NASA CONTRACTOR REPORT

NASA CR-2476

NASA CR-2476

A VISCOUS/POTENTIAL FLOW INTERACTION ANALYSIS METHOD FOR MULTI-ELEMENT INFINITE SWEPT WINGS

Volume I

by F. A. Dvorak and F. A. Woodward

Prepared by
FLOW RESEARCH, INC.
Kent, Wash. 98031
for Ames Research Center

NATIONAL AERONAUTICS AND SPACE ADMINISTRATION • WASHINGTON, D. C. • NOVEMBER 1974

1. Report No.	2. Government Accession No.	3. Recipient's Catalog No.
NASA CR - 2476		

4. Title and Subtitle	5. Report Date
A VISCOUS/POTENTIAL FLOW INTERACTION ANALYSIS METHOD FOR MULTI-ELEMENT INFINITE SWEPT WINGS, VOLUME I	November 1974
	6. Performing Organization Code
7. Author(s)	8. Performing Organization Report No.
F. A. Dvorak and F. A. Woodward	
	10. Work Unit No.
9. Performing Organization Name and Address	11. Contract or Grant No.
Flow Research, Inc. Kent, Washington 98031	NAS 2-7048
	13. Type of Report and Period Covered
12. Sponsoring Agency Name and Address	Contractor Report
National Aeronautics and Space Administration Washington, D.C. 20546	14. Sponsoring Agency Code

15. Supplementary Notes

16. Abstract

An analysis method and computer program have been developed for the calculation of the viscosity dependent aerodynamic characteristics of multi-element infinite swept wings in incompressible flow. The wing configuration consisting at the most of a slat, a main element and double slotted flap is represented in the method by a large number of panels. The inviscid pressure distribution about a given configuration in the normal chord direction is determined using a two dimensional potential flow program employing a vortex lattice technique. The boundary layer development over each individual element of the high lift configuration is determined using either integral or finite difference boundary layer techniques. A source distribution is then determined as a function of the calculated boundary layer displacement thickness and pressure distributions. This source distribution is included in the second calculation of the potential flow about the configuration. Once the solution has converged (usually after 2-5 iterations between the potential flow and boundary layer calculations) lift, drag, and pitching moments can be determined as functions of Reynolds number.

17. Key Words (Suggested by Author(s))	18. Distribution Statement
Aerodynamics, Airfoils, Boundary Layers, Flaps, High Lift, Potential Flow, Slats, Wings, Swept Wings, Viscous Interaction, Viscous Flows	UNCLASSIFIED-UNLIMITED CAT.01

19. Security Classif. (of this report)	20. Security Classif. (of this page)	21. No. of Pages	22. Price*
Unclassified-Unlimited	Unclassified-Unlimited	86	4.00

*For sale by the National Technical Information Service, Springfield, Virginia 22151

TABLE OF CONTENTS

LIST OF FIGURES

LIST OF FIGURES (cont'd)

A VISCOUS/POTENTIAL FLOW INTERACTION ANALYSIS METHOD FOR MULTI-ELEMENT INFINITE SWEPT WINGS

By

F. A. Dvorak and F. A. Woodward
Flow Research, Inc.

SUMMARY

An analysis method and computer program have been developed for the calculation of the viscosity dependent aerodynamic characteristics of multi-element infinite swept wings in incompressible flow.

The wing configuration consisting at most of a slat, a main element and double slotted flap is represented in the method by a large number of panels. The inviscid pressure distribution about a given configuration in the normal chord direction is determined using a two dimensional potential flow program employing a vortex lattice technique. The boundary layer development over each individual element of the high lift configuration is determined using either integral or finite difference boundary layer techniques.

Once the boundary layer development is known, a source distribution is determined as a function of the calculated boundary layer displacement thickness and pressure distributions. This source distribution is included in the second calculation of the potential flow about the configuration, and represents the effect of the boundary layer in the modification of the potential flow. Once the solution has converged (usually after 2-5 iterations between the potential flow and boundary layer calculations) lift, drag, and pitching moments can be determined as functions of Reynolds number.

The new method has a number of features and capabilities which make it a unique method at this time. Some of these features include:

-The inclusion of methods capable of calculating the boundary layer development over infinite yawed wings.

-The inclusion of normal pressure gradient and longitudinal curvature terms in the finite difference program. This has led to much improved predictions of the performance of multi-element airfoils in two dimensions as compared to the predictions of other methods, especially in the calculation of profile drag.

-The use of source distributions rather than the displacement thickness directly to represent the effect of the boundary layer on the potential flow. This approach is much more efficient than the alternate procedure since the influence coefficient matrix representing the geometry of the configuration need be inverted only once. Computer time expenditures are consequently much less with the new method.

-In the future, the effects of tangential injection and suction boundary layer control on aerodynamic performance may be calculated, as well as the effects of fully three dimensional flow.

The computer program is written in Fortran IV for the CDC 6600 and 7600 family of computers. The program occupies 100,000 (octal) words of storage and operates in the overlay mode. The program has been structured in such a way that extension or replacement of individual calculation procedures is straightforward.

INTRODUCTION

Background

The multi-element wing is an essential component of the high-lift systems of existing commercial and military aircraft. Historically the design of these systems has been dependent upon experimental verification of predicted aerodynamic performance. This approach has been and continues to be a very costly and time consuming venture. The advent of high speed computers and of advanced numerical methods is however gradually reducing the reliance on the experimental method. Calculation methods now exist which permit the solution of many practical engineering problems. The prediction of the aerodynamic characteristics of two-dimensional lifting multi-element airfoils including the effect of viscosity is an important example of this capability.

The availability of a three-dimensional version of such a method would be of considerable value to the designers of modern aircraft high-lift systems, particularly with respect to STOL aircraft, where the design problems appear to be the most formidable. Trade-off studies could be made for the design and analysis of individual components such as the leading edge devices or the slotted flaps. A multi-element wing analysis would have other important applications, and it is because of the usefulness of such a method that the procedure described in this report was developed.

The method is currently valid for the infinite yawed wing case, but has been structured in such a way that at a later date, it can be extended to the fully three dimensional case. The addition of viscous effects is accomplished using distributed sources determined from the boundary layer calculations. The need to add viscous effects is clearly demonstrated by the results shown in Figure 1.1 (Ref. 1.). Obviously, the inviscid solution grossly over estimates the performance of the airfoil section.

It was Prandtl who first suggested adding the boundary layer displacement thickness to the original geometry to account for the displacement of the inviscid flow streamlines by the boundary layer. This approach has since been used successfully by many researchers. A practical computational difficulty arises with this approach however, and that is the need in the potential flow calculation to re-invert at each pass a large matrix resulting in large computer time expenditures. In order to obtain smooth pressure distributions it is also usually necessary to smooth the new geometry before each potential flow calculation resulting in further computer time expenditures. An alternative procedure stemming from an idea first suggested by Preston, Ref. 2, has been successfully adopted in the computer program described in this report. Briefly, a source or sink (negative source) distribution is determined as a function of the known displacement thickness, entrainment rate, and velocity distributions ($q = d/ds\ (\rho_e U_e \delta^*)$. With the introduction of a source distribution a new vortex distribution is determined given

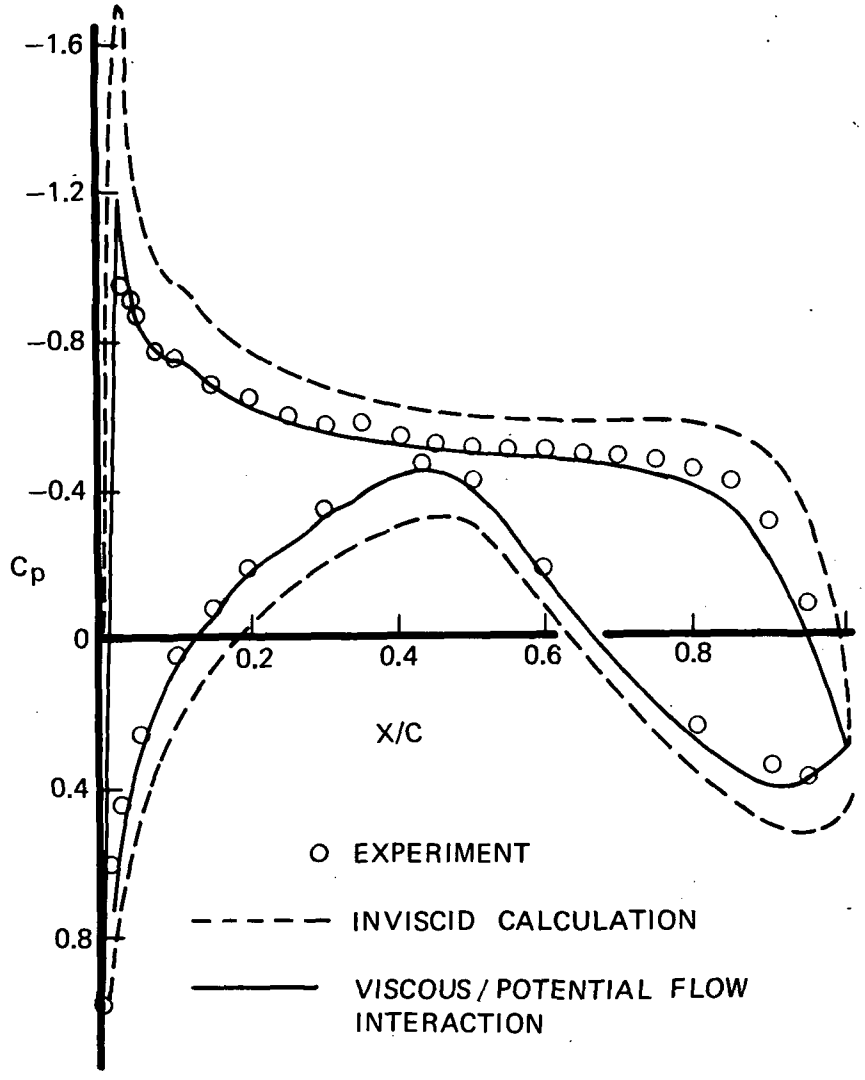

FIG. 1.1 COMPARISON BETWEEN THEORETICAL AND EXPERIMENTAL PRESSURE DISTRIBUTION

the original geometry, consequently, there is no need to invert the matrix a second time. If several iterations between inviscid and viscous flow are required, the potential computer time saving is substantial.

Problem Definition

The calculation of the potential flow about a multi-element configuration represents the first task of any analysis method. Because the analysis is limited to infinite swept wings a two-dimensional potential flow method is adequate. Future expansion to the fully three-dimensional case suggested, however, that any program be written in modular form in order that the two-dimensional method could be readily replaced by a three-dimensional method. In the two-dimensional case, a mathematical model is required for the flow field about a series of arbitrarily shaped bodies in an incompressible, inviscid flow. The model must as a further requirement be able to predict the pressure distribution at selected off-body points above the flap segments. This is necessary because downstream of the wing trailing edge the static pressure normal to the flap surface is greatly influenced both by the proximity of the flap to the wing trailing edge and by the large surface curvature in the flap leading edge region. This static pressure variation (see Figure 1.2) has a considerable influence on the development of the combined wing wake-flap boundary layer downstream of the wing trailing edge.

With the potential flow field specified, it is necessary to predict the boundary layer development over the multi-element configuration. Calculations must include stagnation line initial conditions, laminar, transition and turbulent boundary layer developments and laminar or turbulent separation predictions for each element of the infinite swept wing high lift system. The calculations must include accurate predictions of boundary layer development in the regions where wing or first flap upper surface and cove boundary layers merge with the downstream flap upper surface boundary layer. This requirement is an absolute necessity if accurate drag predictions are to be made. Both longitudinal curvature and normal pressure gradient terms must be included in the governing boundary layer equations as each effect has a significant influence on the boundary layer development and subsequently on the section drag coefficient. These effects are particularly important in the wing trailing edge-flap leading edge region. Once the boundary layer development is known, its effect on the external flow must be determined.

A complete analysis program for the aerodynamic characteristics of multi-element infinite swept wings is developed by combining the separate potential flow and boundary layer calculation procedures. Iteration between the separate procedures results in the prediction of viscosity dependent aerodynamic forces.

The different parts of the flow about a multi-element infinite swept wing high lift system consisting of a leading edge slat, the main wing and double slotted flaps are shown in Figure 1.3. The different calculation schemes that form the elements or modules of the integrated computer program are presented in the following sections.

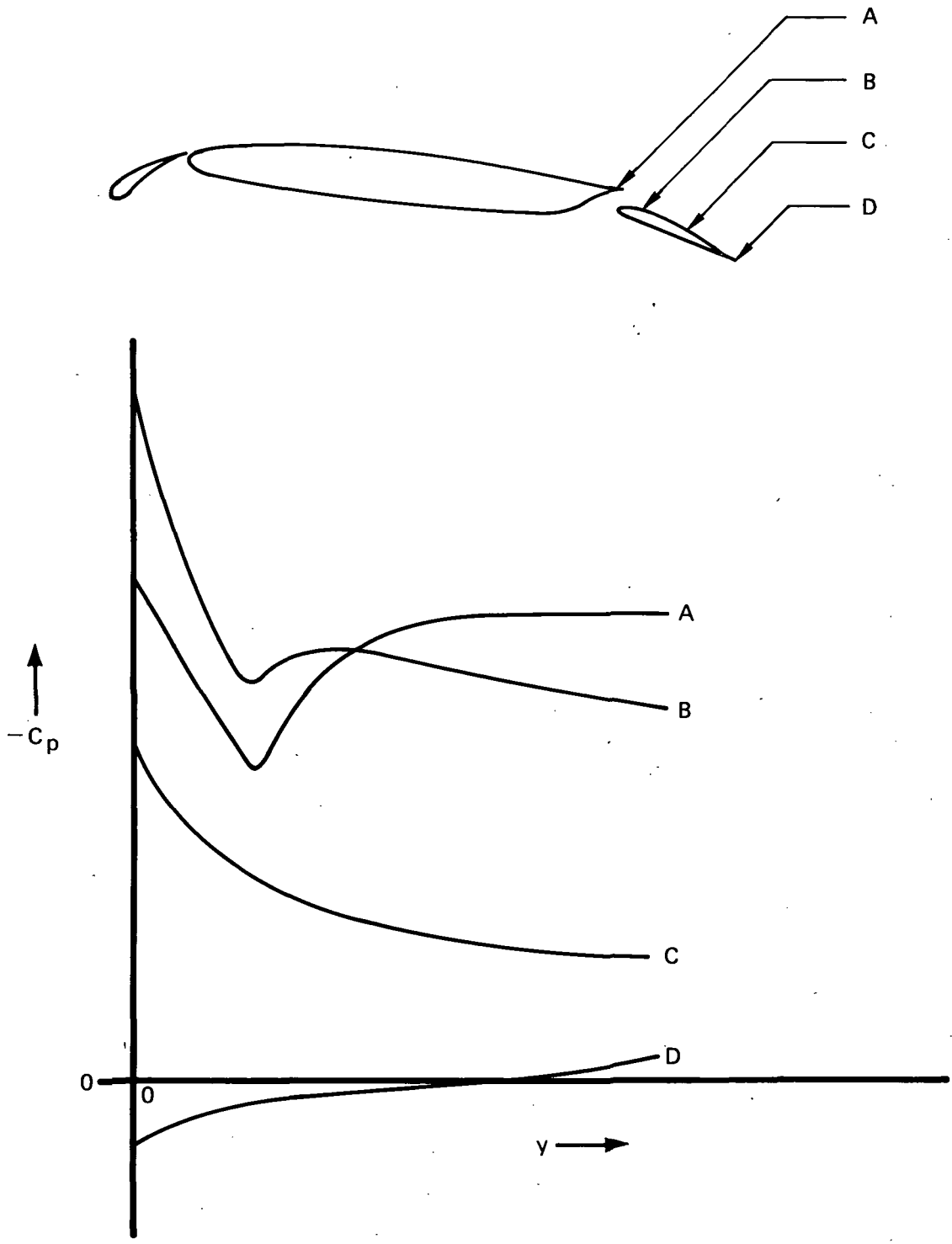

FIG. 1.2 STATIC PRESSURE VARIATION NORMAL TO FLAP SURFACE

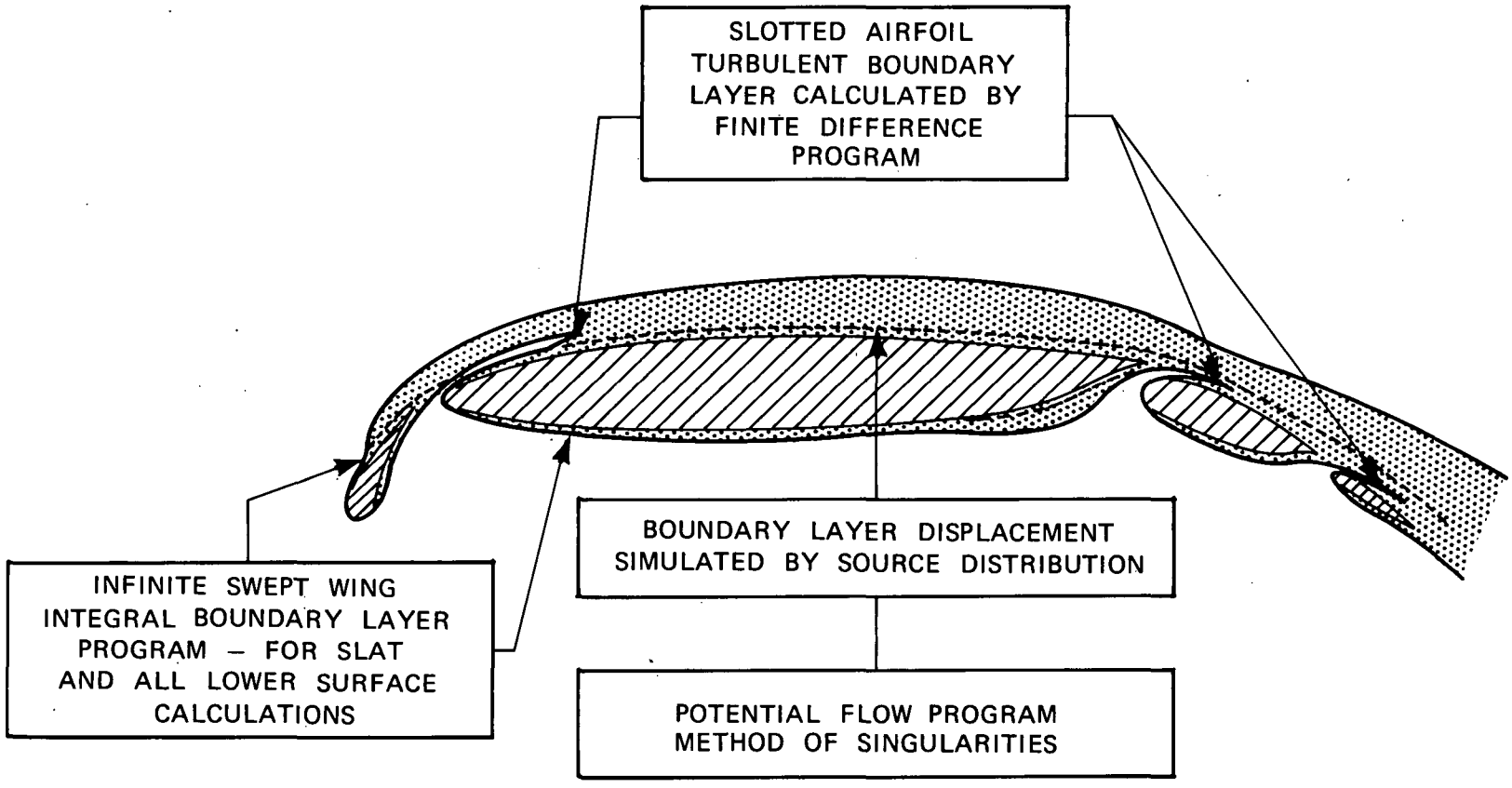

FIG. 1.3 FLOW ABOUT A MULTI-ELEMENT INFINITE SWEPT WING

LIST OF SYMBOLS

a_{ij}	Aerodynamic influence coefficient
A+	Function in Van Driest damping factor
b_{ij}	Normal velocity due to external source
C	Eddy Reynolds number $U_d\sigma/\nu_t$
C*	Reynolds number at stagnation line
C_D	Profile drag coefficient = $\frac{D}{\frac{1}{2}\rho U_\infty^2 c}$
C_L	Lift coefficient = $\frac{L}{\frac{1}{2}\rho U_\infty^2 c}$
C_M	Moment coefficient
c	Airfoil normal chord
c_f	Local skin friction coefficient
C_{f_1}	Streamwise skin friction coefficient
C_{f_R}	Resultant skin friction coefficient
C_{f_2}	Cross flow skin friction coefficient
C_P	Pressure coefficient
D	Drag force/unit span
F, F_o, G, G_o	Universal functions in Curles laminar method
g	Correction term to Thwaites laminar method
H	Shape factor, ratio of displacement to momentum thicknesses (σ^*/θ)
H_1	Shape factor $(\delta - \delta^*)/\theta$
K	Non-dimensional pressure gradient parameter
κ	Von Karman's mixing length coefficient
l	Mixing length l = ky inches
L	Lift force/per unit span
M_L	Local Mach number
M_∞	Free stream Mach number
n_i	Total normal velocity

P	Static pressure, pounds per square inch absolute
q	Source strength
r	Radius of curvature, inches
R	Local radius of curvature
R_c	Chord Reynolds number $U_\infty c/\nu$
R_θ	Momentum thickness Reynolds number $U\theta/\nu$
$R_{\theta\ ins}$	Streamwise momentum thickness Reynolds number at instability point
$R_{\theta\ trans}$	Streamwise momentum thickness Reynolds number at transition
U_R	Resultant velocity
U_S	Local streamwise velocity
U_∞	Free stream velocity
V	Tangential velocity at airfoil surface
u, v, w	Components of velocity in x, y and z directions
U_τ	Friction velocity $(\tau_w/\rho)^{1/2}$
x, y, z	Components of length in the chord, normal and spanwise directions
S	Distance along a streamline
$\delta_1^*\ \delta_2^*$ $\theta_{11}\ \theta_{12}$ $\theta_{21}\ \theta_{22}$	Three-dimensional boundary layer thickness parameters defined in Equation 3.22.
δ	Boundary layer thickness
ρ	Density of air
τ	Shear stress
τ_w	Local surface shear stress

γ_i	Vortex strength
α	Angle between streamline at outer edge of boundary layer and wing normal chord
β	Angle between surface streamline and external streamline directions
ν	Kinematic viscosity
ν_t	Eddy viscosity
$\gamma(y)$	Intermittency function
σ	Standard deviation of intermittency function

Subscripts

e	Value at edge of boundary layer
i	i^{th} value
in	Incompressible
ins	Instability
j	j^{th} value
L	Local value
l	lower
trans	Transition
s	Streamline component
t	Turbulent
u	Upper

POTENTIAL FLOW METHOD

Configuration Definition

The multi-element airfoil configuration is represented by pairs of surface coordinate points. Each element with the exception of the main wing, may be specified in its own or a reference coordinate system. The main element must be given in the reference coordinate system. Individual coordinate systems are related to the reference coordinate system by pivot points. The pivot points are prescribed in both the element and reference coordinate systems. In order to loft the configuration, element rotation angles must also be prescribed. Given the pivot points and rotation angles any element may be translated and rotated to the desired location relative to the main element.

Pivot points may be determined based on such requirements as a specified slot gap and wing-flap overlap. Leading edge coordinates usually provide a convenient element pivot point although in some cases the hinge point of a flap on its mechanical track or linkage mechanism gives a ready reference point. Figure 2.1 shows a four element configuration in both input and lofted positions.

If the configuration is made up of a main element and one or more slotted flaps, then additional analysis is required to determine flap upper surface longitudinal radius of curvature for later use in the finite difference boundary layer calculation methods. Accurate calculations of curvature require the use of very smooth input data. Because of this, it was found necessary to use spline functions to represent the surface being analyzed. A spline under tension* is first passed through the coordinate points representing the flap upper surface. First derivatives dy/dx are then determined from the splined curve using analytic expressions. A second spline under tension is now used to represent a curve through the calculated first derivatives. This spline is likewise differentiated using analytic expressions. Once both first and second derivatives of the surface are known the radius of curvature can be readily calculated. Figure 2.2 indicates the success of this technique in relation to known values of radius of curvature for the NACA 4412 airfoil upper surface contour.

---

* "Splines Under Tension" - a technique developed by Dr. A. Cline of the National Center for Atmospheric Research, Boulder, Colorado, for obtaining smooth continuous curves from sets of imput coordinate points.

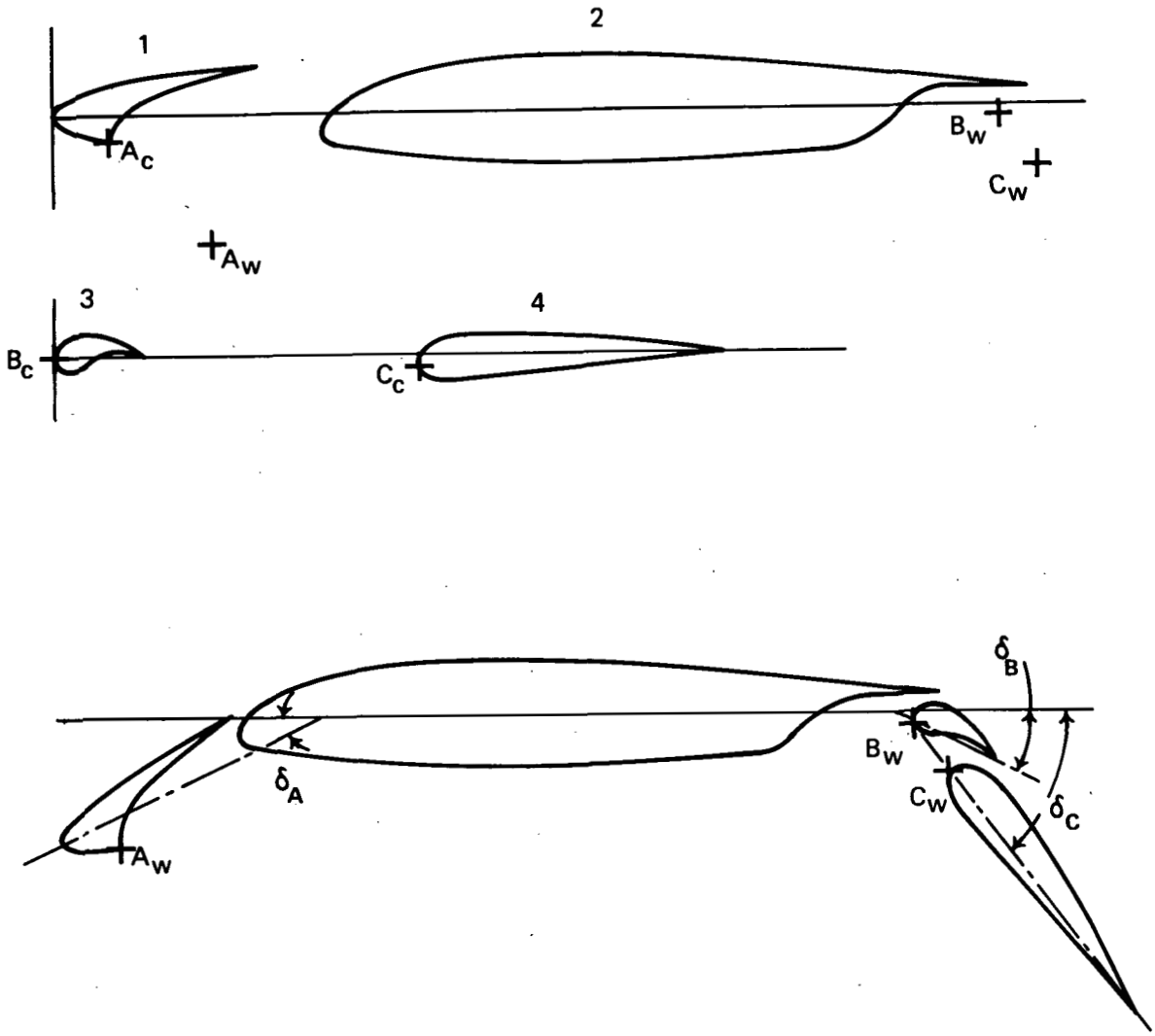

FIG. 2.1 MULTI-ELEMENT AIR FOIL LOFTING PROCEDURE

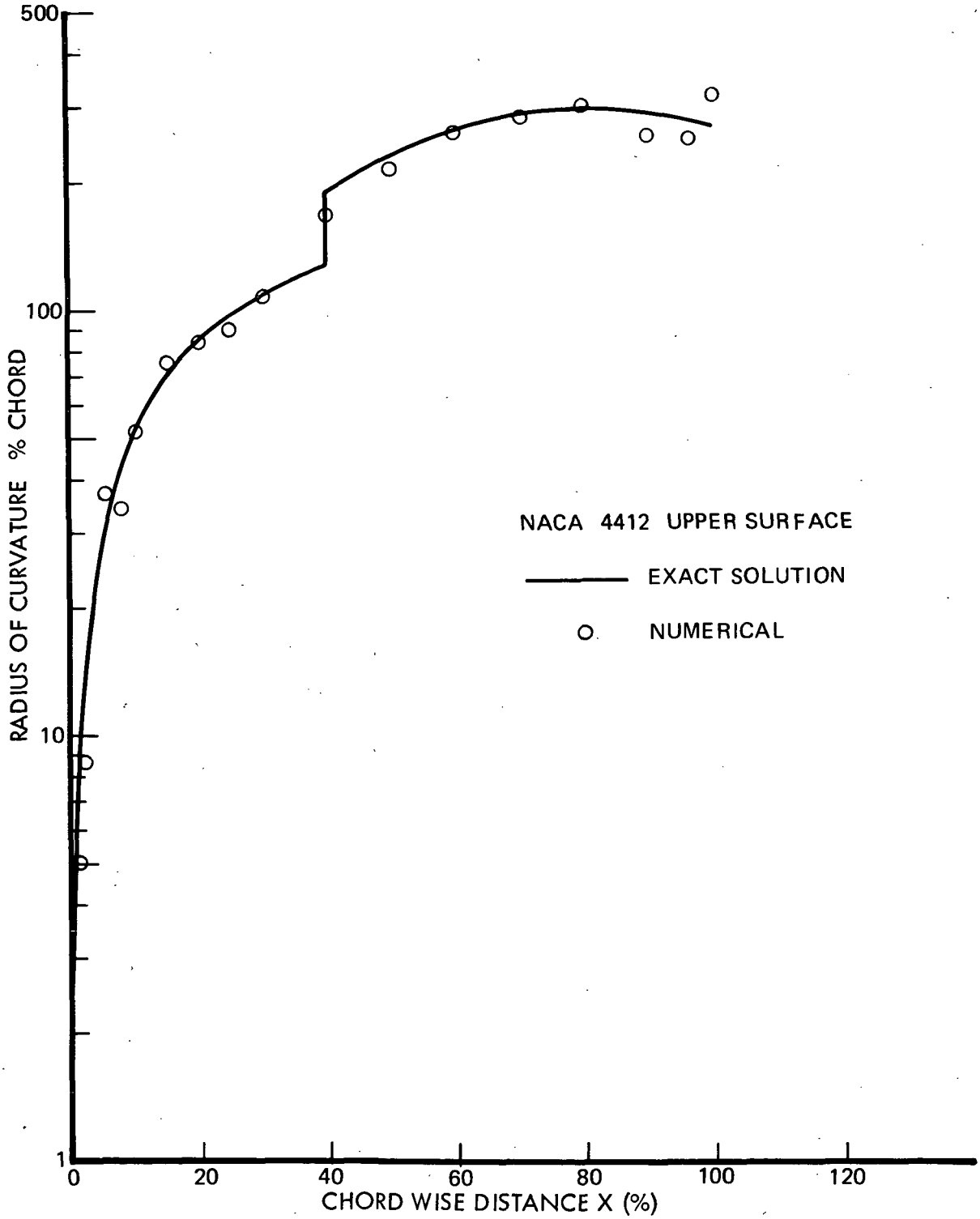

FIG. 2.2 COMPARISON OF EXACT & NUMERICAL CALCULATION OF SURFACE RADIUS OF CURVATURE

Inviscid Method

The airfoil and associated flap system in their lofted configuration is approximated by a large number of planar segments, or panels, with corner points located on the actual airfoil or flap surfaces. The geometry of a typical two element system is illustrated below:

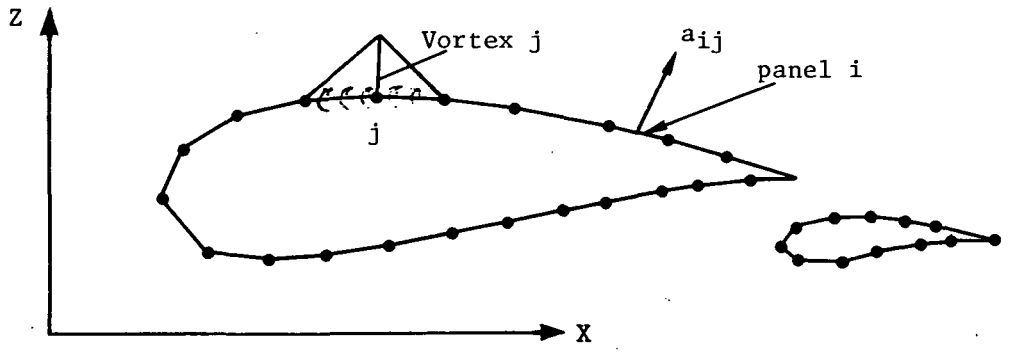

Fig. 2.3 Airfoil Geometry Using Planar Panels

A triangular distribution of vorticity is located on each adjacent pair of panels, as shown above. The vortex distribution is identified by the index of the common edge, and is given unit magnitude at that point. The normal component of velocity induced by the j^{th} vortex distribution at the center of panel i is designated the aerodynamic influence coefficient a_{ij}, and is calculated as follows:

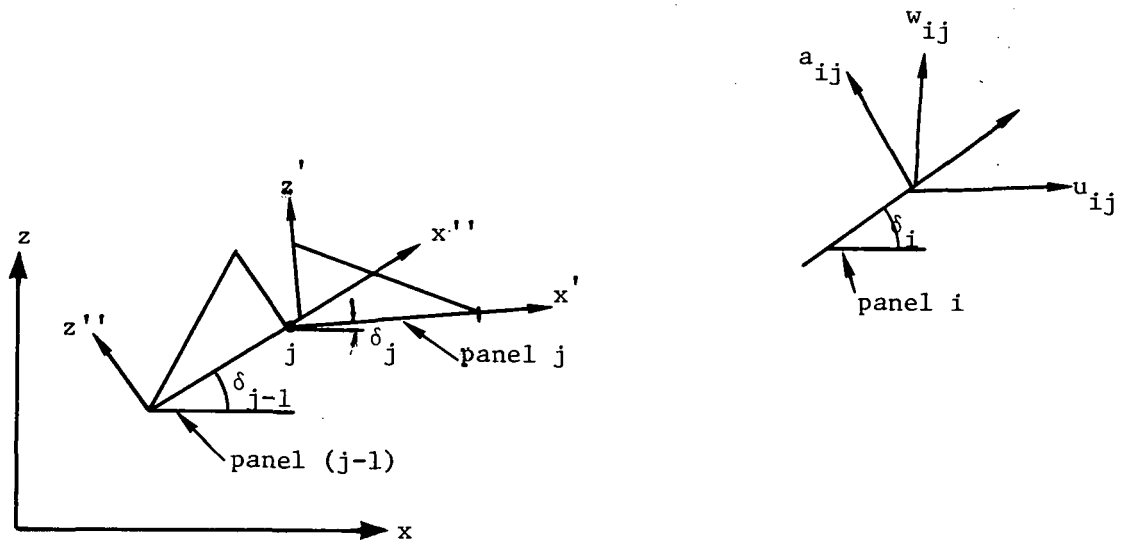

Fig. 2.4 Aerodynamic Influence Coefficients

First, the horizontal and vertical components of velocity u_{ij} and w_{ij} are obtained by summing the influences of a linearly varying vortex distribution on panel (j-1) having unit value at the trailing edge, and a linearly varying vortex distribution on panel j having unit value at the leading edge. Formulas for the u and w components induced by these vortex distributions in terms of the primed coordinate system associated with the influencing panel are given in Appendix I.

$$u_{ij} = u''_{i,j-1} \cos\delta_{j-1} - w''_{i,j-1} \sin\delta_{j-1} + u'_{ij} \cos\delta_j - w'_{ij} \sin\delta_j \qquad (2.1)$$

$$w_{ij} = w''_{i,j-1} \cos\delta_{j-1} + w''_{i,j-1} \sin\delta_{j-1} + w'_{ij} \cos\delta_j + w'_{ij} \sin\delta_j \qquad (2.2)$$

The normal velocity a_{ij} is then

$$a_{ij} = w_{ij} \cos\delta_i - u_{ij} \sin\delta_i \qquad (2.3)$$

A series of overlapping triangular vortex distributions are placed on the upper and lower surfaces of the airfoil, as indicated:

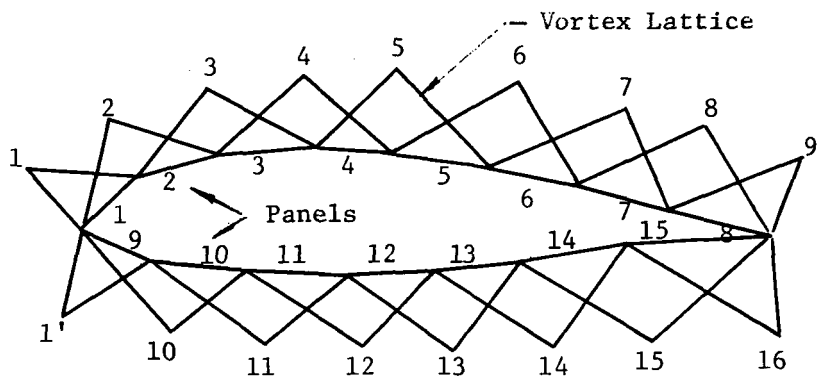

Fig. 2.5 Vortex Distribution on Airfoil

It should be noted that the number of panels on the upper and lower surfaces are not necessarily equal. At the leading edge, the vortex strengths of the upper and lower vortices are set equal, to insure a smooth flow around the leading edge. At the trailing edge the "Kutta" condition specifies that the magnitudes of the surface velocity on the upper and lower surfaces have a common limit. This implies that the vortex strengths on the upper and lower surfaces must be equal and opposite.

In the above example, the airfoil has 8 panels on the upper surface and 7 on the lower, for a total of 15 panels. If the leading edge vortices 1 and 1' are set equal ($\gamma_1 = \gamma_1'$) and the trailing edge vortices 9 and 16 are set equal and opposite ($\gamma_9 = -\gamma_{16}$) a total of 15 unknown vortex strengths remain. The unknown vortex strengths are determined by specifying that the sum of the induced velocity and the normal component of the free stream velocity go to zero at each panel control point. For an airfoil having N panels, the total normal velocity at panel i may be written

$$n_i = \sin(\alpha - \delta_i) + \sum_{j=1}^{N} a_{ij}\,\gamma_j = 0 \qquad (2.4)$$

The first term represents the normal component of a unit free stream velocity at the control point of panel i, and the second is the sum of the products of the influence coefficients and the N unknown vortex strengths. Writing this boundary condition equation for each of the N panels results in a linear system of N equations in the N unknown vortex strengths. In matrix form,

$$\begin{bmatrix} a_{11} & a_{12} \cdots\cdots & a_{1N} \\ a_{21} & & \\ \vdots & & \\ a_{N1} & & a_{NN} \end{bmatrix} \begin{Bmatrix} \gamma_1 \\ \gamma_2 \\ \\ \gamma_N \end{Bmatrix} = - \begin{Bmatrix} \sin(\alpha - \delta_1) \\ \vdots \\ \sin(\alpha - \delta_N) \end{Bmatrix} \qquad (2.5)$$

This matrix equation can then be solved for the vortex strengths. Direct inversion is employed for single element airfoils, and either a direct method or an iterative procedure (described in Appendix II) can be employed for multi-element airfoils.

Airfoils with blunt trailing edges can be analyzed successfully using the Kutta condition that the trailing edge vortex strengths are equal and opposite (i.e. $\gamma_9 = -\gamma_{16}$ in Figure 2.5). If the trailing edge closes to a point, the strengths of the trailing edge vortices must go to zero, since the trailing edge will be a stagnation point in the flow. Although this result is given automatically by the solution of the above system of equations, it has been found that an alternate formulation of these equations is desirable for airfoils with trailing edge closure. In this case the coefficients in the last column of the matrix (eqn. 2.5) become very small resulting in a poorly conditioned system of equations.

In the alternate formulation, the Kutta condition is specified by setting the strengths of the vortices associated with the trailing ege panels equal to zero (i.e., $\gamma_9 = \gamma_{16} = 0$ in Figure 2.5). However, this procedure eliminates the last column of influence coefficients in Eqn. (2.5) leaving an indeterminate system of N equations in N-1 unknowns.

An additional unknown is provided by adding the influence of a constant strength source distribution just inside the airfoil surface. The source is distributed on the inner side of each panel used to represent the airfoil. The velocities induced by a constant strength source distribution are given in Appendix I, and are used to calculate new values for the last column of influence coefficients in the boundary condition equations. The unknown source strength is added to the remaining N-1 unknown vortex strengths to give a well conditioned set of equations. It should be noted that the unknown source strength is always very close to zero for airfoils with trailing edge closure.

The pressure coefficient at the mid point of panel i is calculated as follows:

$$C_{p_i} = 1 - u_i^2 - w_i^2 \qquad (2.6)$$

where

$$u_i = \sum_{j=1}^{N} u_{ij}\, \gamma_j$$

$$w_i = \sum_{j=1}^{N} w_{ij}\, \gamma_j$$

and u_{ij}, w_{ij} are given by Eqns (2.1) and (2.2). The lift and pitching moment coefficients are obtained by integrating the pressures around the airfoil configuration.

Viscous/Potential Flow Interaction

The inviscid flow around an airfoil can be modified to account for viscous effects through the addition of the boundary layer displacement thickness δ^* to the original airfoil geometry. The potential flow method described in the previous section can then be used to calculate the flow field about the new geometry. A modified pressure field results, which in turn causes a change in the calculated boundary layer development. After several iterations both the pressure field and boundary layer developments should become convergent. This procedure is used in both the Lockheed and McDonnel-Douglas programs (Refs 1 and 3), and while it would seem at first glance to be a straightforward approach, several requirements are necessary to ensure a satisfactory solution. These include:

- The necessity to calculate and invert a new influence coefficient matrix at each iteration due to the change in resultant geometry.

- The necessity to smooth the geometry each time the displacement thickness is added, to ensure a smooth pressure distribution.

- The necessity during each iteration to modify to a considerable extent the calculated pressure and boundary layer developments in the trailing edge region in order to ensure a convergent calculation procedure.

An alternate procedure is available which uses the same influence coefficient matrix throughout the calculation, and it is this method which is used in the present program.

The effect of the boundary layer on the potential flow is represented by a distribution of sources on the panels connecting points of the original airfoil surface (Figure 2.3). The strength q_j of the source distribution is made proportional to the rate of entrainment of mass into the boundary layer (i.e. $q = \frac{d}{ds}(\rho_e U_e \delta^*)$)† Thus the calculated pressure distribution and boundary layer displacement thickness developments can be used to determine the source strengths for the next iteration of the analysis. The source distribution has the effect of modifying the boundary conditions to the original problem by altering the right hand side of Eqn 2.5. The influence coefficients a_{ij} (or u_{ij}, w_{ij}) remain unchanged as does the geometry of the configuration being analyzed.

The effect of the source distribution on the boundary conditions is determined in the following manner. Consider a panel representing a portion of the airfoil geometry; the source strength is known as is the normal velocity induced by the source distribution at the boundary point on the panel. This normal velocity is the new boundary condition to be satisfied by all sources and vortices representing the geometry and the boundary layer effects. However, the source distribution of the same panel already satisifies this new boundary condition, therefore, the remaining sources and vortices must satisfy the boundary condition of tangential flow to the surface.

Source influence coefficients $u_{s_{ij}}$ and $w_{s_{ij}}$ are defined as induced velocities per unit source strength q_j at a corner point where the source distribution on a panel is represented by two overlapping triangles. This definition is completely analogous to the vortex influence coefficients u_{ij} and w_{ij}.

The total induced velocities at the i-th boundary point can be described by

$$u_i = \sum_{j=1}^{N} u_{ij}\,\gamma_j + \sum_{j=1}^{N} u_{s_{ij}}\,q_j \qquad (2.7)$$

$$w_i = \sum_{j=1}^{N} w_{ij}\,\gamma_j + \sum_{j=1}^{N} w_{s_{ij}}\,q_j \qquad (2.8)$$

†With this technique the normal velocity component at the surface n_i and the source strength q_i are equal.

Because of the introduction of a source distribution, the Kutta condition at the trailing edge of the airfoil takes a form different from those used for blunt and closed trailing edges in the inviscid flow calculation. With the trailing edge being a stagnation point the sum of the vortex and source velocities is zero. With the trailing edge sources known the vortex strengths γ_u and γ_l can be determined by the condition that the component of velocity normal to the trailing edge panel is zero at the trailing edge on the upper and lower surfaces.

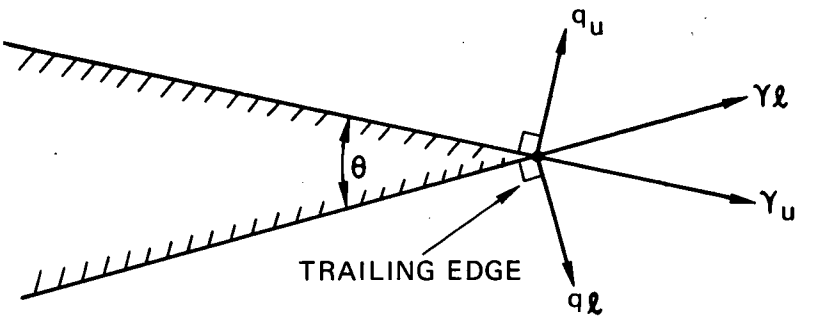

Fig. 2.6 Kutta Condition - Modified by Source Distribution

From the preceeding figure,

$$\gamma_u = (-q_l + q_u \cos\theta)/\sin\theta \qquad (2.9)$$

$$\gamma_l = (-q_u + q_l \cos\theta)/\sin\theta \qquad (2.10)$$

It should be noted that the above equations imply equal pressure coefficients on the upper and lower surfaces at the trailing edge. Taking the difference of the squares of each equation,

$$\gamma_u^2 - \gamma_l^2 = q_l^2 - q_u^2$$

or

$$Cp_u = 1 - \gamma_u^2 - q_u^2$$

$$= 1 - \gamma_l^2 - q_l^2 = Cp_l$$

The addition of the source distribution external to the airfoil modifies the normal velocity at the control point of panel i. Referring to Eqn. (2.4),

$$q_i = n_i = \sin(\alpha-\delta_i) + \sum_{j=1}^{N} a_{ij}\,\gamma_j + \sum_{j=1}^{N} b_{ij}\,q_j \qquad (2.11)$$

where

$$b_{ij} = w_{s_{ij}} \cos\delta_i - u_{s_{ij}} \sin\delta_i$$

is the normal velocity induced by the external source on panel j.

Since the q_j are known, the right hand side of Eqn. (2.5) becomes

$$c_i = -\sin(\alpha-\delta_i) - \sum_{j=1}^{N} b_{ij}\,q_j + q_i \qquad (2.12)$$

Since the vortex strengths at the trailing edge of the upper and lower surfaces are also specified in terms of the external source strength by Eqns. (2.9 and (2.10), an additional unknown constant source distribution inside each airfoil surface is required to solve Eqn (2.5), as described in the previous section.

The advantage in computer time of this procedure results from having to calculate the influence coefficients only once. At each successive iteration only matrix multiplication is required to determine the new vortex strengths. As in the displacement method the effect of the boundary layer corrections tends to cause an overshoot or correction in the pressure field solution at each iteration. This undesirable feature is avoided and rapid convergence assured if the boundary layer development and resultant source distribution is determined from a pressure field weighted using fifty percent of the current solution and fifty percent of the previous solution.

Although the precedure does not require extensive smoothing as in the displacement methods some limitation on the source strength is required in the trailing edge region if rapid convergence is to be achieved. Rapid growth of the boundary layer approaching separation in strong adverse pressure gradients (typical of configurations at high angles-of-attack) cause abnormally fast growth of the displacement thickness, and in turn the source strength. Numerical experiments indicate that if a limit is placed on the maximum source strength convergence can occur between two and five iterations. The calculations also indicate that this limit is different for slotted airfoil cases, where the boundary layer growth on the flap is very much greater than that typical of single element cases. More will be said of this limit in a following section.

Because the pressure coefficients are determined from the velocities on the boundary points of a panel rather than from the vortex strengths at the corner points, the trailing edge pressures are not known a priori. Therefore, they are calculated by simple linear extrapolation of the pressures from the last two boundary points on the upper and lower surfaces respectively.

A special situation arises if any element of the geometry does not have a closed trailing edge. In this case the solution for the inviscid flow about the particular element is determined using the Kutta condition $\gamma_u = -\gamma_l$. No internal distributed source is required to complete the problem definition. Consequently, when boundary layer effects are included in the first iteration (with the Kutta condition determined from Eqns. (2.9) and (2.10)), an internal source is required to complete the problem definition and it is necessary to recalculate the influence coefficient to include the effect of the distributed source. Subsequent iterations require only matrix multiplication to obtain the vortex strengths.

BOUNDARY LAYER CALCULATION METHODS

The boundary layer development is calculated from the stagnation line of each element. For the infinite swept wing case two separate calculation procedures are used, each for a particular region of the flow. On the upper surfaces of the leading edge slat and main wing and for the lower surface of every element of the configuration an integral method is used. This method is about 100 times faster than the corresponding finite difference method in two dimensions. Economy of computer time is essential in an iterative method particularly when a multi-element configuration is considered, if the method is to be of practical use to the designer. In all cases where passive blowing (slotted flaps) or powered blowing is considered, the finite difference method is used. This method could be used for the complete boundary layer analysis if desired by the user.

Descriptions of the individual boundary layer and transition analyses are presented in the following sections.

Stagnation Line Initial Conditions

It has been predicted theoretically by Cumpsty and Head 4 and Bradshaw 5 amongst others that flow along the stangation line of a infinite yawed wing appraoches an asymptotic condition. This condition is one where the rate of growth of the boundary layer due to frictional forces is balanced by the divergence of the flow from the spanwise to the streamwise direction. Cumpsty and Head later demonstrated in an experimental study (Ref 6) their earlier theoretical prediction. They were able to show that whether the flow is laminar or turbulent its integral properties can be determined directly as a function of a single non-dimensional parameter C*. The parameter C* ($\equiv V^2/\nu\ dU/dx$), where V is the spanwise velocity, ν the kinematic viscosity and dU/dx the chordwise velocity gradient at the stagnation line) is a form of Reynolds number which correlates well with the streamwise shape factor H, momentum thickness θ and skin friction coefficient $C_f/2$. The correlations for H and θ are presented in tabular form in Table 1. Initial integral boundary layer parameters are determined from the table for the calculated C*. If $C^* < 1.35 \times 10^5$ the flow is laminar otherwise it is turbulent. The appropriate calculation method is then used to determine the downstream boundary layer growth (See Figure 3.1).

Integral Boundary Layer Methods

Laminar Method

A variety of methods exist for the calculation of laminar boundary layer developments, the most general of these being based on finite difference methods. In the case of the infinite swept wing substantial regions of laminar flow (10% chord or more), are likely only at the lower Reynolds numbers and sweep angles and in cases where large flap deflections result in considerable laminar flow on the lower surfaces of the flaps. In these instances the effect of the laminar flow on the external flow is negligible and the drag contribution very small.

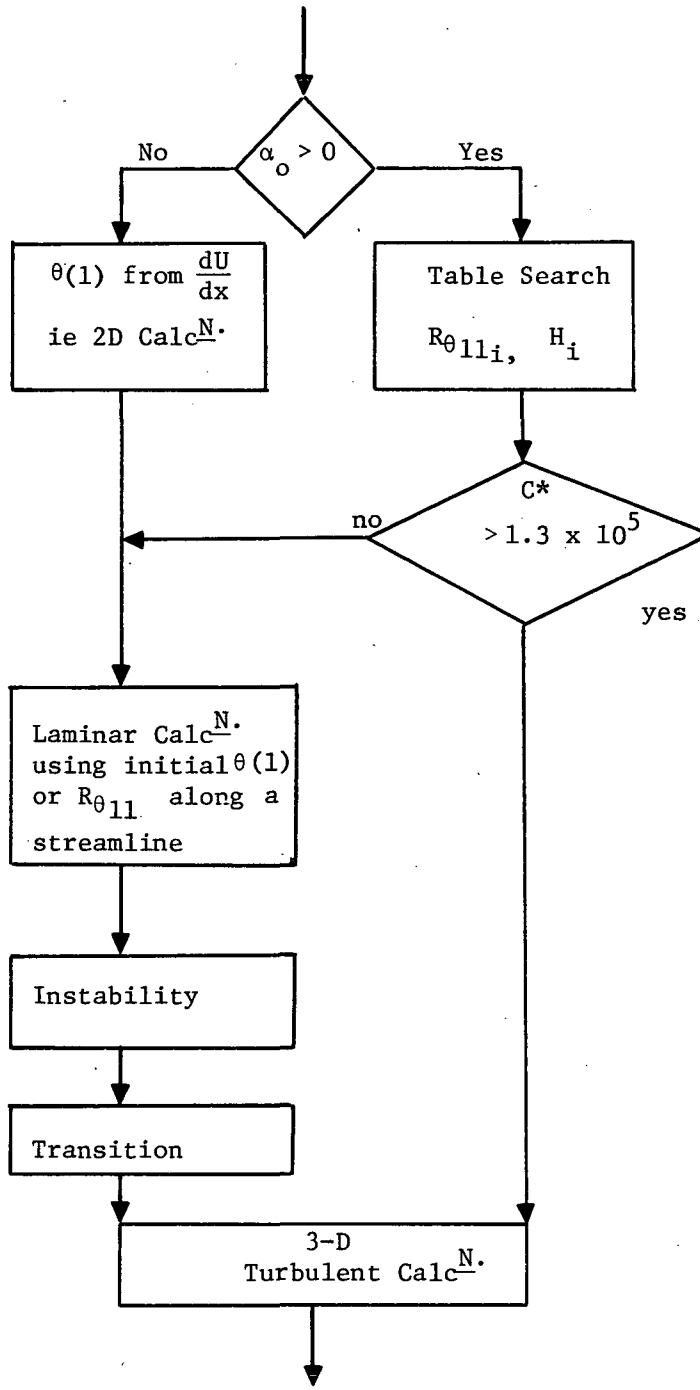

Fig. 3.1 Flow Chart for Boundary Layer Calculations

$C^* \times 10^{-5}$	H	$R_{\theta_{11}}$
0.	2.54	0.
.2	2.54	57.1
.4	2.54	80.88
.6	2.38	100.00
.8	1.78	200.00
1.0	1.70	245.00
1.2	1.60	295.00
1.4	1.56	350.00
1.6	1.54	400.00
1.8	1.53	430.00
2.0	1.51	450.00
2.5	1.50	550.00
3.0	1.47	640.00
3.5	1.45	720.00
4.0	1.44	805.00
4.5	1.43	875.00

Table 1. Stagnation Line Correlation of C^* with H and $R_{\theta_{11}}$.

Because of this, all laminar boundary layer calculations are made using a two-dimensional integral approach along external streamlines. The finite difference method to be described in a following section can also be used to determine the laminar boundary layer development but for the infinite swept wing case as will be seen later it appears to be unnecessary for practical calculations.

The two dimensional method is an adaptation by Curle [7] of a method developed by Thwaites [8]. In Thwaite's method the momentum integral equation

$$d\theta/dx = C_f/2 - (H+2)\theta/U(dU/dx) \qquad 3.1$$

is written in the form

$$d/dx(K/U) = L/U \qquad 3.2$$

where

$$\begin{aligned} K &= \theta^2/\nu \ (dU/dx) \\ L &= [\ell - K(H+2)] \\ \ell &= \theta/U(\partial U/\partial y)_{y=0} \end{aligned} \qquad 3.3$$

Thwaites used exact solutions to a variety of laminar flows to determine the relationship between L and K,

$$L = 0.45 - 6\,K \qquad 3.4$$

Curle has pointed out that Eqn. 3.4 is not adequate in flows approaching separation, and he has suggested an extension or correction to Eqn. 3.4 giving:

$$L = 0.45 - 6\,K + g(K,\mu) \qquad 3.5$$

The parameter μ is a function of both the pressure gradient and the curvature or second derivative of velocity.

$$\mu = K^2U\,(d^2U/dx^2)/(dU/dx)^2 \qquad 3.6$$

Curle rewrote Eqn. 3.5 in the form

$$L = F_o\,(K) - \mu\,G_o(K) \qquad 3.7$$

where F_o and G_o are universal functions determined from a series of exact solutions to laminar flows in the same way as did Thwaites for Eqn. 3.4. After substitution of Eqn. 3.5 into Eqn. 3.2 and with subsequent integration, the result can be rearranged in the form

$$\theta^2 = 0.45\nu/U^6 \int_0^x (1 + 2.22g)\ U^5\,dx. \qquad 3.8$$

This equation is conveniently solved by iteration, g initially equal to zero. With values of K and μ determined in the first iteration. a second iteration is carried out using Eqn. 3.7. At each step in the calculation the local skin friction coefficient, $C_f/2$ and the shape factor H can be calculated using Eqn 3.3. The local skin friction coefficient has been defined as

$$C_f = (\mu/\rho\theta U)\ell \qquad 3.9$$

where ℓ in Eqn. 3.3 is determined in a similar manner to L from a series of known solutions to give

$$\ell^2 = F_1(K) - \mu G_1(K) \qquad 3.10$$

The functions F_0, F_1, G_0 and G_1 are tabulated in the computer program. Calculations begin at the stagnation line in the swept wing case, with the initial momentum thickness θ given as a function of C*. If the flow is two dimensional K takes a initial value $K_o = 0.0855$ at the stagnation point from which the initial momentum thickness θ_o is

$$\theta_o = (.0855\nu/dU/dx)^{1/2} \qquad 3.11$$

The calculation proceeds either to laminar separation or to the end of the airfoil whichever occurs first. The calculated boundary layer development is then interrogated to determine if transition, laminar separation or forced transition (boundary layer tripping) has taken place. If any of these phenomena have occurred the downstream flow is assumed to be turbulent.

Turbulent Method

Several methods have been developed for the calculation of infinite swept wing three dimensional boundary layers. Among the more useful of the methods are those by Cumpsty and Head 9, Nash 10, and Bradshaw 5. Nash's method (a finite difference procedure) is also applicable to fully three dimensional boundary layers but in the words of the originator is cumbersome and inflexible when applied to complex geometries. In practical cases the methods of Cumpsty and Head and of Bradshaw appear to give similar results, with Cumpsty and Heads method having a considerable advantage both in speed and convenience. Because of this, their method was chosen for use in the viscous/potential flow interaction program.

In developing their method, Cumpsty and Head chose an orthogonal curvilinear system of coordinates based on the projections of external streamlines on the surface. In this system streamwise turbulent boundary layer velocity profiles resemble very closely two-dimensional profiles. When the streamwise profiles are known the cross-flow velocity profiles can be calculated as functions of the streamwise profiles and the angle between the surface streamline and the projection of the external streamline on the surface (angle β).

Cumpsty and Head wrote the streamwise and cross flow equations in integral equation form as follows:

Streamwise Momentum Equation

$$\frac{\partial \theta_{11}}{\partial s} - K \frac{\partial \theta_{12}}{\partial s} + \frac{1}{U_s}\frac{\partial U_s}{\partial s}(2 + H)\,\theta_{11} - \frac{\partial \alpha}{\partial s}(\theta_{11}-\theta_{22})K = C_{f_1}/2 \quad (3.12)$$

Cross Flow Momentum Equation

$$\frac{\partial \theta_{21}}{\partial s} - K\frac{\partial \theta_{22}}{\partial s} + \frac{2}{U_s}\frac{\partial U_s}{\partial s}\theta_{21} - \frac{K}{U_s}\frac{\partial U_s}{\partial s}\{\theta_{11}(H+1) + \theta_{22}\} - 2K\frac{\partial \alpha}{\partial s}\theta_{21} \quad (3.13)$$

$$= C_{f_2}/2$$

where $k = \tan \alpha$.

Equations (3.12) and (3.13) contain several unknowns and before turbulent boundary layer predictions can be made further relationships are required between the streamwise and cross flow momentum thicknesses, the streamwise shape factor H and the streamwise skin friction coefficient C_f.

Entrainment Equations

The fact that the streamwise velocity profiles are similar to two dimensional velocity profiles led Cumpsty and Head to assume that the rate of entrainment along a streamline in the infinite swept wing case could be determined using relationships developed for two-dimensional flow. This is a credible assumption since the entrainment process is a function of the velocity defect in the outer part of the boundary layer, a region where the streamwise and two dimensional profiles are expected to agree most closely. Cumpsty and Heads entrainment equation takes the form

$$\frac{\partial(\delta-\delta_1^*)}{\partial s} + K\frac{\partial \delta_2^*}{\partial s} = F(H_1) + (\delta-\delta_1^*)\left(K\frac{\partial \alpha}{\partial s} - \frac{1}{U_s}\frac{\partial U_s}{\partial s}\right) \quad (3.14)$$

where $H_1 = (\delta-\delta_1^*)/\theta_{11}$.

The function $F(H_1)$ is taken in the form presented by Head [11].

$$H_1 = F(H_1) \quad (3.15)$$

Likewise the expression relating H_1 to the more usual shape factor H is also given by Head.

$$H_1 = G(H) \tag{3.16}$$

The functions F and G in Eqns 3.15 and 3.16 can be analytically defined as follows:

$$F(H_1) = \exp\,[-3.512 - 0.617\ \ln\,(H_1-3)]. \tag{3.17}$$

$$G(H) = 3.3 + \exp\,[0.4667 - 2.722\ \ln\,(H-0.6798) \tag{3.18}$$

for $H \leq 1.6$ or

$$G(H) = 3.3 + \exp[0.4383 - 3.064\ \ln\,(H-0.6798) \tag{3.19}$$

for $H > 1.6$.

Streamwise Velocity Profiles

Cumpsty and Head demonstrated that the streamwise turbulent boundary layer velocity profiles could be represented quite accurately by the two dimensional velocity profile family derived by Thompson 12. The law of the wall - law of the wake velocity profile family of Coles 13 gives results which are in good agreement with Thompsons profiles and could easily be used as an alternate approach.

Cross Flow Profiles

The cross flow profiles have been specified by the simple relationship between streamwise and cross flow velocities suggested by Mager 14,

$$v/u = (1 - \zeta/\delta)^2 \tan\beta \tag{3.20}$$

where β is the angle between the surface streamline (resulting skin friction direction) and the projection of the external streamline on the surface, ζ is the direction normal to the surface, and u and v are the streamwise and cross flow velocities.

Cross Flow Thicknesses

The cross flow thicknesses have been defined using a power law velocity profile instead of one of the more complicated two parameter profile relationships, in the streamwise direction. This approach greatly simplified the definition of the cross flow thicknesses without any great loss in accuracy. The use of the power law relationship

$$u/U = (\zeta/\delta)^{(H-1)/2} \tag{3.21}$$

in Equation (3.20) gives the cross flow thicknesses as defined by:

$$\delta_2^* = \theta_{11} D(H) \tan\beta \quad ; \quad D(H) = -(H + H_1)\left[\frac{2}{H+1} - \frac{4}{H+3} + \frac{2}{H+5}\right]$$

$$\theta_{12} = \theta_{11} J(H) \tan\beta \quad ; \quad J(H) = -(H + H_1)\left[\frac{1}{H} - \frac{4}{H+1} + \frac{1}{H+2} + \frac{4}{H+3} - \frac{2}{H+5}\right]$$

$$\theta_{21} = \theta_{11} E(H) \tan\beta \quad ; \quad E(H) = -(H + H_1)\left[\frac{1}{H} - \frac{2}{H+1} + \frac{1}{H+2}\right] \tag{3.22}$$

$$\theta_{22} = \theta_{11} C(H) \tan\beta \quad ; \quad C(H) = -(H + H_1)\left[\frac{1}{H} - \frac{4}{H+1} + \frac{6}{H+2} - \frac{4}{H+3} + \frac{1}{H+4}\right]$$

Skin Friction Coefficient

The streamwise skin friction coefficient is determined using Thompson's two parameters skin friction law although here again Cole's skin friction law could also have been used. The relationship is of the form

$$C_{f_1} = f(H, R_\theta) \quad \text{and is given as} \quad C_f = \exp(AH + B) \tag{3.23}$$

where

$$A = .01952 - .3868Z + .02834Z^2 - .0007Z^3$$

$$B = .19151 - .8349Z + .06259Z^2 - .001953Z^3$$

$$Z = \ln R_{\theta_{11}}$$

The cross flow skin friction coefficient C_{f_2} is then determined from C_{f_1} as $C_{f_2} = C_{f_1} \tan\beta$ and the resultant skin friction coefficient C_f as $C_f = C_{f_1}/\cos\beta$.

Calculation Procedure

With initial values of θ_{11} and H known either from the laminar boundary layer calculation or the stagnation line initial conditions Equations 3.12, 3.13 and 3.14 are integrated using standard integration procedures. The parameters θ_{11}, H and β in conjunction with the skin friction coefficient, and the cross flow thicknesses are determined along streamlines as functions of the known pressure distribution.

The streamwise free stream velocity U_s and angle α are determined as shown in the sketch, also shown is the angle β, the angle between the projection of the external streamline on the surface, and the resultant skin friction direction.

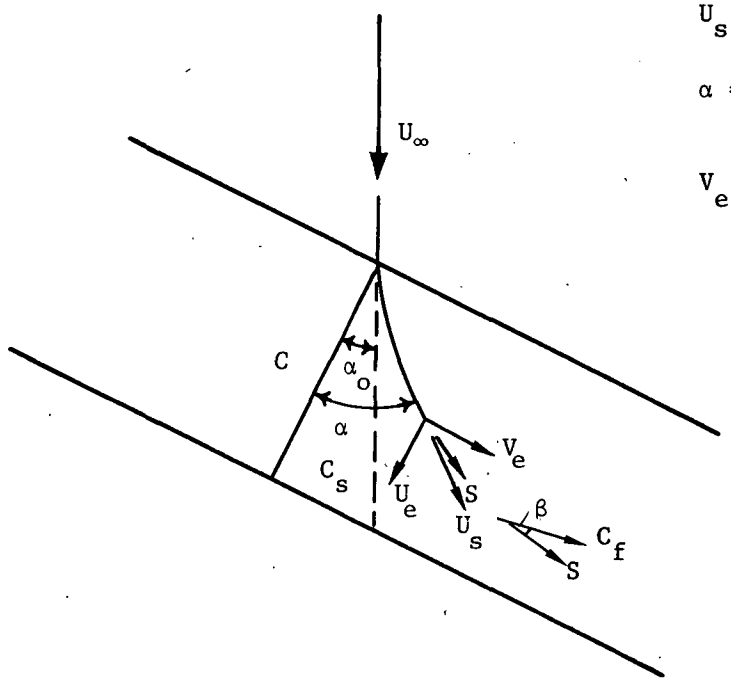

$$U_s = (U_e^2 + V_e^2)^{1/2}$$

$$\alpha = \sin^{-1}\left(\frac{\sin\alpha_o}{U_s/U_\infty}\right)$$

$$V_e = U_\infty \sin\alpha_o$$

The sum of the two angles α and β is continuously monitored during the calculation. If this sum reaches 90^o the flow is completely spanwise and by definition turbulent separation has occurred. The calculation is stopped at this point.

Boundary Layer Transition and Laminar Separation

Boundary layer transition is a very complex phenomenon and to date no reliable theoretical method has been developed for its prediction. Reynolds number is a controlling parameter, but it has been shown that the Reynolds number at transition can be increased a considerable amount by careful elimination of disturbances. At very low Reynolds numbers, laminar boundary layers are stable to small disturbances, however, at higher Reynolds numbers the boundary layer is unstable, and small disturbances can be amplified.

Amplification of these disturbances cause the flow to become turbulent. The point at which flow break down occurs depends on the strength and dominant frequency of the initial disturbance. Disturbances may be due to freestream turbulence, surface roughness, noise or vibration of the surface. As there is no detailed analysis of the transition process, transition prediction is accomplished by means of empirical correlations. Granville 15 has developed a procedure based on the determination of the neutral stablility point and the transition point. The neutral stability point is defined as that point downstream of which small disturbances are amplified within the boundary layer. It is this amplification of small disturbances that ultimately leads to transition. The neutral stability point is reached when the Reynolds number based on the local momentum thickness and the local flow properties attains some critical value, $R_{\theta_{ins}}$. Schlichting and Ulrich (Ref. 16) have shown that $R_{\theta_{ins}}$ can be correlated with the local pressure gradient parameter $K = \theta^2/\nu(dU/ds)$. Correlations by Smith 17 and others have been reduced to analytical form as follows:

Instability Curves

$$K = -0.4709 + 0.11066 \ln R_\theta - 0.0058591 \ln^2 R_\theta \qquad (3.24)$$

for $0 < R_{\theta_{ins}} \leq 650$

and

$$K = 0.69412 - 0.23992 \ln R_\theta + 0.0205 \ln^2 R_\theta \qquad (3.25)$$

for $650 < R_{\theta_{ins}} \leq 10{,}000.$

If for a given R_θ the pressure gradient parameter K as calculated by Eqn. 3.24 or 3.25 is greater than that determined by the boundary layer development the flow has passed from a stable to an unstable region. Once the flow passes into the unstable region, the transition process begins, and Granville has been able to show that a correlation similar to the instability process can be used to determine the transition point.

Granville formed an average pressure gradient parameter $\bar{K}$ defined as

$$\bar{K} = \frac{\int_{s_{ins}}^{s_{trans}} K \, ds}{s_{trans} - s_{ins}} \qquad (3.26)$$

which correlated reasonably well with the momentum thickness Reynolds number at transition $R_{\theta_{trans}}$. This correlation is presented in analytical form as follows:

Transition Curves

$$\bar{K} = -0.0925 + 7.0 \times 10^{-5} R_\theta \quad \text{for } 0 < R_{\theta\,trans} \leq 750 , \tag{3.27}$$

$$\bar{K} = -0.12571 + 1.14286 \times 10^{-4} R_\theta \quad \text{for } 750 < R_{\theta trans} \leq 1100 , \tag{3.28}$$

$$\text{and } \bar{K} = 1.59381 - 0.45543 \ln R_\theta + 0.032534 \ln^2 R_\theta \quad \text{for } 1100 < R_{\theta trans} \leq 3000. \tag{3.29}$$

When the $\bar{K}$ calculated by one of the above expressions for a given R_θ is greater than the value determined from the boundary layer development, transition is predicted.

With transition predicted, initial values of the momentum thickness θ and the shape factor H are required to start the turbulent boundary layer calculation. Because the boundary layer growth is continuous the momentum thickness at transition is used as the initial turbulent momentum thickness. Since the shape factor varies from values greater than 2.0 to less than 1.5 through the transition region an empirical expression is used to determine the initial turbulent shape factor. The empirical relation between H and $R_{\theta_{trans}}$ was determined from data obtained by Coles [18]:

$$H_t = \frac{1.4754}{\text{Log}_{10} R_{\theta trans}} + 0.9698 \tag{3.30}$$

In many cases the pressure gradient is of sufficient strength to separate the laminar boundary layer prior to transition. Except in extreme cases the boundary layer will then reattach, usually as a turbulent boundary layer. Only recently have researchers been able to analyze this phenomenon (Ref. 19) and as yet the procedure is extremely complicated and cumbersome, consequently empirical relationships are still required. From the measurements of Gaster (Ref. 20), and others a correlation is formed which is capable of predicting both the occurrence of separation and later the reattachment as a turbulent boundary layer or the catostrophic separation.

The correlation is of the form:

$$K = 0.027 - 0.0007575\ R_\theta - 0.000001157\ R_\theta^2 \qquad (3.31)$$

for $R_\theta > 125$

and

$$K = -0.09$$

for $R_\theta < 125$. (3.32)

If K becomes less than -0.09 separation occurs, and if R_θ is less than 125 the boundary layer is not able to re-attach. However, if R_θ is greater than 125 the value of K determined by the boundary layer development must be less than that calculated by Eqn. 3.31 before separation without reattachment is predicted. If reattachment is predicted, the turbulent boundary layer calculation is initiated using the momentum thickness calculated at the separation point.

Finite Difference Boundary Layer Method

On elements of a high lift configuration where the flow field is particularly complex, such as in the region where the wing wake mixes or interacts with the flap upper surface, integral boundary layer methods are not capable of completely analyzing the flow. A more satisfactory method can be developed using finite difference methods. Such a method is described in the following paragraphs.

Governing Equations

The governing equations of mean motion for three-dimensional incompressible flow in a general system of curvilinear orthogonal coordinates are:

$$\alpha : \frac{u}{h_1}\frac{\partial u}{\partial \alpha} + v\frac{\partial u}{\partial \beta} + \frac{w}{h_3}\frac{\partial u}{\partial \gamma} + \frac{uv}{h_1}\frac{\partial h_1}{\partial \beta} + \frac{uw}{h_1 h_3}\frac{\partial h_1}{\partial \gamma} - \frac{w^2}{h_1 h_3}\frac{\partial h_3}{\partial \alpha}$$

$$= -\frac{1}{\rho h_1}\frac{\partial P}{\partial \alpha} + \frac{1}{\rho}(\nabla\cdot\tau)_\alpha \tag{3.33}$$

$$\beta : \frac{u^2}{h_1}\frac{\partial h_1}{\partial \beta} + \frac{w^2}{h_3}\frac{\partial h_3}{\partial \beta} = \frac{1}{\rho}\frac{\partial P}{\partial \beta} \tag{3.34}$$

$$\gamma : \frac{u}{h_1}\frac{\partial w}{\partial \alpha} + v\frac{\partial w}{\partial \beta} + \frac{w}{h_3}\frac{\partial w}{\partial \gamma} + \frac{uw}{h_1 h_3}\frac{\partial h_3}{\partial \alpha} + \frac{vw}{h_3}\frac{\partial h_3}{\partial \beta} - \frac{u^2}{h_1 h_3}\frac{\partial h_1}{\partial \gamma}$$

$$= -\frac{1}{\rho h_3}\frac{\partial P}{\partial \gamma} + \frac{1}{\rho}(\nabla\cdot\tau)_\gamma \tag{3.35}$$

Continuity Equation

$$\frac{\partial}{\partial \alpha}(h_3 \rho u) + \frac{\partial}{\partial \beta}(h_1 h_3 \rho v) + \frac{\partial}{\partial \gamma}(h_1 \rho w) = 0 \ . \tag{3.36}$$

The shear stress terms in Eqs. (3.33) and (3.35) are:

$$\frac{1}{\rho}(\nabla\cdot\tau)_{\alpha} = \frac{1}{\rho h_1 h_3}\left[\frac{\partial}{\partial\beta}\{h_1^2 h_3 \mu \frac{\partial}{\partial\beta}\left(\frac{u}{h_1}\right)\}\right] + \frac{\mu}{\rho}\frac{\partial h_1}{\partial\beta}\frac{\partial}{\partial\beta}\left(\frac{u}{h_1}\right) \tag{3.37}$$

$$\frac{1}{\rho}(\nabla\cdot\tau)_{\gamma} = \frac{1}{\rho h_1 h_3}\left[\frac{\partial}{\partial\beta}\left(h_1 h_3^2 \mu \frac{\partial}{\partial\beta}\left(\frac{w}{h_3}\right)\right)\right] + \nu\frac{\partial h_3}{\partial\beta}\frac{\partial}{\partial\beta}\left(\frac{w}{h_3}\right) - \frac{2\nu}{h_1}\frac{h_1}{\partial\gamma}\frac{1}{h_1}\frac{\partial u}{\partial\alpha}$$

$$- 2\nu\frac{1}{h_1^2 h_3}\frac{\partial h_1}{\partial\gamma} v \frac{\partial h_1}{\partial\beta} - 2\nu\frac{1}{h_1^2 h_3^2}\frac{\partial h_1}{\partial\gamma} w \frac{\partial h_1}{\partial\gamma} \quad . \tag{3.38}$$

If a practical three-dimensional high-lift system is considered where it can be assumed that curvature effects in the spanwise direction are negligible compared to the normal chord direction, a surface coordinate system can be employed, where

$$x = \alpha \qquad h_1 = 1 + ky \qquad k = f(x)$$

$$y = \beta \qquad h_2 = 1$$

$$z = \gamma \qquad h_3 = 1$$

where k is the longitudinal surface curvature.

The equations can then be written in the following form:

$$x: \quad \frac{u}{1+ky}\frac{\partial u}{\partial x} + v\frac{\partial u}{\partial y} + w\frac{\partial u}{\partial z} + \frac{uvk}{1+ky} = -\frac{1}{\rho(1+ky)}\frac{\partial P}{\partial x} + \nu\frac{\partial}{\partial y}\left(\frac{\partial u}{\partial y}\right) + \nu\frac{k}{1+ky}\frac{\partial u}{\partial y}$$

$$- u\nu\left(\frac{k}{1+ky}\right)^2 \tag{3.39}$$

$$y: \quad \frac{u^2 k}{1+ky} = \frac{1}{\rho}\frac{\partial P}{\partial y} \tag{3.40}$$

$$z: \quad \frac{u}{1+ky}\frac{\partial w}{\partial x} + v\frac{\partial w}{\partial y} + w\frac{\partial w}{\partial z} = -\frac{1}{\rho}\frac{\partial P}{\partial z} + \nu\frac{\partial}{\partial y}\left(\frac{\partial w}{\partial y}\right) + \frac{\nu k}{1+ky}\frac{\partial w}{\partial y} \tag{3.41}$$

Continuity

$$\frac{\partial}{\partial x}(\rho u) + \frac{\partial}{\partial y}[(1+ky)\rho v] + \frac{\partial}{\partial z}[(1+ky)\rho w] = 0 \tag{3.42}$$

Equations (3.39) to (3.42) represent the laminar boundary layer equations in incompressible flow. The corresponding equations in turbulent flow are:

$$x: \frac{u}{1+ky}\frac{\partial u}{\partial x} + v\frac{\partial u}{\partial y} + w\frac{\partial u}{\partial z} + \frac{uvk}{1+ky} = -\frac{1}{\rho(1+ky)}\frac{\partial P}{\partial x}$$

$$+ \frac{\partial}{\partial y}\left[\nu\frac{\partial u}{\partial y} - \overline{u'v'}\right] + \frac{2k}{1+ky}\left[\nu\frac{\partial u}{\partial y} - \overline{u'v'}\right]$$

$$- \frac{k}{1+ky}\nu\frac{\partial u}{\partial y} - \nu u\left(\frac{k}{1+ky}\right)^2 \tag{3.43}$$

$$y: \quad \frac{u^2 k}{1+ky} = \frac{1}{\rho}\frac{\partial P}{\partial y} \tag{3.44}$$

$$z: \frac{u}{1+ky}\frac{\partial w}{\partial x} + v\frac{\partial w}{\partial y} + w\frac{\partial w}{\partial z} = -\frac{1}{\rho}\frac{\partial P}{\partial z} + \frac{\partial}{\partial y}\left[\nu\frac{\partial w}{\partial y} - \overline{v'w'}\right]$$

$$+ \frac{k}{1+ky}\left[\nu\frac{\partial w}{\partial y} - \overline{v'w'}\right] \tag{3.45}$$

The continuity equation is unchanged. The terms $\overline{u'v'}$ and $\overline{v'w'}$ represent the Reynolds stresses in the normal chord and spanwise directions. The shear stress term $\overline{u'v'}$ is represented by the expression

$$-\overline{u'v'} = \nu_{t_x}(\partial u/\partial y - uk/1+ky) \tag{3.46}$$

where ν_{t_x} is the eddy viscosity, which in this case is determined using a two dimensional model. Then, if the shear stress vector is considered to be aligned with the rate of strain vector (Nash and Patel (21)), the eddy viscosity in the "z" direction may be determined from the expression

$$\overline{u'v'} \Big/ \left(\frac{\partial u}{\partial y} - \frac{uk}{1+ky}\right) = \overline{v'w'} \Big/ \frac{\partial w}{\partial y} \tag{3.47}$$

or the equivalent form

$$\nu_{t_x} = \nu_{t_z} \tag{3.48}$$

Eddy Viscosity Model

The eddy viscosity model used in the calculation procedure is a modification of one developed for two-dimensional turbulent boundary layers and wall jets over curved surfaces (Ref. 22). The basic two layer model consists of inner and outer regions. The inner region profile is calculated using the modified Van Driest relation

$$\nu_t(y) = \ell^2 \left[1 - \exp -\left(\frac{U_\tau y}{A\nu}\right)\right]^2 \left|\frac{\partial u}{\partial y}\right| \tag{3.49}$$

where

$$\ell = 0.435y$$

$$u_\tau = (\tau_w/\rho)^{1/2}$$

$$A = f\ (dP/dx,\ vw)$$

The outer region eddy viscosity profile is determined from the Eddy Reynolds number $(u_d\ \sigma/\nu_t)$ and the intermittency function $(\gamma(y))$ formulations described in Reference 22. These functions are combined to give:

$$\nu_t(y) = (u_d\sigma/C)\ \gamma(y) \tag{3.50}$$

where the velocity scale u_d and the length scale σ (standard deviation of the intermittency function γ) are known functions of the shape factor H and the displacement thickness δ^* for conventional boundary layers.

The extension of the eddy viscosity model to the mixed flow case associated with slotted flaps is based on observations made of the development of walls jets exhibiting both velocity maxima and minima in the profile (see sketch).

In the region below the velocity maxima (Region A) the conventional eddy viscosity model is used to describe the flow. The outer region of the profile (Region C) represents the remnant of the upstream boundary layer having a large value of the shape factor H. Measurements of the standard deviation of the intermittency σ indicate that an asymptotic value is approached at high values of H. Similar behavior is observed for the velocity defect U_d. By employing the asymptotic values of σ and U_d in the Eddy Reynolds number relation $u_d\sigma/\nu_t$, a third layer is established which when joined to the conventional two layer eddy viscosity profile provides a completed eddy viscosity model.

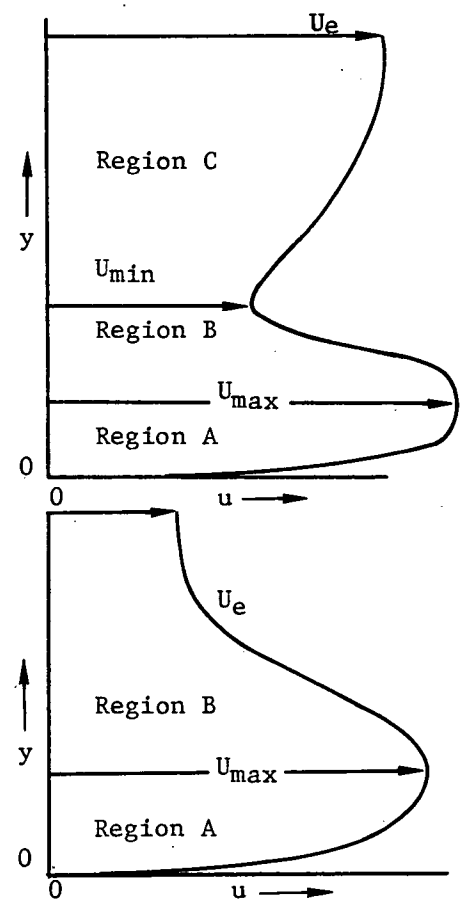

Wall jets exhibiting only a maximum in velocity have been studied by many researchers. Measurements of the standard deviation σ of the intermittency function γ for these flows allow predictions to be made of the eddy viscosity in the outer region of the profile (Region B of sketch). The velocity defect U_d in this case is simply $U_{max} - U_e$. Region A is again described using the conventional boundary layer model for the eddy viscosity.

The slotted airfoil (passive blowing) case results in velocity profiles which are very similar to those for tangential injection; profiles with velocity maxima in the case of the leading edge slotted slat, and profiles with velocity maxima and minima for slotted flaps. As a consequence it was assumed that the same eddy viscosity approach as developed for tangential injection could be applied to the slotted airfoil case. The initial velocity profile for the slotted case is shown in Figure 3.2. Two factors make the problem slightly different from the tangential injection case. These are:

(i) With slotted configurations, the persistence of the potential core, and

(ii) on the flap surface the possibility of considerable laminar flow at least to the suction peak.

Consequently the flow may consist of a laminar boundary layer, above which is a potential core. Above the potential core is the remnant of the cove and upper surface turbulent boundary layers of the wing or preceding flap segment. To account for the presence of the laminar boundary layer and the potential core, the eddy viscosity is set to zero in these regions. In the potential core region the remaining viscous terms are negligible in comparison with the inertia terms, resulting in a form of Bernoullis' equation. Three different eddy viscosity distributions are possible depending on the flow regime (Figure 3.3).

The inclusion of curvature terms is essential to the success of the calculation method as is the necessity of including the static pressure variation in the direction normal to the airfoil surface. In regions away from the wing trailing edge - flap leading edge Eq. (3.44) is adequate; however, if the aforementioned region is of interest, then a pressure field $P(x,y)$ in the two-dimensional and infinite swept wing case or $P(x,y,z)$ in the full three-dimensional case must be prescribed. The pressure field above the individual flap surfaces is determined directly from the known induced velocity field.

Once the eddy viscosity distribution, the surface curvature and the pressure field $P(x,y)$ are known, Eqns. 3.43, 3.44 and 3.45 can be solved in conjunction with the continuity equation. In the present calculation all spanwise gradients have been neglected. The resulting equations are solved using a modification of the Crank - Nicholson procedure (23) first described in Ref. 24.

The initial velocity profile is determined by combining known or assumed velocity distributions in the wing trailing edge - potential core region. The integral method (IBL) is used to calculate the boundary layer development to transition or to some point on the flap surface downstream of the wing trailing edge if transition takes place in the slot region. The calculated integral parameters at the slot exit are then used to determine the laminar or turbulent boundary layer velocity distribution and thickness. If the flow is laminar, the laminar boundary layer profile on the flap upper surface is represented by a Pohlhausen polynomial. If the flow is turbulent, Thompson's velocity profile family is used to calculate the velocity distribution.

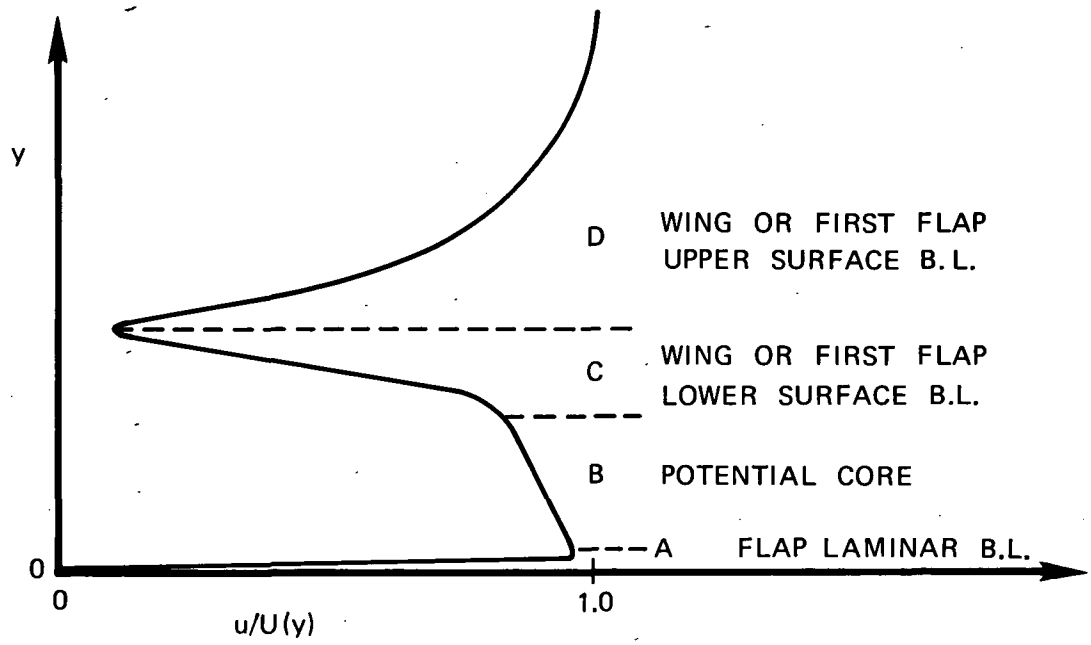

FIG. 3.2 INITIAL VELOCITY DISTRIBUTION FOR A SLOTTED AIRFOIL CONFIGURATION

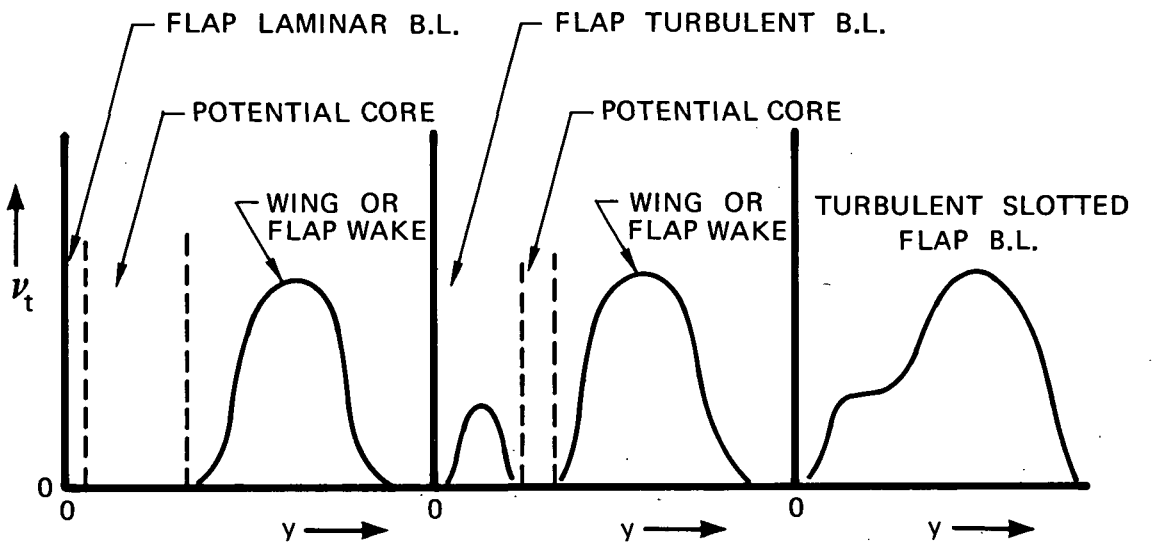

FIG. 3.3 POSSIBLE EDDY VISCOSITY PROFILES ON A SLOTTED FLAP

The potential core velocity distribution is determined from the calculated off-body pressures (P(x,y)). The wing lower surface boundary layer profile is represented by a power law profile, while the wing upper surface trailing edge velocity profile is determined using Thompson's velocity profile family (12) and the values of H, R_θ and C_f at the wing trailing edge.

Aerodynamic Forces

The aerodynamic lift coefficient for a given configuration can be determined in several ways. For closed trailing edge airfoils, the most accurate procedure involves summing the individual vortex sheet strengths.

$$\Gamma = \sum_{i=0}^{N} \gamma_i \tag{3.51}$$

from which

$$C_L = \frac{2\Gamma}{U_\infty C} \tag{3.52}$$

where

Γ = circulation about airfoil

γ_i = vortex strength of i^{th} singularity

U_∞ = freestream velocity

C = reference chord.

When the airfoil trailing edge remains open Eqn. 3.51 does not necessarily give the correct circulation even though the vortex distribution is a valid solution for the given boundary conditions. The pressure distribution determined from the vortex distribution is in very poor agreement with experiment (see Figure 3.4). Consequently it has been found that more satisfactory pressure distributions can be determined from the expression

$$C_{p_i} = 1 - u_i^2 - w_i^2 \tag{3.53}$$

The lift is then determined by integration of the pressure coefficients about the airfoil.

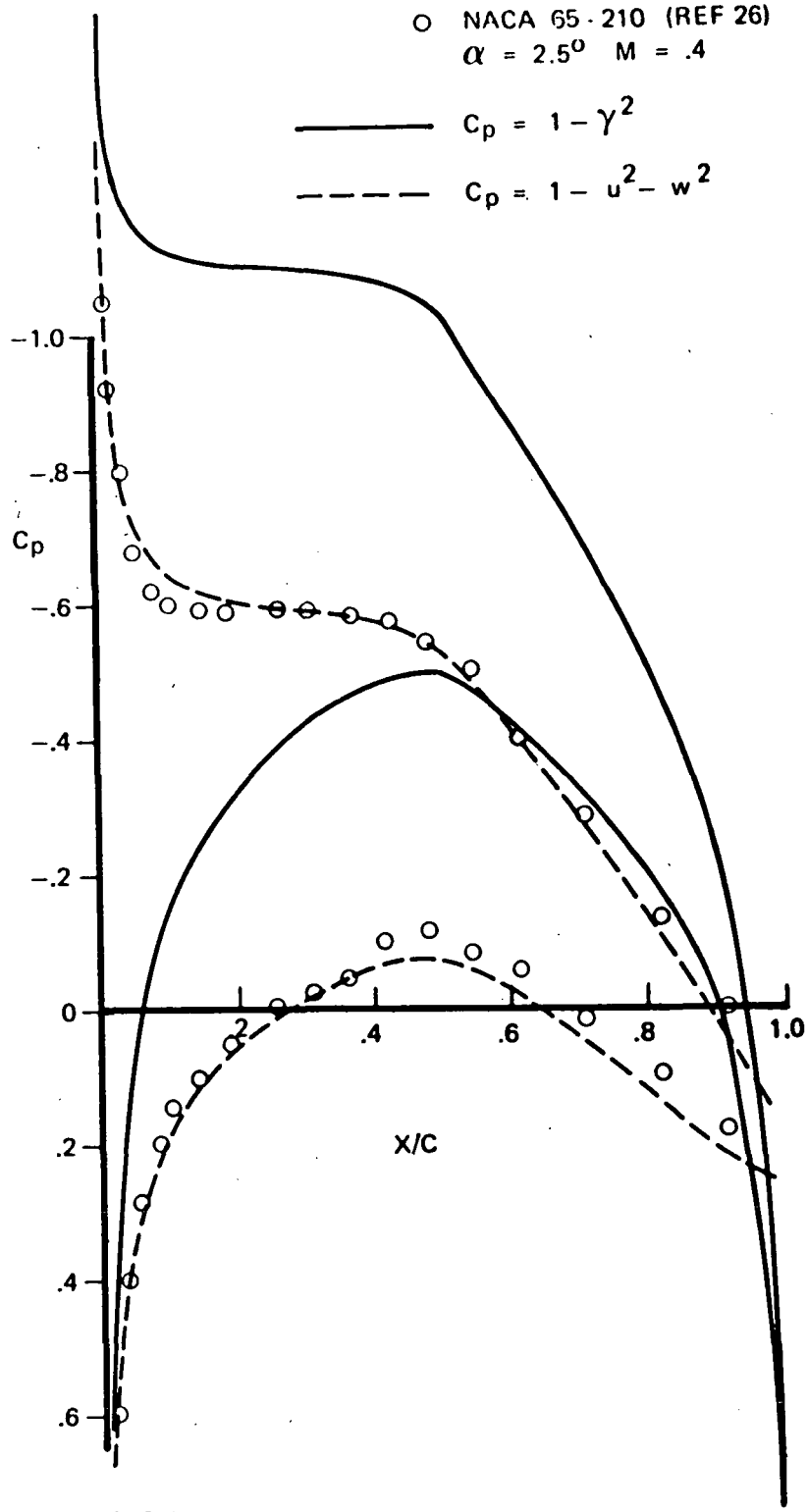

FIG. 3.4 COMPARISON OF METHODS FOR CALCULATING PRESSURE COEFFICIENTS

The flow model used to represent open trailing edge airfoils is being reviewed. It is possible that with the Kutta condition $\gamma_u = -\gamma_l$ a small amount of circulation inside the airfoil gives rise to non-zero tangential velocities inside the airfoil and consequently vorticity strength which is greater than if the flow inside the airfoil was stagnant.

Pitching moment characteristics are determined as follows: It is presumed that incremental resultant pressure forces act at the center of pressure of a small panel of a prescribed length. Consequently, the pressure force times the moment arm to some reference point gives the increment in pitching moment for that point. The sum of the incremental pitching moments for each calculated pressure gives the pitching moment for the system.

The profile drag is determined for a streamwise section of the infinite span wing by using the Squire and Young drag formula (25).

$$C_D = 2 \frac{\theta}{C}_{T.E.} (U_{T.E.}/U_\infty)^{\frac{H_{T.E.}+5}{2}} \qquad (3.54)$$

The streamwise momentum thickness θ_s, velocity U_s and shape factor H_s are used in Eqn. 3.54. The skin friction drag coefficient is determined by the summation of the local skin friction forces in the drag direction. Pressure drag is determined by taking the difference between profile drag and friction drag.

CALCULATION PROCEDURES

All of the calculation methods, potential flow and boundary layer, are incorporated into a single computer program. The calculation sequence is outlined below:

(i) The potential flow pressure field is computed for a multi-element infinite swept wing configuration (consisting of up to four elements, a leading edge slat, the main airfoil, and a double-slotted flap).

(ii) The boundary layer properties are then computed for each element of the configuration as a function of the potential flow pressure distribution. Included in these calculations are the locations of transition or laminar separation and turbulent separation, if present.

(iii) Source distributions are determined to represent the displacement effects of the boundary layer on each element and of the wing wake-flap boundary layer interaction.

(iv) A new potential flow solution is then computed taking into account the source distribution computed in step (iii) above.

Steps (ii) through (iv) are repeated until convergence (based on the pressure distribution and lift coefficient) is achieved, or until the case is abandoned for reasons such as large separation zones. Lift, drag and pitching moment coefficients are then calculated for the given configuration. The approach is illustrated in Figure 4.1.

The actual program overlay structure is given in Figure 4.2. The main supervisor program has been called VIP (for viscous/potential flow interaction). This program directs the overall flow of the calculation. The other programs include POTFLOW (potential flow), IBL (integral boundary layer method, INSPAN (infinite span finite difference method, and FELDPT (field point calculation for off-body pressures).

CALCULATIONS AND DISCUSSION OF RESULTS

The ultimate test of any analysis method is in how well does it predict actual aerodynamic performance. This can be determined in the case of potential flow methods by comparison with exact solutions; for boundary layer methods, the usual recourse however, is comparison with experiment. Evaluation of the overall viscous/potential flow interaction analysis can also be made only through comparison with experiment. The comparisons that follow represent a cross-section of the possible configurations that can be treated by the analysis method.

The potential flow method developed as part of the contract effort has been compared with several exact potential flow analyses. Of considerable interest is the comparison for the highly cambered Karman-Trefftz airfoil shown in Figure 5.1. Hess (27) has used this case to demonstrate the degree of agreement between his new method and other classical methods. It is therefore encouraging to note that our analysis is in almost total agreement with the exact case in comparison with other methods. A second comparison with an exact solution is for the two element slotted flap airfoil configuration of Williams (28). Here again agreement between the numerical approach and the exact solution is excellent (Figure 5.2).

Two calculations have been included to demonstrate some of the capability of the finite difference boundary layer method in two-dimensions (see Ref. 22). The effect of longitudinal surface curvature on the boundary layer development is shown in Figure 5.3. It will be seen that when curvature effects are ignored the calculation is in poor agreement with the data. The calculations shown in Figure 5.4 demonstrate that velocity profiles typical of those found on the upper surfaces of slotted or blown flaps can be predicted quite accurately.

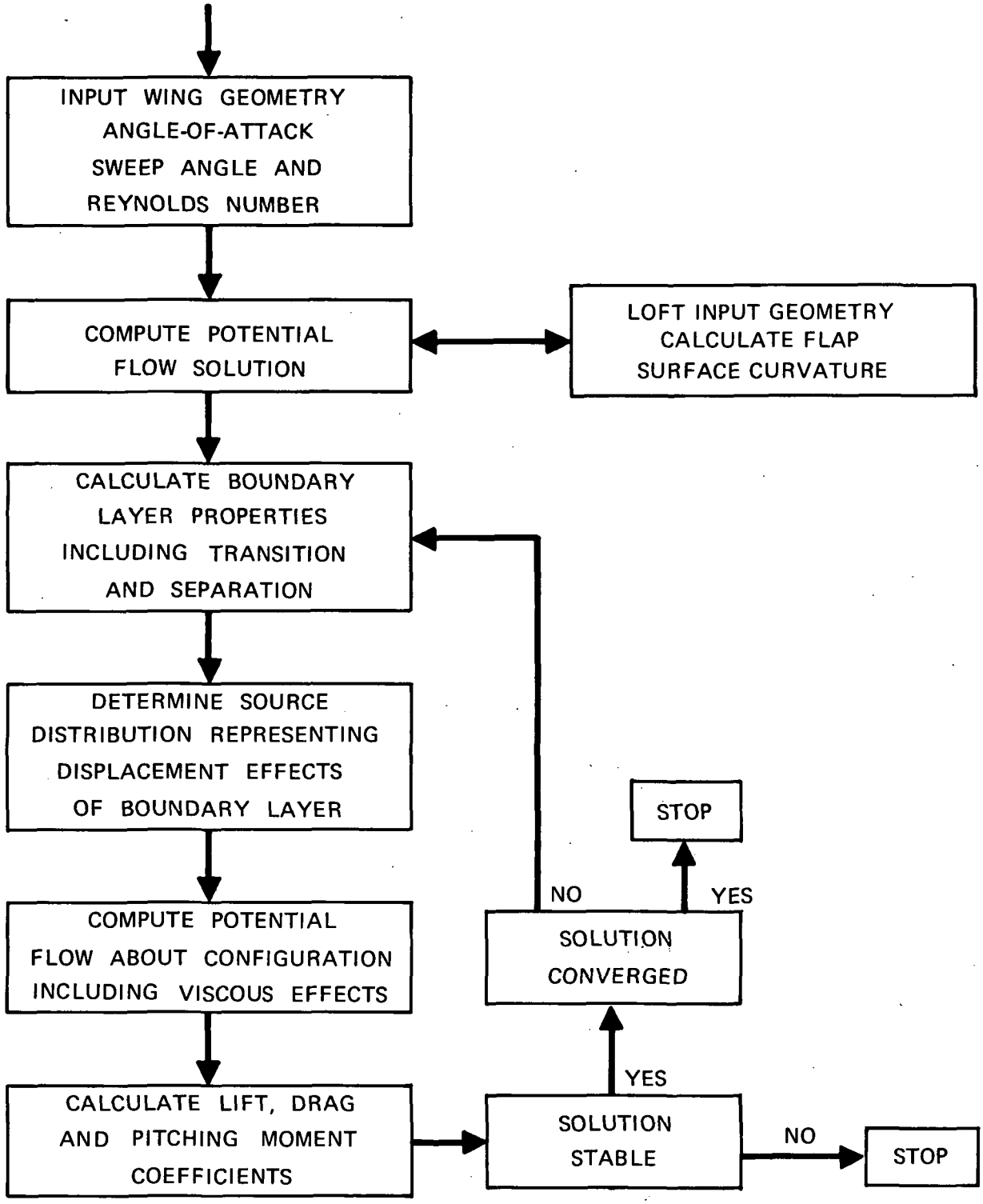

FIG. 4.1 COMPUTATION PROCEDURE FOR AERODYNAMIC FORCES

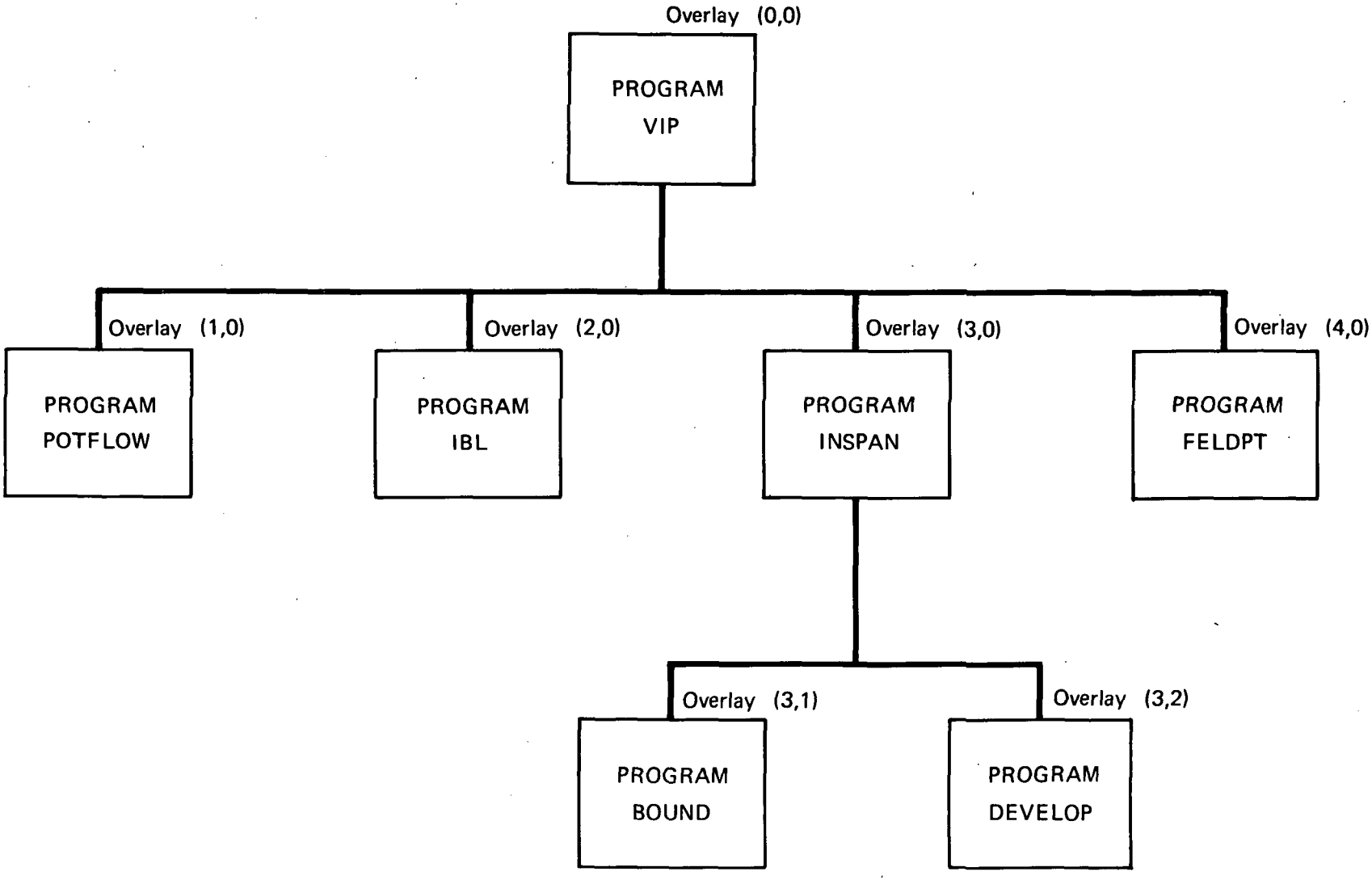

FIG. 4.2 VISCOUS/POTENTIAL FLOW PROGRAM OVERLAY STRUCTURE

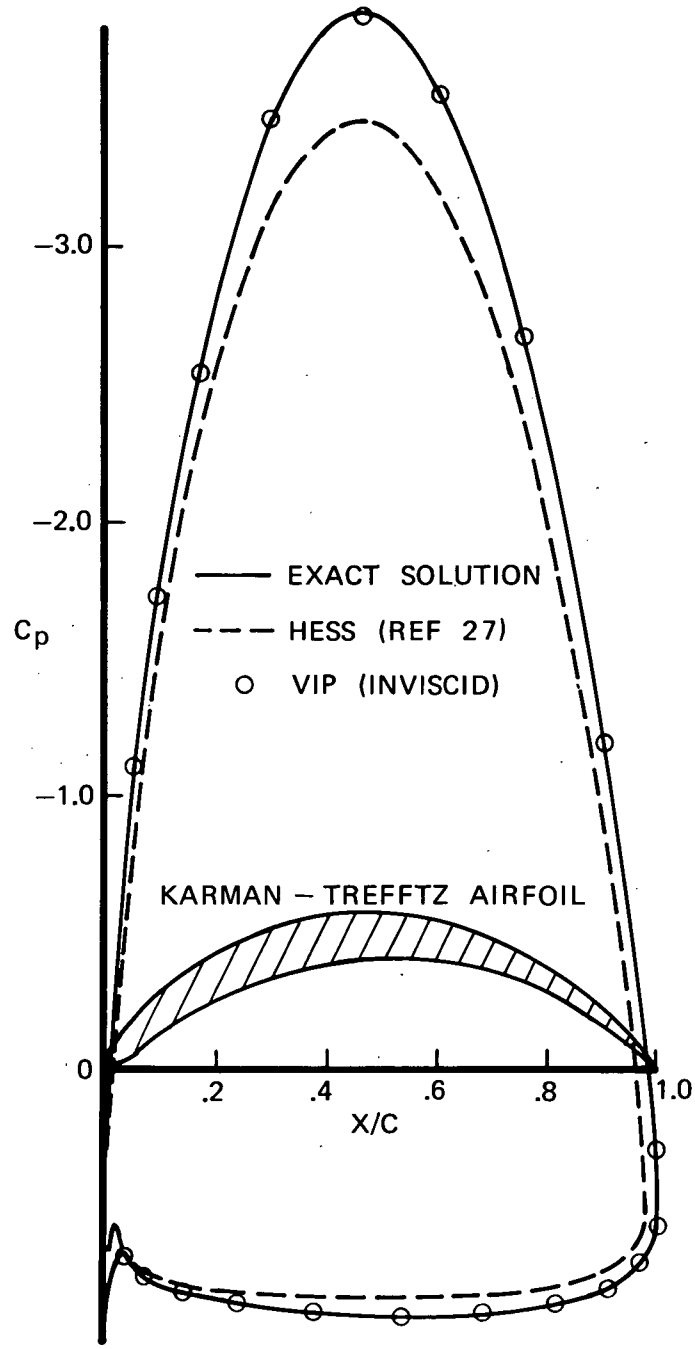

FIG. 5.1 COMPARISON BETWEEN NUMERICAL AND EXACT POTENTIAL FLOW SOLUTIONS

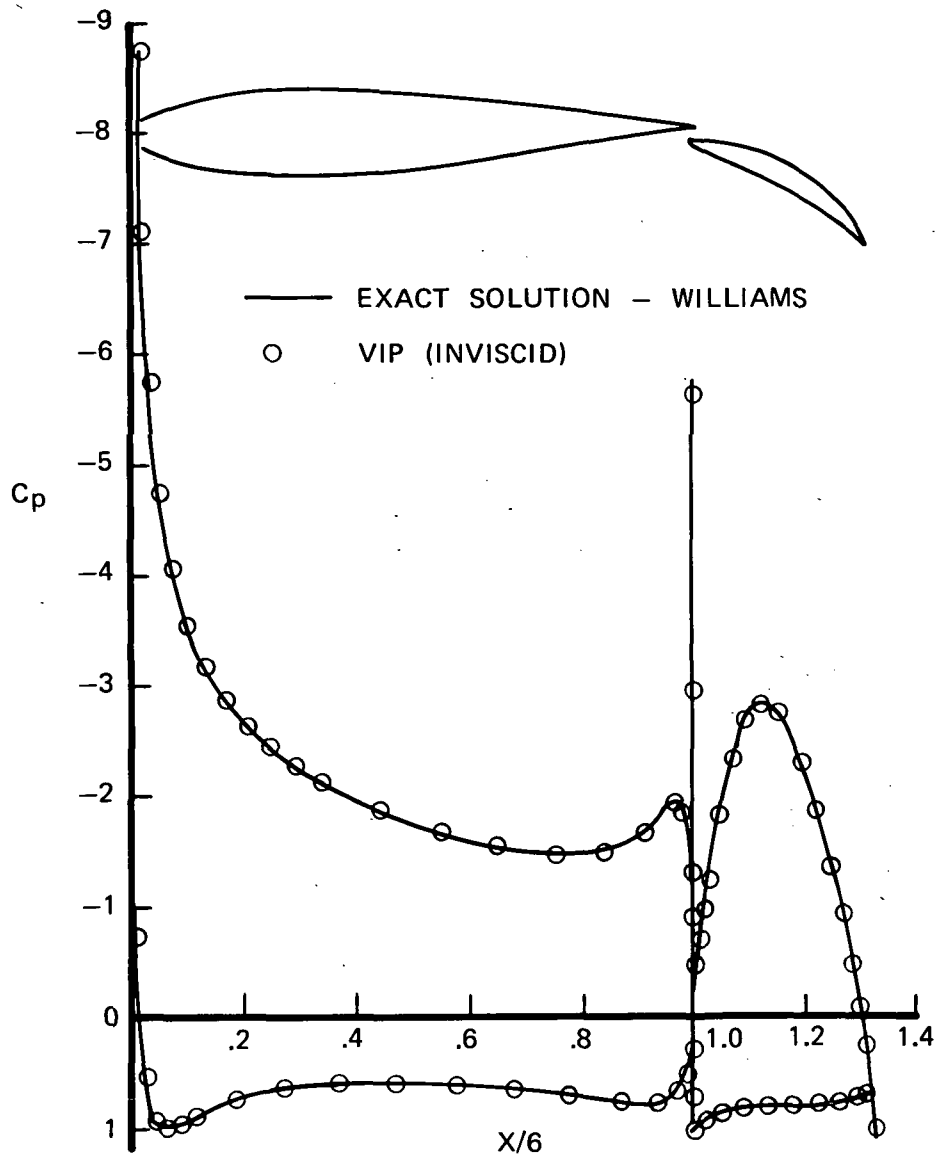

FIG. 5.2 COMPARISON BETWEEN NUMERICAL AND EXACT POTENTIAL FLOW SOLUTIONS

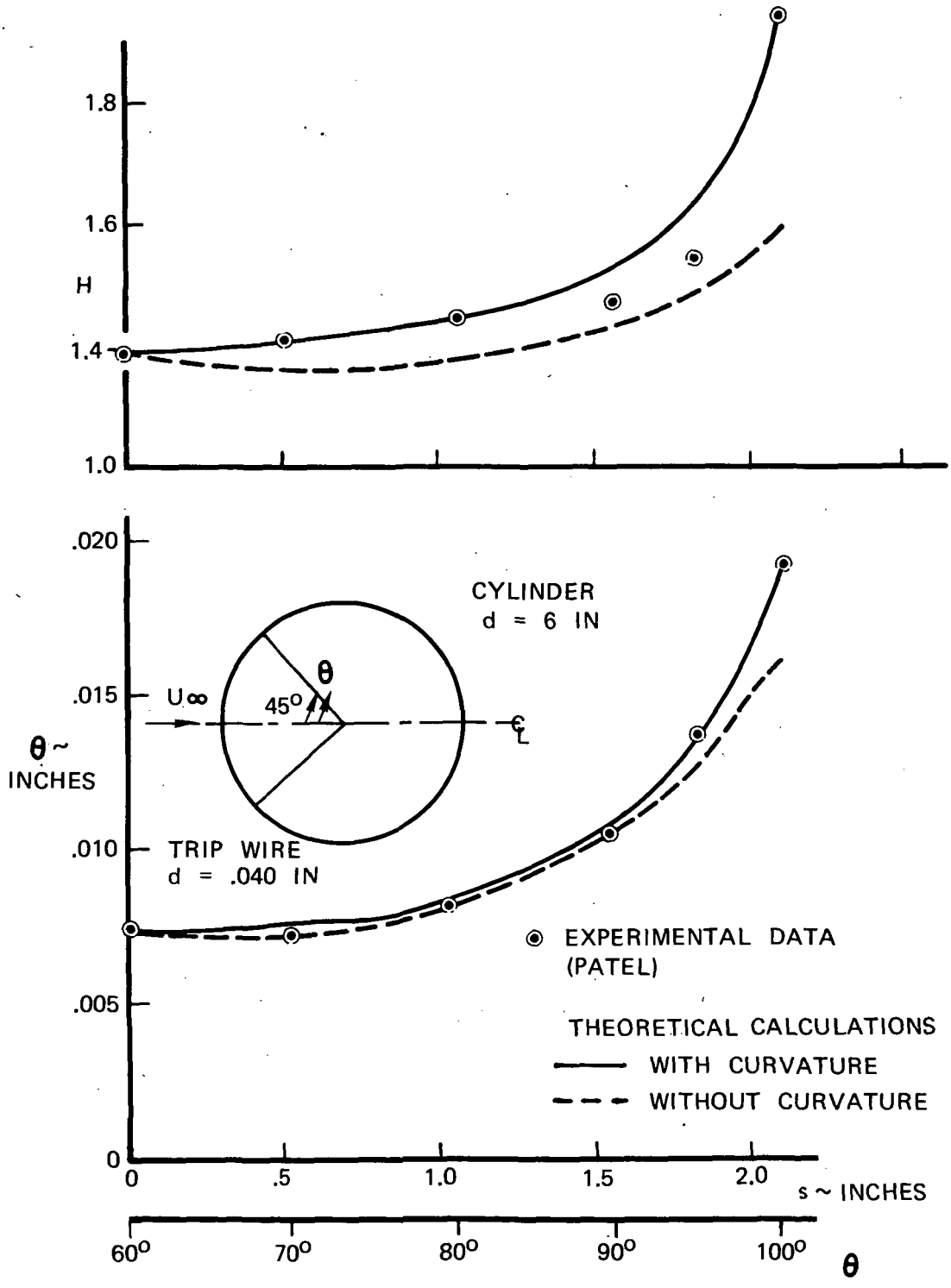

FIG. 5.3 COMPARISON OF CALCULATED AND MEASURED TURBULENT BOUNDARY LAYER

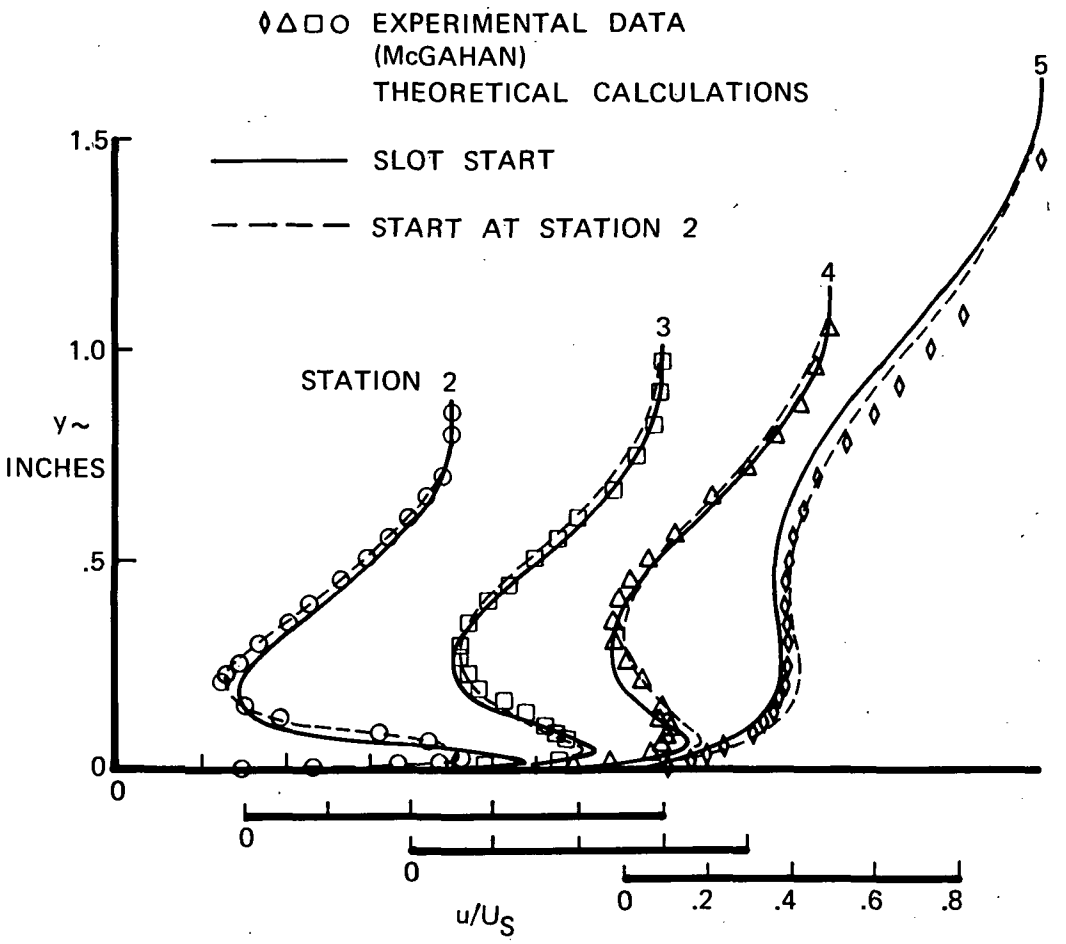

FIG. 5.4 COMPARISON OF CALCULATED AND MEASURED VELOCITY PROFILE DEVELOPMENTS DOWNSTREAM OF A BLOWING SLOT

Calculations were made for a series of angles-of-attack for the new NASA GA(w)-1 airfoil. Comparisons were made with the NASA measurements and with calculations made by Morgan (29) using the Lockheed program. The results are shown on Figures 5.5, 5.6 and 5.7. Both methods give excellent agreement with experiment in comparison with measured lift and pitching moment coefficients (Figure 5.5). At the higher angles-of-attack the source method appears to be in better agreement with experiment. In all cases however the Lockheed program is in slightly better agreement with experiments in the trailing edge region in the prediction of pressure coefficients. In the present program (VIP) the pressure coefficients are calculated on the original airfoil surface, and it is believed that if the pressures are determined at off-body points defined by the displacement thickness that improved agreement with experimental pressures will result. This procedure will be tried at a later date. Measured and calculated drag polars are shown in Figure 5.6. No allowance has been made for trip drag or separation effects in the calculations although these are present in the measurements. Calculated and measured pressure distributions are compared in Figure 5.7. Currently neither theoretical approach is capable of predicting the effects of separation present in the measurements. A further set of calculations were made for the NACA 23012 airfoil. Comparisons between theory and experiment for lift coefficient versus angle-of-attack (Figure 5.8) and lift versus drag (Figure 5.9) are in good agreement.

The multi-element prediction capability of the program is demonstrated in Figures 5.10 through 5.14. The first case considered is that of the NACA 23012 airfoil with a 25 percent chord slotted flap (Ref. 30). As shown in Figure 5.10 the present method is in better agreement with experiment than is the Lockheed program. It is believed that the use of a finite difference boundary layer method including the effects of curvature and normal pressure gradients results in an improved physical representation of the flow in the wing trailing edge-flap upper surface region. This in turn results in an improved prediction of the circulation about the complete configuration when viscous effects are included. Similar conclusions can be drawn from the results of Figure 5.11 for the NACA 23012 configuration having a leading edge slot and a slotted flap (Ref. 31).

The NACA 64A010 airfoil with leading edge slot and a double slotted flap (Ref. 32) is considered in Figure 5.12. Also shown for comparison are the results for the same configuration from the Lockheed program. The comparison is similar to that of Figure 5.11 in that the greatest difference between the two results is in the prediction of the pressure distribution for the main element. It is believed that the difference is a result of the way in which the two programs treat the mixing between the main element and the double slotted flaps.

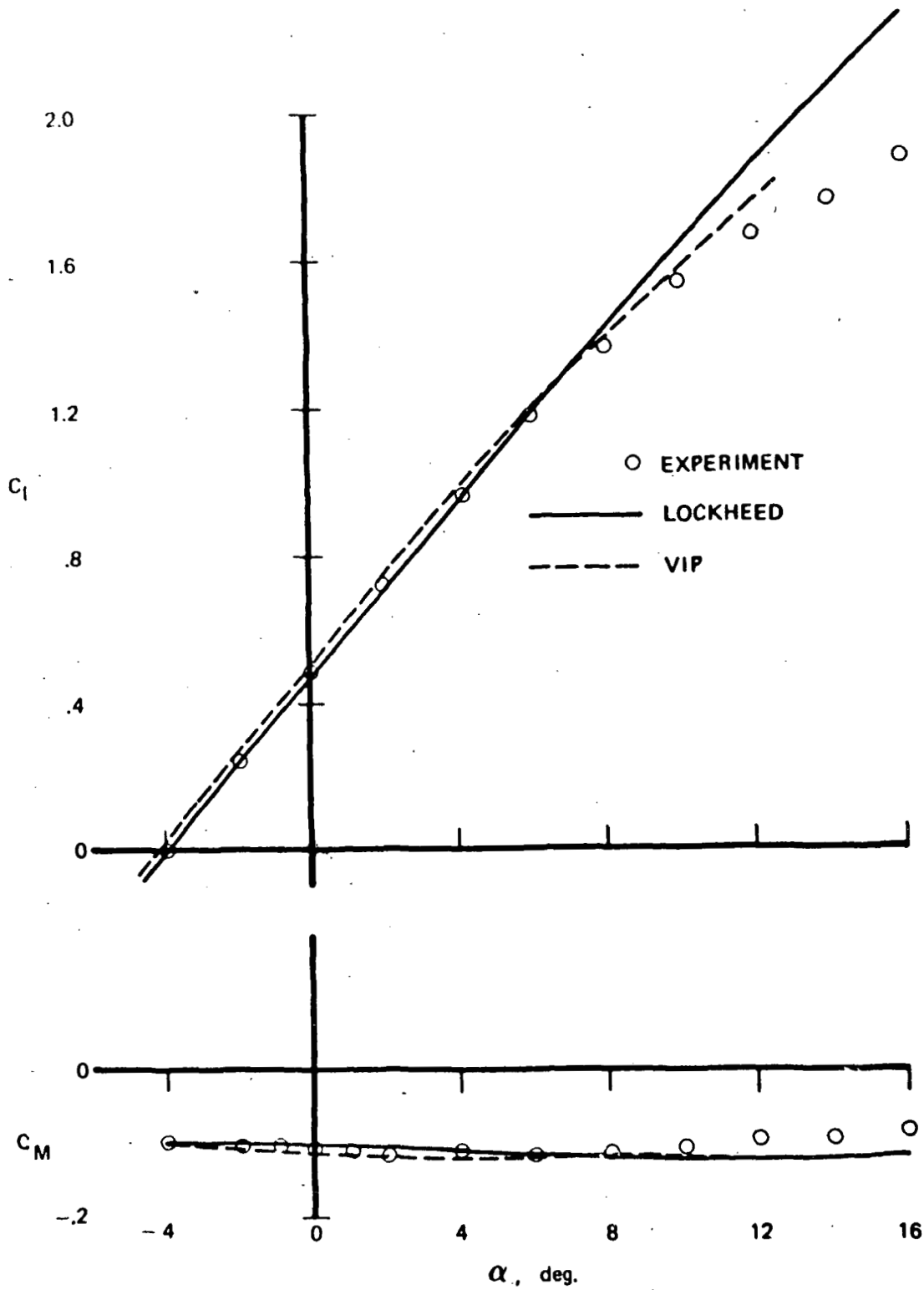

FIG. 5.5 LIFT AND MOMENT COEFFICIENTS FOR NASA GA (W) -1 AIRFOIL

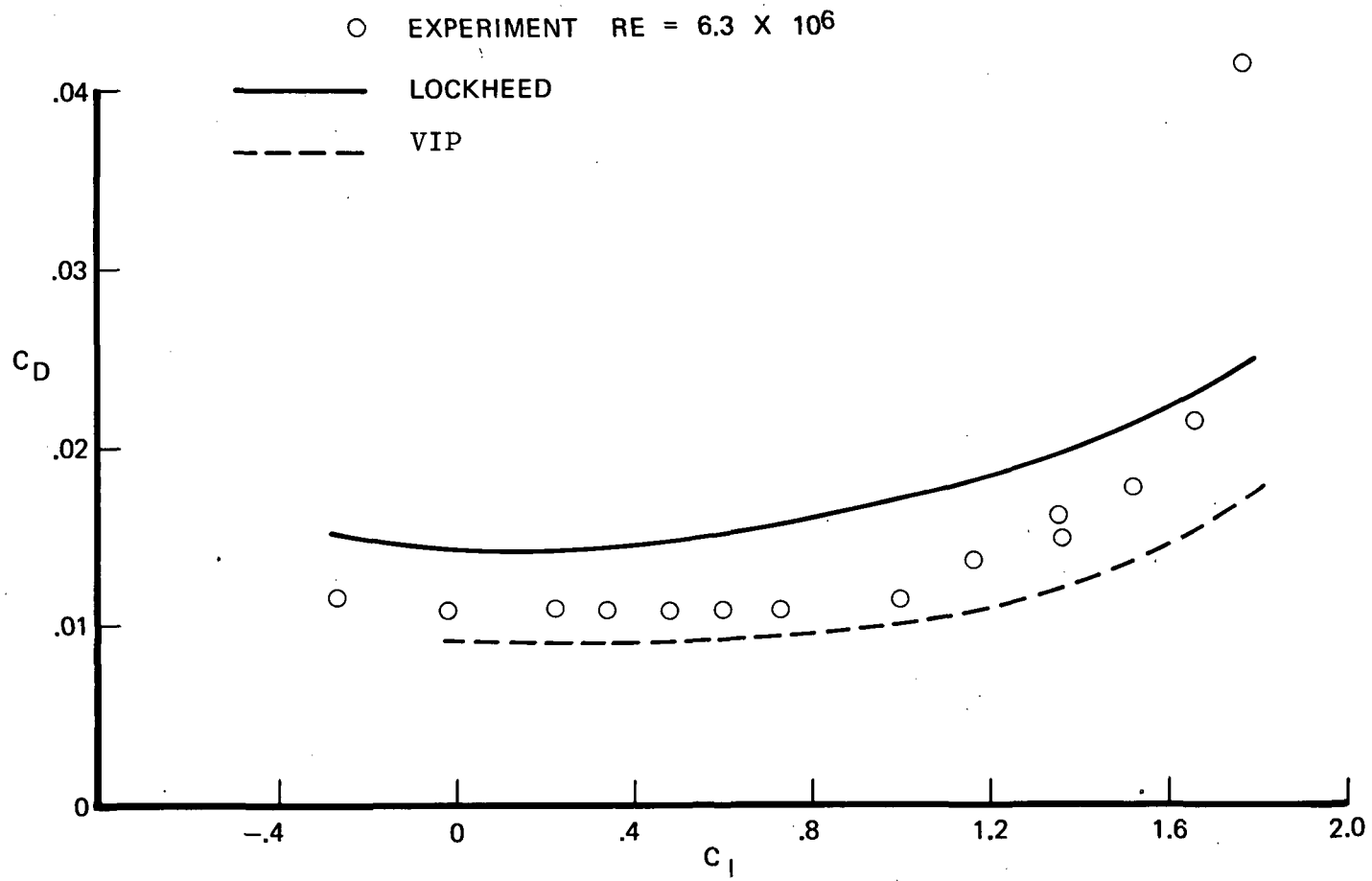

FIG. 5.6 DRAG POLAR NASA GA (W) –1 AIRFOIL

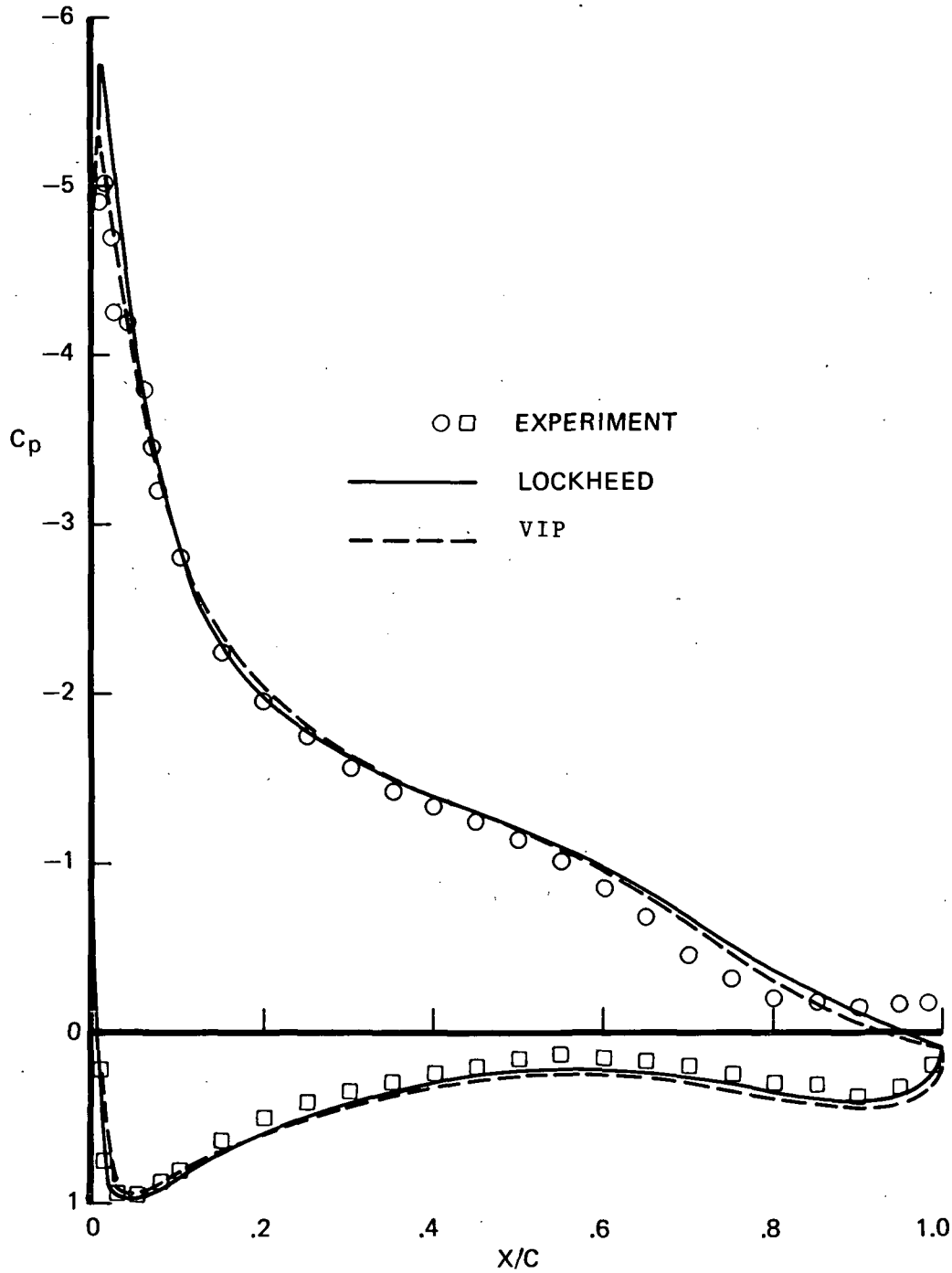

FIG. 5.7 PRESSURE DISTRIBUTION NASA GA (W) −1 AIRFOIL (12.04°)

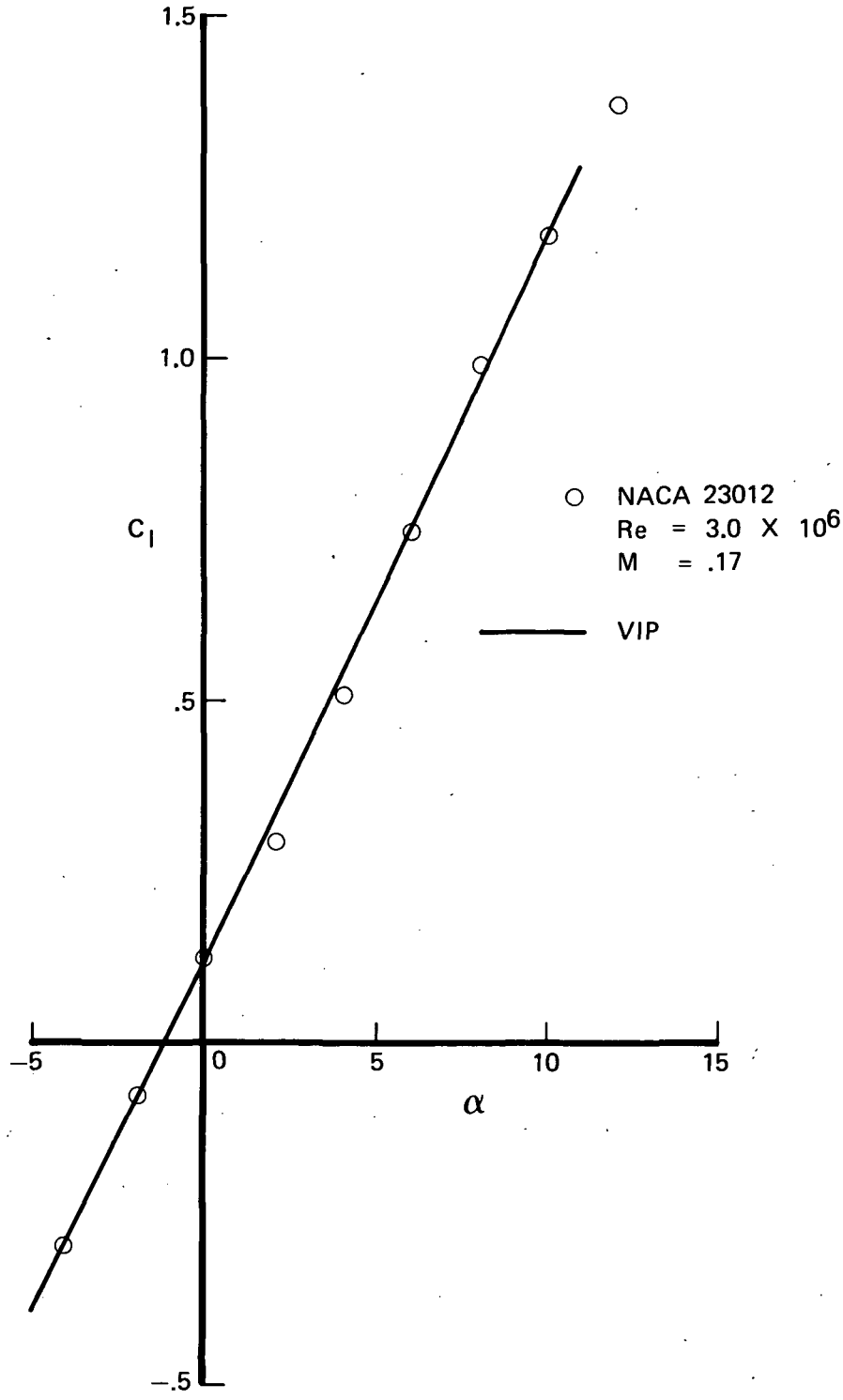

FIG. 5.8 LIFT COEFFICIENTS FOR NACA 23012 AIRFOIL

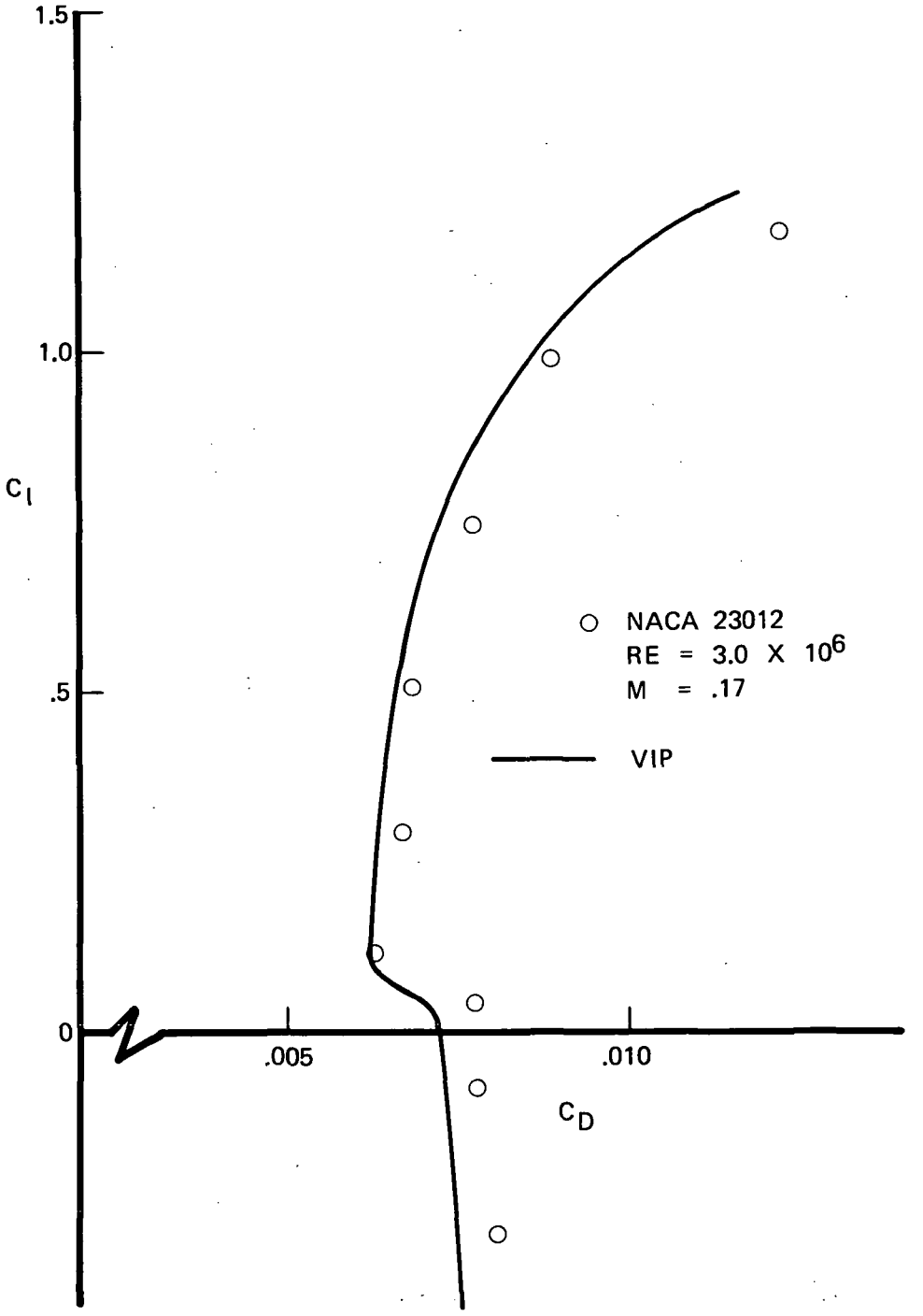

FIG. 5.9 DRAG POLAR FOR NACA 23012 AIRFOIL

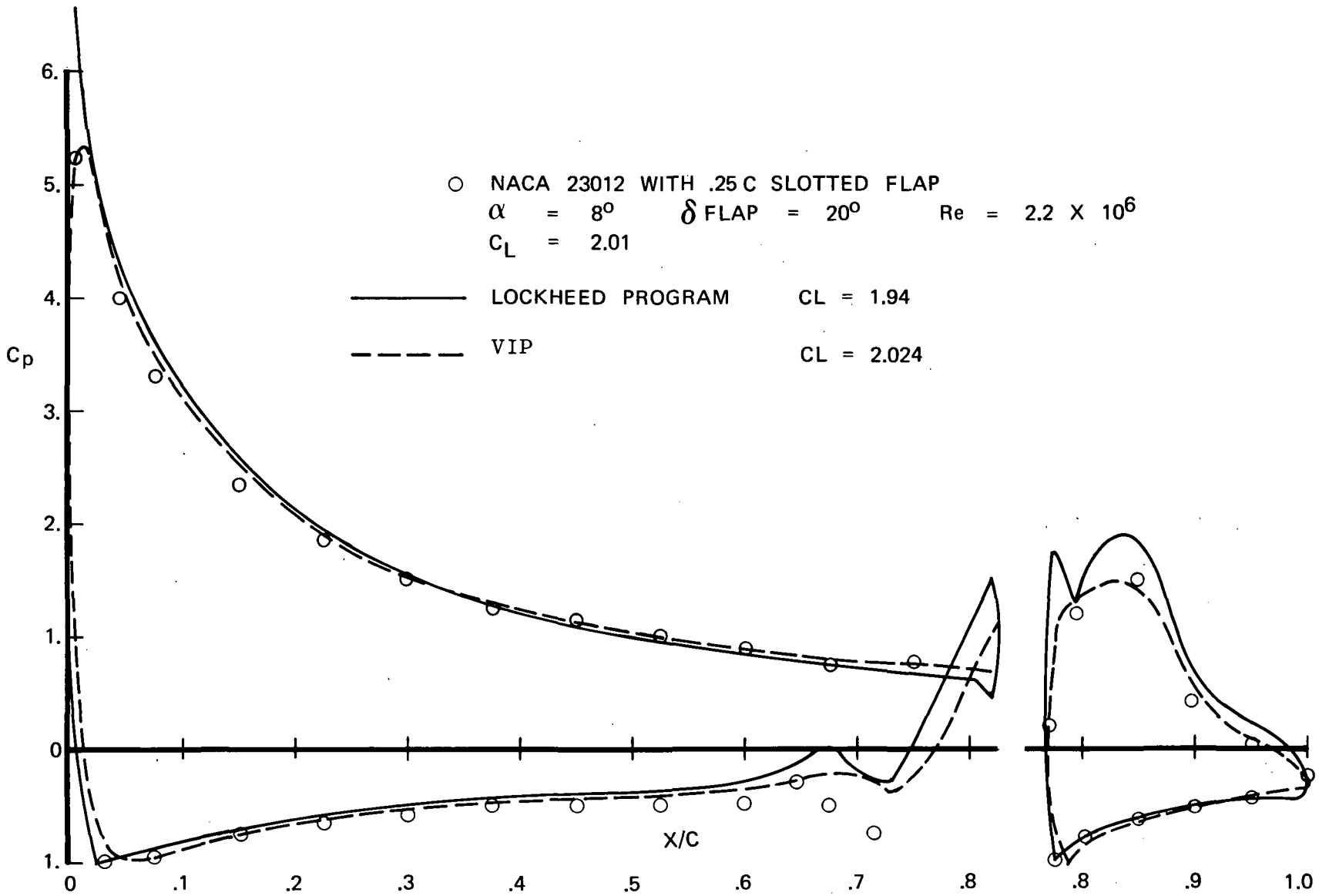

FIG. 5.10 COMPARISON OF MEASURED AND PREDICTED PRESSURE DISTRIBUTIONS FOR NACA 23012 AIRFOIL WITH 25% SLOTTED FLAP

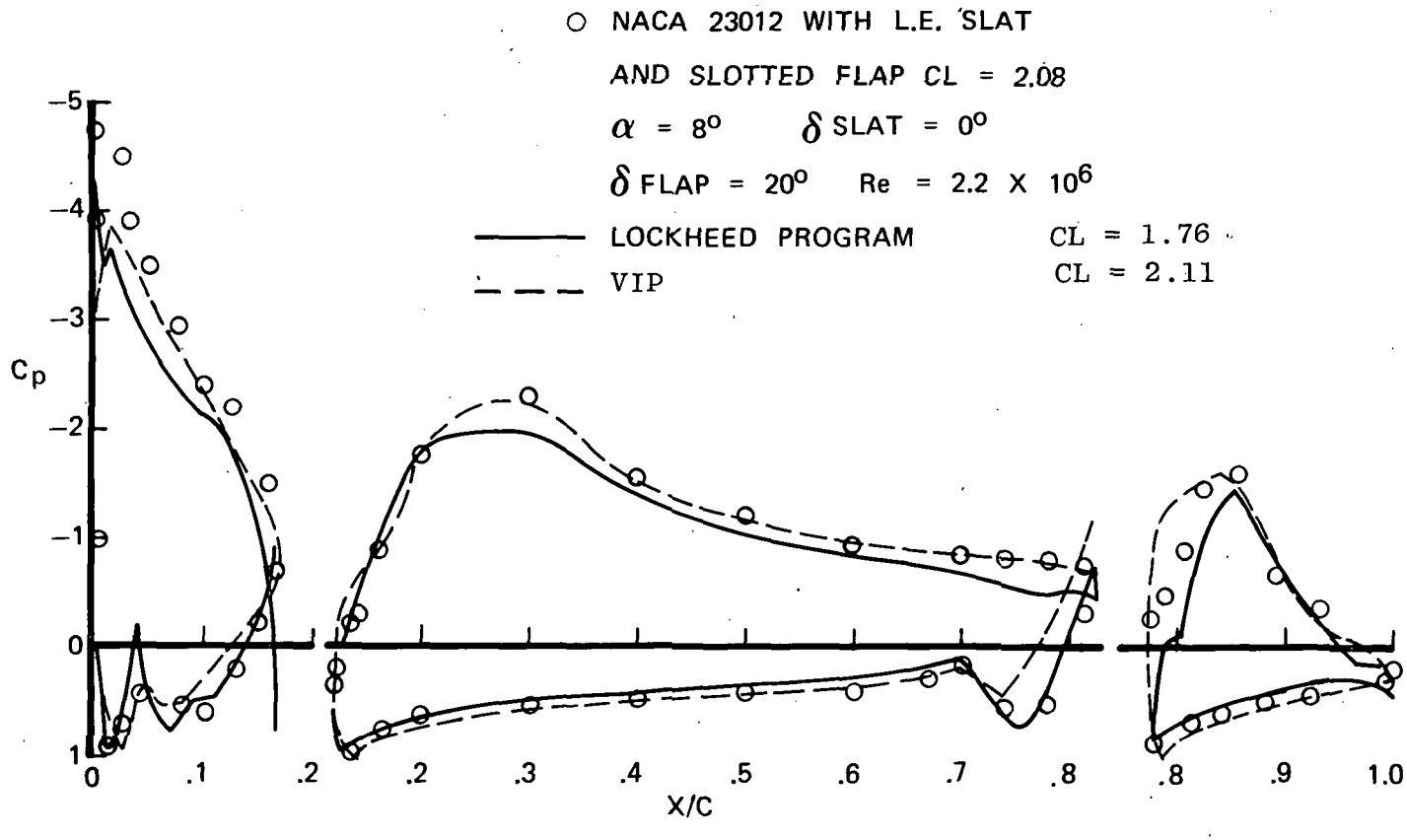

FIG. 5.11 COMPARISON OF MEASURED AND PREDICTED PRESSURE DISTRIBUTIONS FOR NACA 23012 AIRFOIL WITH L.E. SLAT AND 25% SLOTTED FLAP

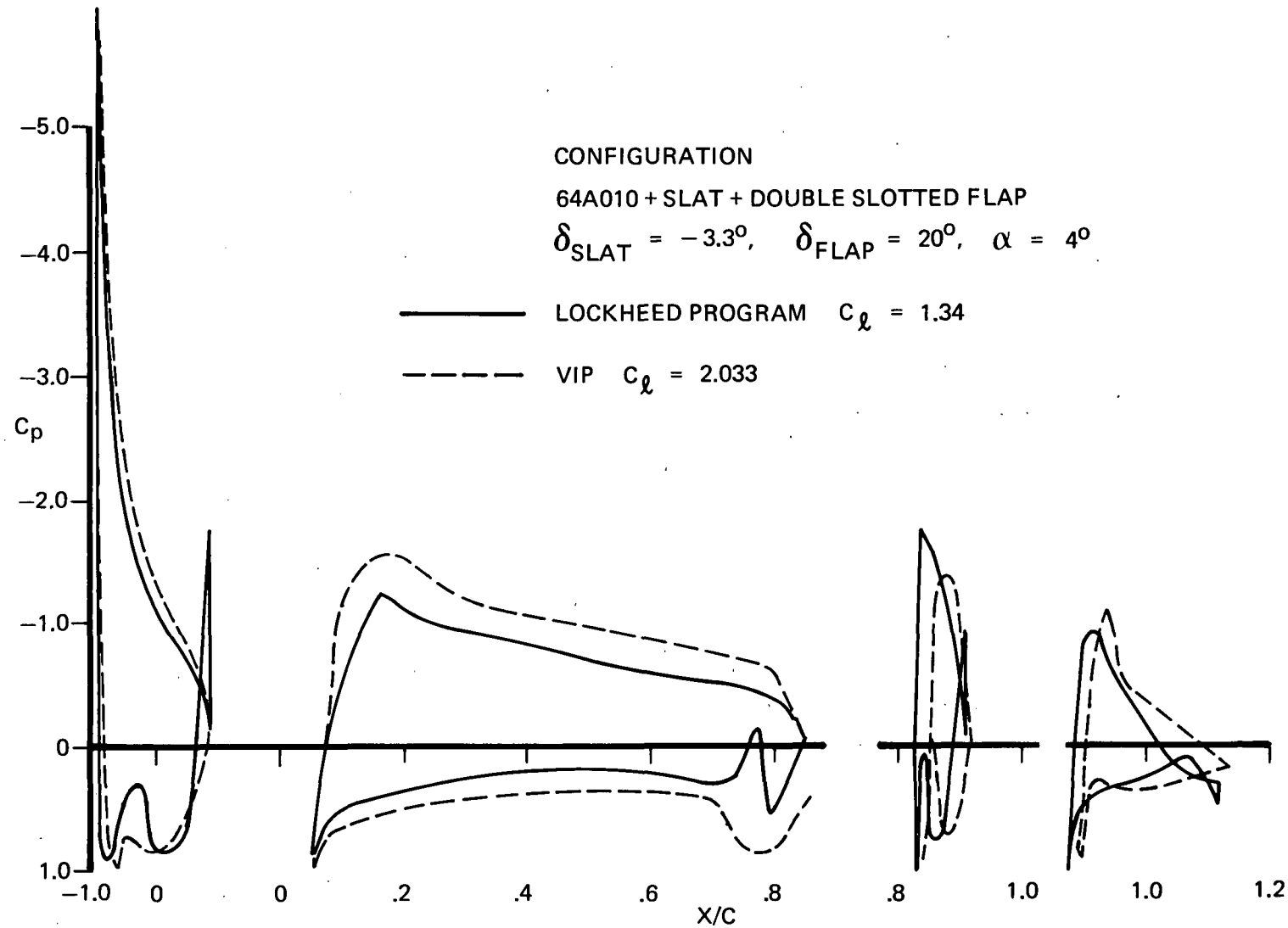

FIG. 5.12 COMPARISON OF PREDICTED PRESSURE DISTRIBUTIONS FOR NACA 64A010 AIRFOIL WITH L.E. SLAT AND DOUBLE SLOTTED FLAP

A second and considerably more challenging case has been investigated using the same basic four element geometry. In this example the slot and double slotted flaps are positioned in a landing configuration ($\delta_{slat} = -26.1^{o}$, $\delta_{flap} = 52.7^{o}$). Two problems have been encountered at this time and they will require further study. The first problem centers on the iterative procedure for solution of the influence coefficient matrix. Each element is initially analyzed in isolation with respect to its neighboring components. Interference effects are then determined and the analysis continued until convergence is achieved. The problem arises when interference effects are added to the slot loading (initially strongly negatively loaded because of the negative angle-of-attack), and change the loading to strongly positive lift. The result is a divergent solution. Another possible difficulty with the configuration analysis may be with the method of solution. Linearly varying vorticity methods do not have a strong diagonally dependent matrix as in the case of constant source panel methods. Iterative methods of solution rely to a considerable extent on the strong diagonal for their success. More work is definitely needed in the area of fast reliable solution techniques.

When the problem with the iterative solution was encountered, the direct technique was used to obtain the inviscid pressure distribution. As a result of a very high suction peak in the trailing edge region of the upper surface of the main element (probably due to the very high camber effect resulting from the highly deflected flaps) the starting velocity profile to the finite difference program had unacceptably high velocities. More work is needed to resolve this problem.

The RAE 2815 configuration tested by Foster (33) consisting of a main element and a single slotted flap has been considered in Figures 5.13 and 5.14. The comparisons in Figure 5.13 include measurements and calculations for two configurations. The spike in pressure measured by Foster is not duplicated by NASA Ames, nor is it reproduced in the calculated pressure distributions. This has a marked effect on the velocity profiles shown in Figure 5.14. Although the initial velocity profiles are in reasonable agreement, the different pressure gradient conditions experienced by the measured and calculated boundary layer developments results in quite different downstream profiles. It is interesting to note, however, that the aerodynamic load comparisons shown in Table 2 are in generally good agreement. Comparisons are also made for the RAE 2815 configuration having a drooped leading edge, and a slotted flap deflected 30 degrees. All comparisons were at 9^{o} angle-of-attack and at a Reynolds number of 3.8 million.

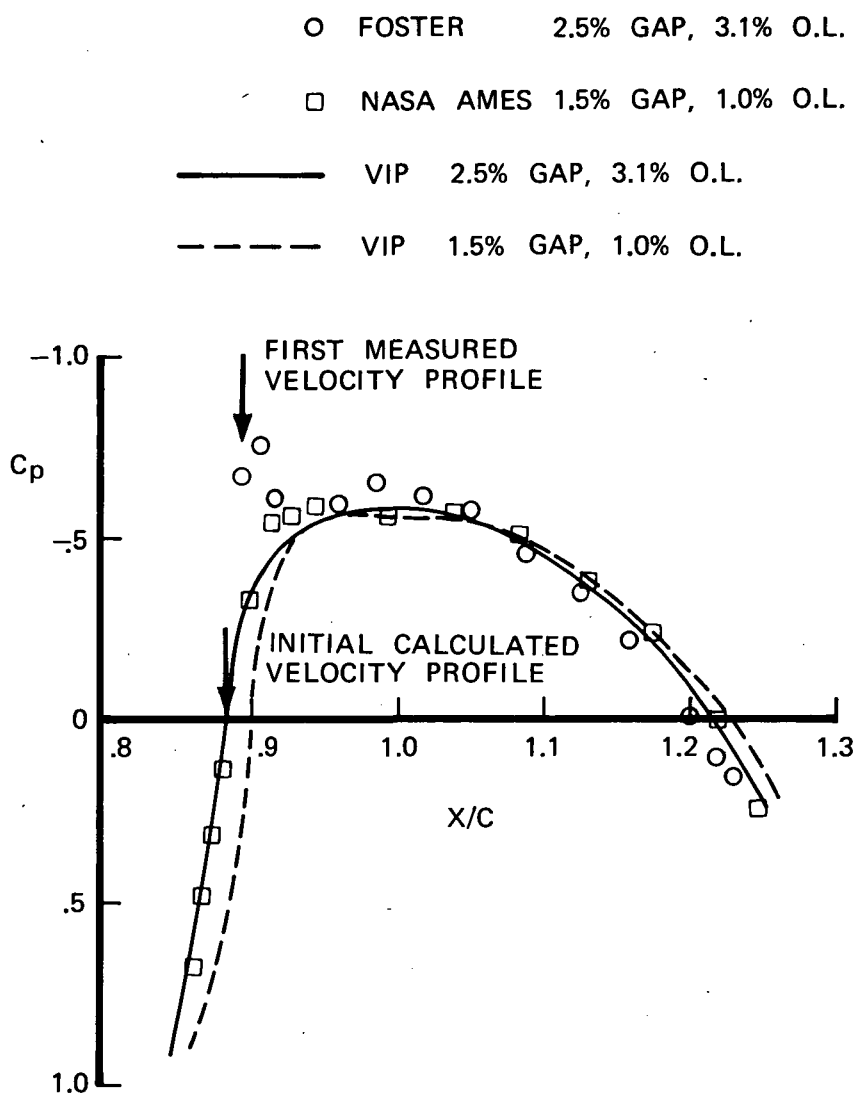

FIG. 5.13 COMPARISON OF MEASURED AND PREDICTED PRESSURE DISTRIBUTION FOR FOSTER'S AIRFOIL FLAP COMBINATION

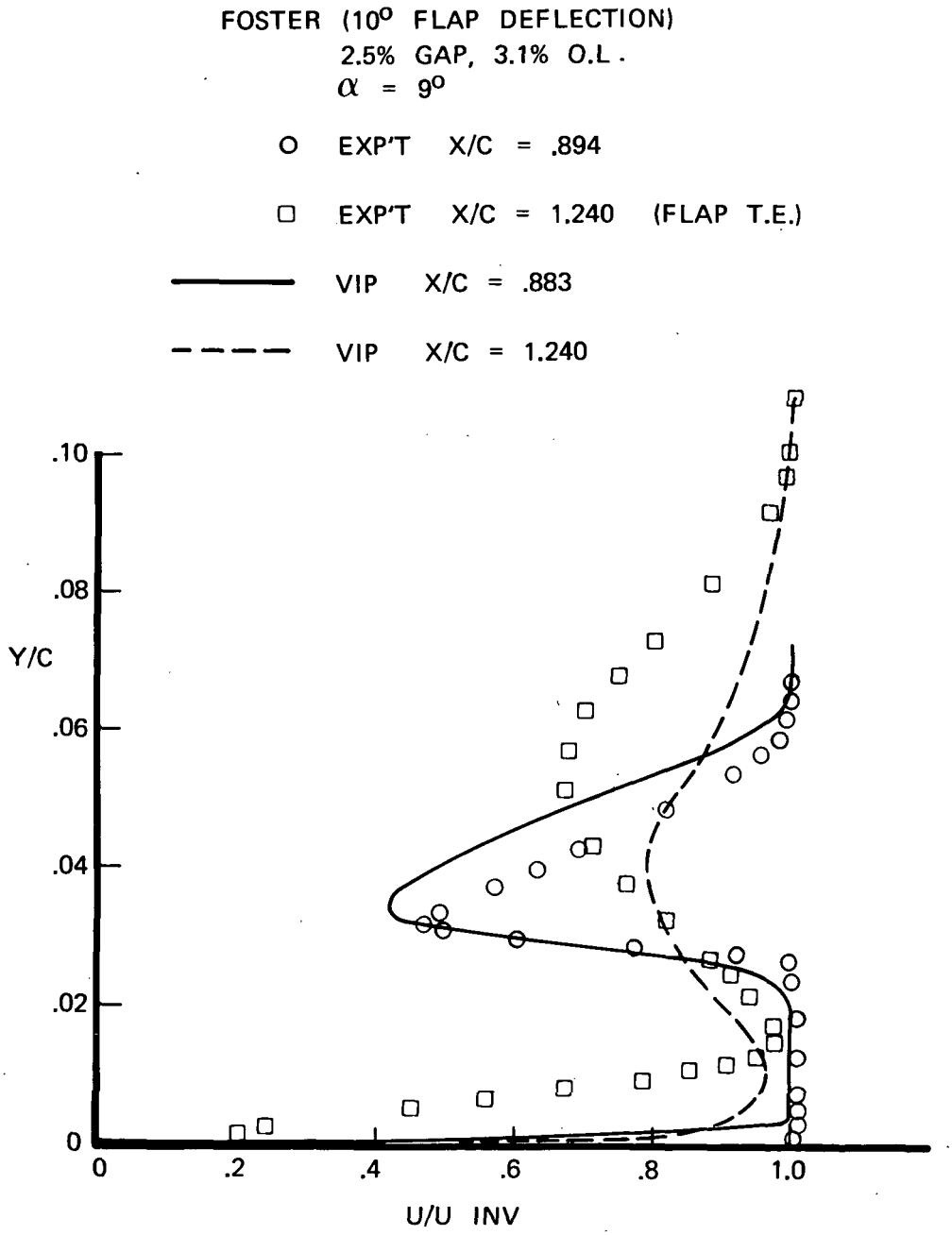

FIG. 5.14 COMPARISON OF MEASURED AND PREDICTED VELOCITY PROFILES ON FLAP UPPER SURFACE

Table 2 - RAE 2815

Flap Configuration	$C_{L_{meas.}}$	$C_{L_{Calc.}}$	$C_{D_{meas.}}$	$C_{D_{Calc.}}$
10° flap .025C Gap	1.897	1.885	.0222	.025
10° flap .015C Gap	1.84	1.835	.0203	.024
30° flap .020C Gap	3.40	3.56	$\approx$ .05 - .06	$\approx$ .065

The infinite swept wing capability of the program is considered in Figures 5.15 through 5.19. Calculations have been made for comparison with Cumpsty and Heads measurements (Ref. 34) on a 61.1° swept wing. Unfortunately the configuration tested had a large region of separated flow on both the upper and lower surfaces. As shown in Figure 5.15 the measured and calculated pressure distributions are in reasonable agreement in the forward section of the airfoil although the separated flow greatly modifies the pressures in the trailing edge region. The predicted streamwise momentum thickness variation is in good agreement with experiment away from the separation region as shown in Figure 5.16. The comparison between predicted and measured values of the angle β is good only in the region far removed from separation, while the predicted shape factor H is in poor agreement with experiment (Figure 5.17). The behavior of H is a result of much larger calculated pressure gradients than exist in the experimental case.

Figures 5.18 and 5.19 represent the results of calculations for the RAE 2815 airfoil flap configuration swept 25 degrees. The pressure distribution resulting from 5 iterations of program VIP is shown in Figure 5.18. Also included are the calculated aerodynamic lift drag and moment coefficients for both the 25 degree and zero degree cases. In this comparison the lift and moment coefficients are reduced slightly, while the drag as a result of the increased streamwise distance is considerably greater for the swept wing. Flap trailing edge streamwise and cross flow velocity profiles are shown in Figure 5.19. For this particular case the cross-flow profiles on the flap upper surface are very small, a result both of the moderate sweep angle, and the moderate loading on the flap.

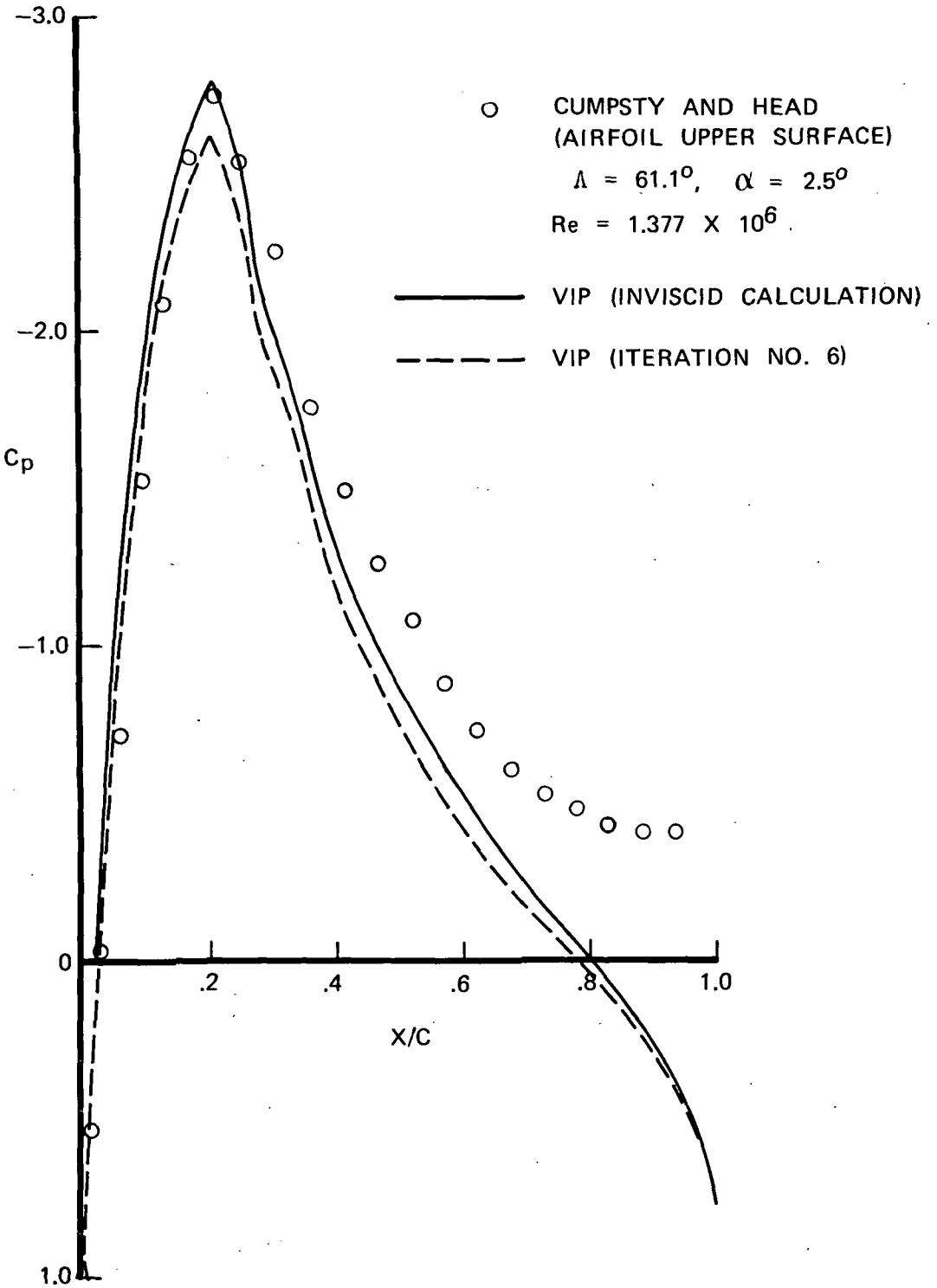

FIG. 5.15 COMPARISON OF MEASURED AND PREDICTED PRESSURE DISTRIBUTIONS FOR AN INFINITE SWEPT WING.

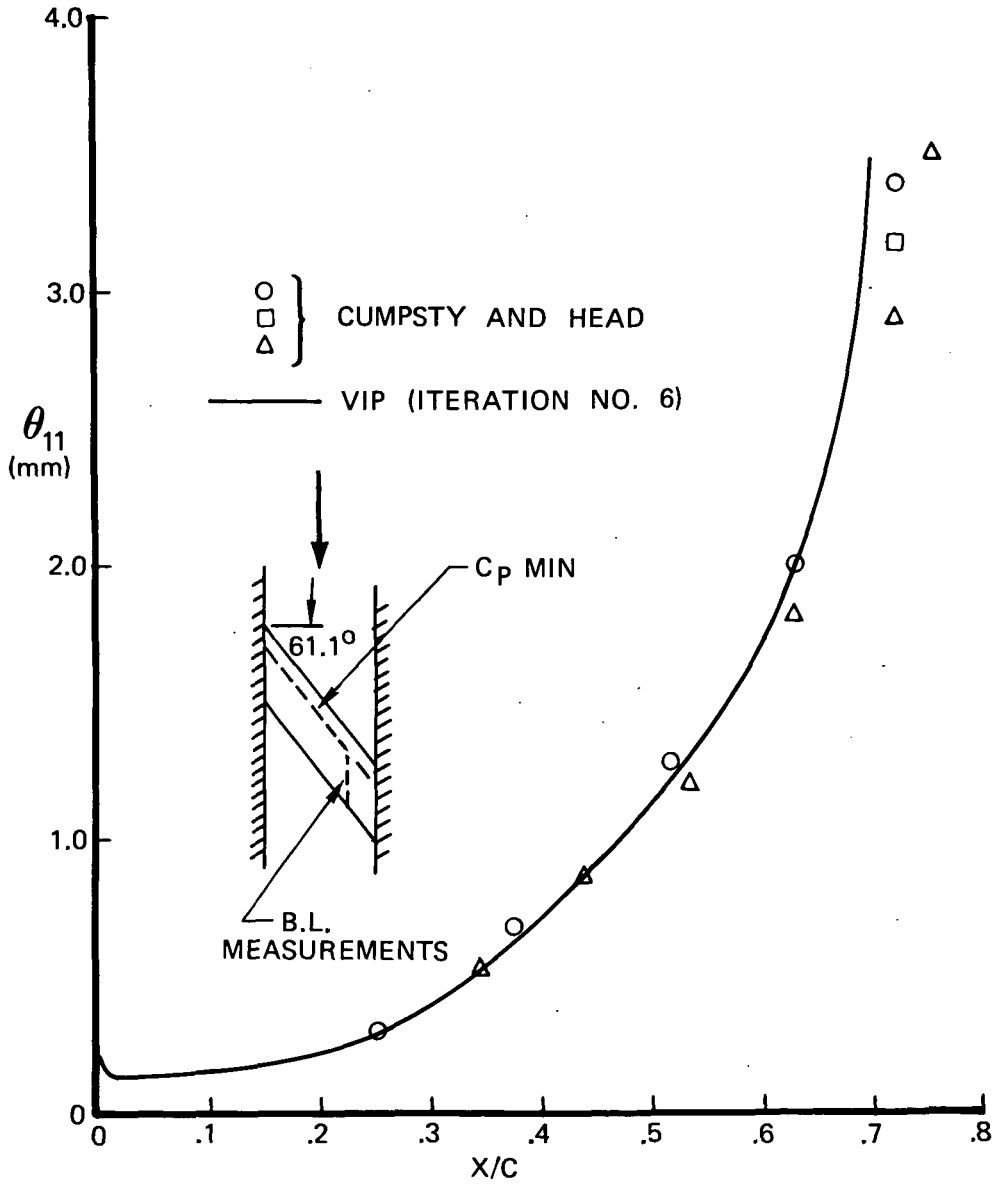

FIG. 5.16 COMPARISON OF MEASURED AND PREDICTED STREAMWISE MOMENTUM THICKNESS DEVELOPMENT

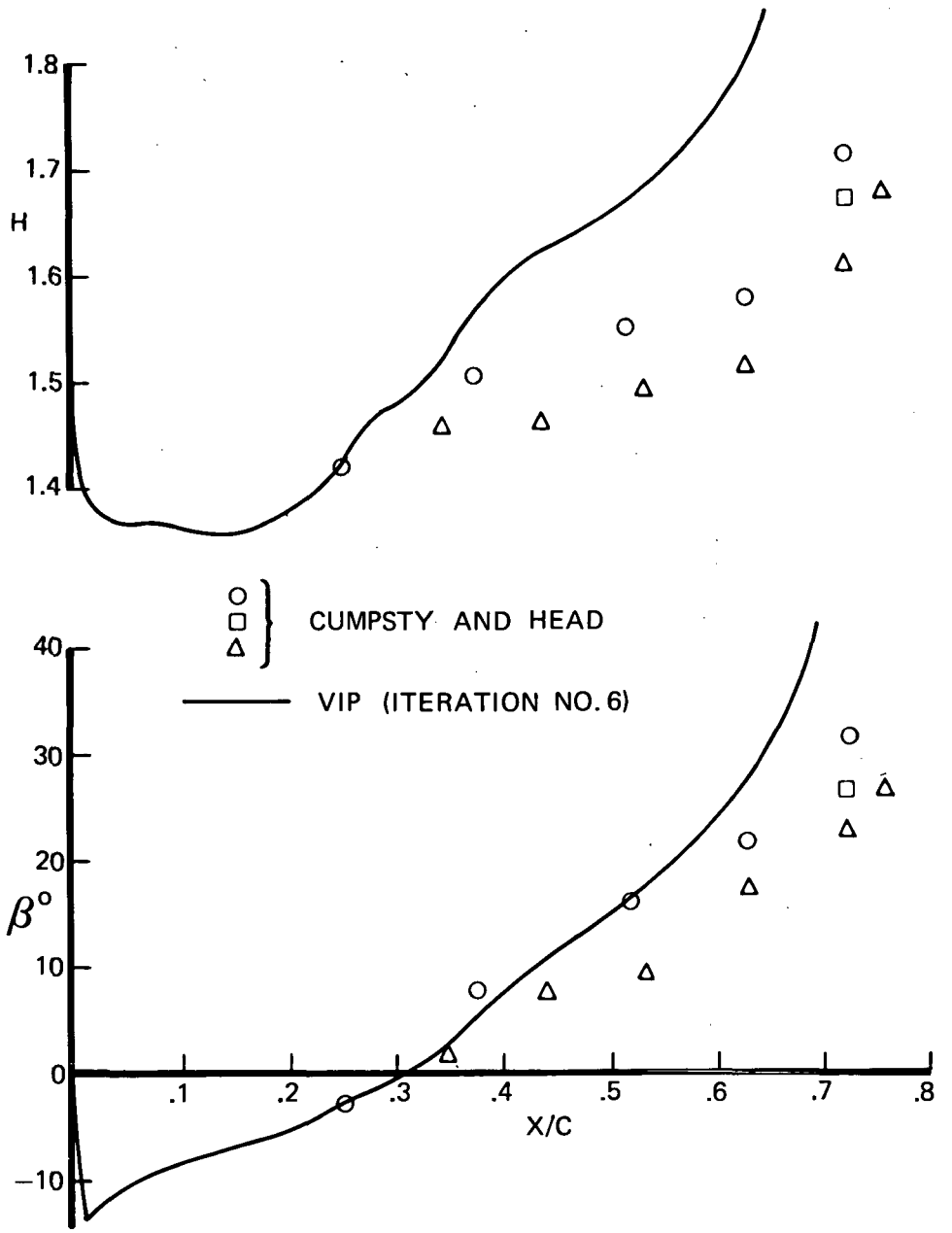

FIG. 5.17 COMPARISON OF MEASURED AND PREDICTED SHAPE FACTOR AND ANGLE β DEVELOPMENTS FOR AN INFINITE SWEPT WING

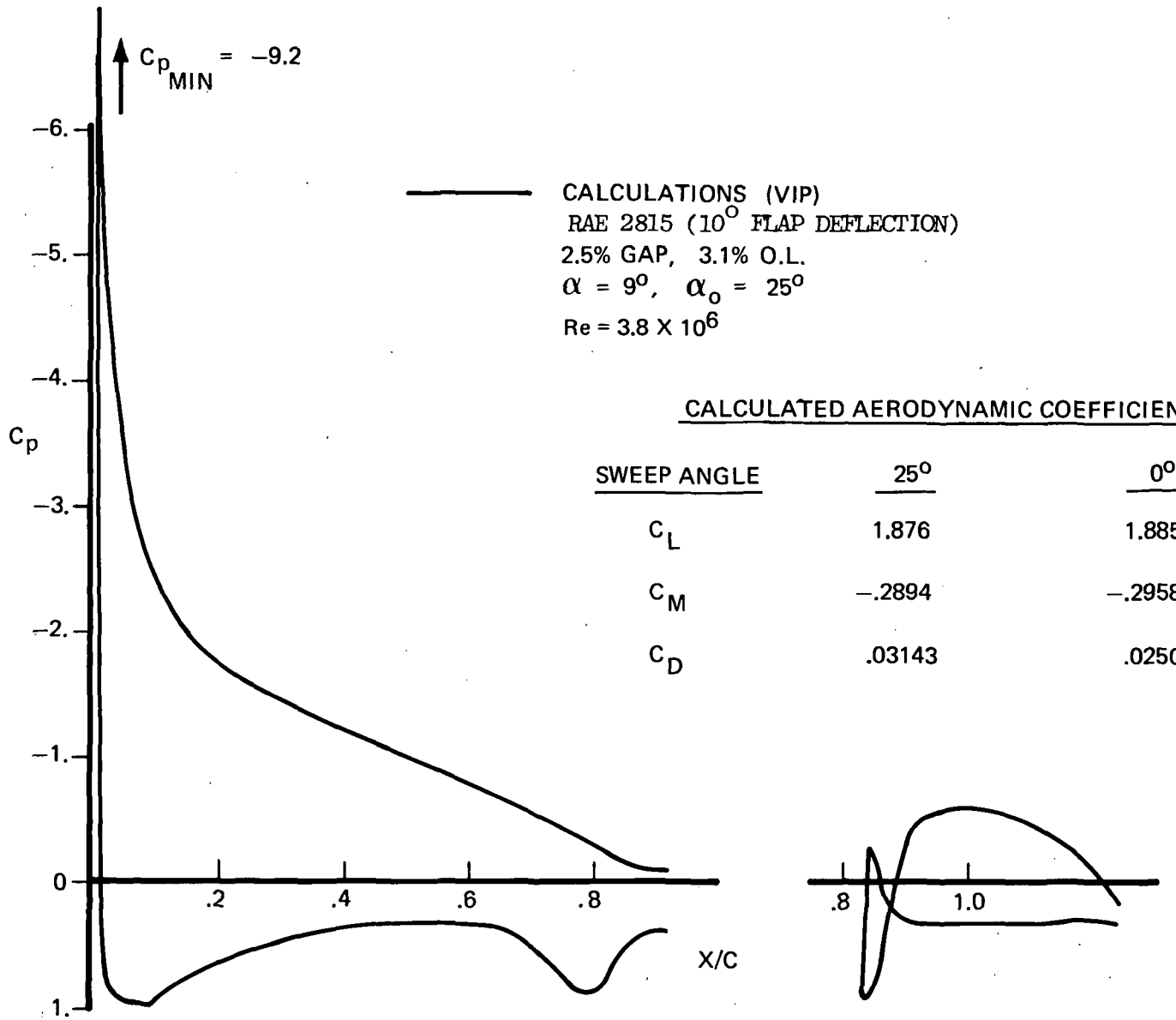

CALCULATED AERODYNAMIC COEFFICIENTS

SWEEP ANGLE	25°	0°
C_L	1.876	1.885
C_M	−.2894	−.2958
C_D	.03143	.0250

FIG. 5.18 PREDICTED PRESSURE DISTRIBUTIONS FOR FOSTER'S AIRFOIL–FLAP CONFIGURATION SWEPT 25 DEGREES

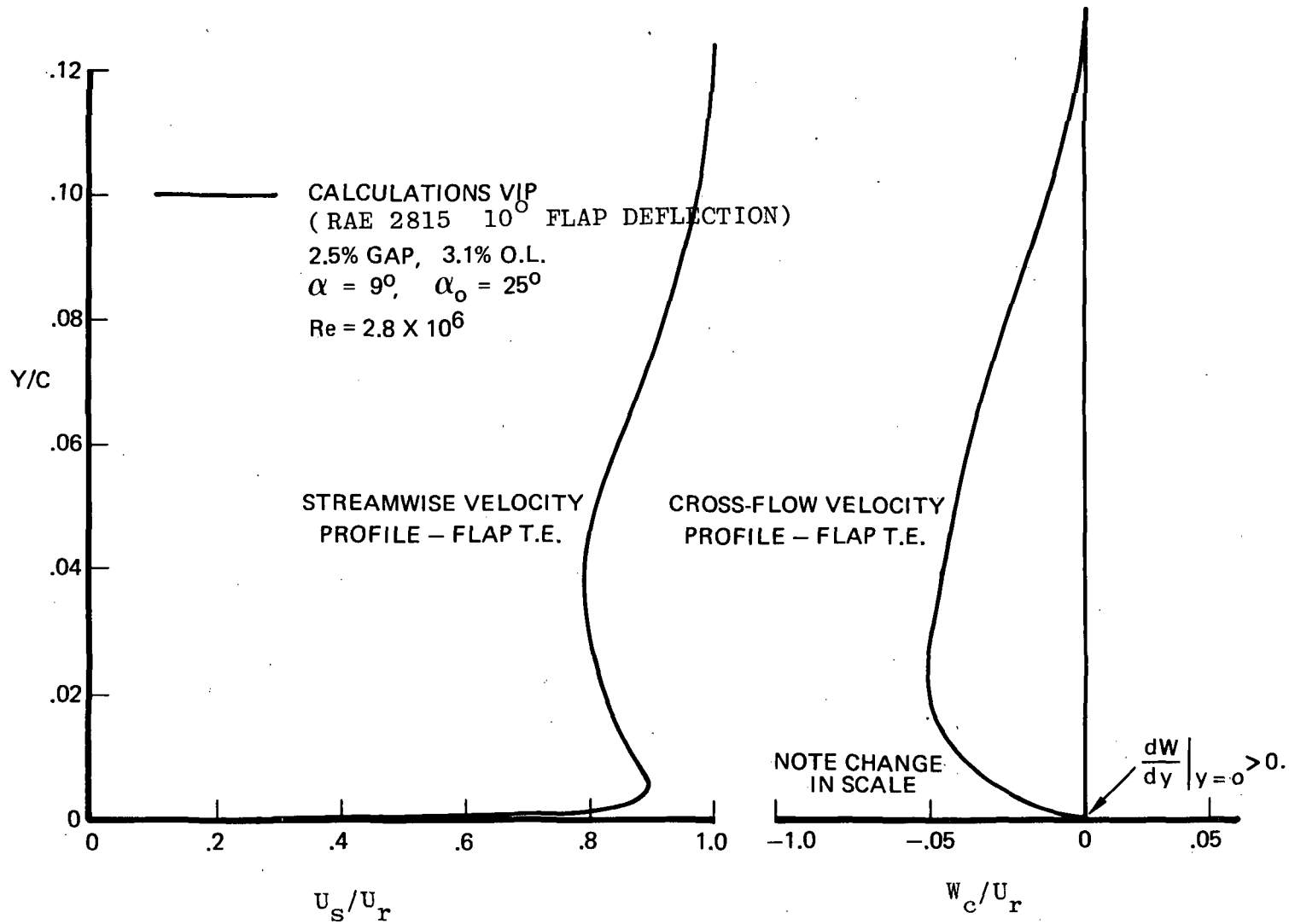

FIG. 5-19 PREDICTED STREAMWISE AND CROSS-FLOW VELOCITY PROFILES AT FLAP TRAILING EDGE FOR FOSTER'S AIRFOIL FLAP CONFIGURATION SWEPT 25 DEGREES.

PROGRAM LIMITATIONS

Although it is believed that the calculation procedure and computer program is capable of analyzing a wide variety of airfoil configurations, limitations both in theoretical methods and due to program structure restrict the range of application. These limitations include restriction to:

- Infinite swept wings consisting of at most four elements two of which can be slotted flaps.

- Incompressible flow; although the pressure distributions are corrected for Mach number effects using Gotherts rule.

- Small regions of separation. Although the source method lends itself readily to the development of a separated flow model, the current model does not have this capability (as apparent from the results of Figure 5.15). If separation is predicted the existing approach is to simply extrapolate the source strength to the trailing edge of the airfoil.

Oscillations in lift occurred in early calculations having predicted regions of separation. It was finally determined that this was due to unacceptably large source strengths at the trailing edge of the airfoil. A numerical experiment demonstrated that monotomically convergent solutions can be obtained if the maximum value of the source strength at the trailing edge of single element airfoils be limited using the criterion

$$q_{max} = 0.115 - 0.01\ (ITR-1)$$

where $1 \leq ITR \leq ITRMAX$

For configurations having slotted flaps the maximum value of q currently allowed in the program is 0.15. In all cases analyzed to date the behavior of the lift coefficient has been a monotonic decrease with increasing number of iterations.

CONCLUSIONS AND RECOMMENDATIONS

The viscous/potential flow interaction program described in this report employs potential flow and boundary layer procedures which are currently unique to this method and it is believed that because of this the analysis represents a considerable advance on other methods of its type. The program in its present form is applicable to a wide variety of problems, in particular, to the infinite swept wing case. There is however considerable scope for extension to a general three-dimensional wing calculation procedure. Specific conclusions regarding each of the major components of the program are given in the following paragraphs.

- The vortex lattice potential flow method developed for this program is an accurate numerical approach, adapted for two-dimensions, from a general three dimensional lifting potential flow method developed by one of the authors. The extension to the three dimensional case is therefore relatively straightforward.

- The integral boundary layer method used for single element airfoils and currently on all but the flap upper surfaces in the multi-element mode, is quite accurate, as witnessed by the good drag prediction capability. At the same time the method uses only a fraction of a second of computer time per boundary layer development.

The inclusion of curvature and normal pressure gradient effects in the finite difference boundary layer method enables complicated boundary layer flows to be represented more accurately than is possible by other procedures now available. It is believed that the improved physical representation of the flow over slotted flaps is responsible for the greater degree of agreement with experiment than is achieved by other methods.

- The use of sources to represent the displacement effects of the boundary layer on the potential flow, while not necessarily more accurate a procedure than the direct employment of the displacement thickness, has two distinct advantages. The first advantage is in the computational superiority of such a procedure. The influence coefficient matrix need by inverted only once, with succeeding iterations requiring only matrix multiplication. If one is ever to contemplate a viscous/potential flow interaction program applied to general three dimensional airplane configurations such a procedure will be almost mandatory. The second advantage is related to the modelling of separated flow regions in a potential flow analysis by distributed sources. It has been demonstrated in the literature that such an approach is possible, and it is recommended that one of the first extensions of the present program should be to include separation effects. The program would then be capable of predicting $C_{\ell_{max}}$ as a function of Reynolds number.

Another useful extension to the program would be the inclusion of compressibility effects in the boundary layer development. Even at low free stream Mach numbers the high suction peaks experienced by a slot or main element of a high lift system can lead to compressibility problems.

With some modification the finite difference boundary layer program module can be used to predict the effect of tangential blowing or boundary layer suction in the overall context of a viscous/potential flow interaction method for high lift systems.

REFERENCES

1. Stevens, W. A., Goradia, S. H., and Braden, J. A., "Mathematical Model for Two-Dimensional Multi-Component Airfoils in Viscous Flow", NASA CR-1843, July 1971.

2. Preston, J. H., "The Effect of the Boundary Layer and Wake on the Flow Past a Symmetrical Airfoil at Zero Incidence", A. R. C. R. and M 2107, 1947.

3. Callaghan, J. G., and Beatty, T. D., "A Theoretical Method for the Analysis and Design of Multielement Airfoils:, J. Aircraft, Vol. 9, No. 12, December 1972.

4. Cumpsty, N. A., and Head, M. R., "The Calculation of Three-Dimensional Turbulent Boundary Layers, Part II: Attachment - Line Flow on an Infinite Swept Wing", *Aero Quart.*, Vol. XVIII, May 1967.

5. Bradshaw, P., "Calculation of Three-Dimensional Turbulent Boundary Layers", J. Fluid Mech., Vol. 46, 1971.

6. Cumpsty, N. A. and Head, M. R., "The Calculation of the Three-Dimensional Turbulent Boundary Layer, Part III: Comparison of Attachment - Line Calculations with Experiment", *Aero Quart.*, Vol. XX, May 1969.

7. Curle, H., "A Two Parameter Method for Calculating the Two-Dimensional Incompressible Laminar Boundary Layer", *J. R. Aero Soc.*, Vol. 71, 1967.

8. Thwaites, B., "Approximate Calculation of the Laminar Boundary Layer", *Aero Quart.*, Vol. I, 1949.

9. Cumpsty, N. A. and Head, M. R., "The Calculation of Three-Dimensional Turbulent Boundary Layers, Part I: Flow Over the Rear of an Infinite Swept Wing", *Aero Quart.*, Vol. XVIII, February 1967.

10. Nash, J. F., "The Calculation of Three-Dimensional Turbulent Boundary Layers in Incompressible Flow", J. Fluid Mechanics, 37, 1969.

11. Head, M. R., "Entrainment in the Turbulent Boundary Layer", R&M 3152, Aero Research Council, Great Britain, 1958.

12. Thompson, B. G. J., "A New Two Parameter Family of Mean Velocity Profiles for Incompressible Turbulent Boundary Layers on Smooth Walls", R&M 3463, Aero Research Council Great Britain, 1965.

13. Coles, D. E., "The Law of the Wake in the Turbulent Boundary Layer", J. Fluid Mech., Vol. 1, 1956.

14. Mager, H., "Generalization of Boundary Layer Momentum Integral Equations to Three-Dimensional Flows Including Those of Rotating Systems", NACA TR 1067, 1952.

15. Granville, P. S., "The Calculation of the Viscous Drag of Bodies of Revolution", David W. Taylor Model Basin Report 849, 1953.

16. Schlichting, J. and Ulrich, A., "Zur Berechnung Des Unsellages Laminar-Turbulenten" (On the Calculation of Laminar-Turbulent Transition), Jahrbuch 1942 Der Deutschen Luftfahrt-Forschung.

17. Smith, A. M. O., "Transition, Pressure Gradient and Stability Theory", Proc. 9th Internat. Congress of Appl. Mech., Brussels, Vol. 7, 1957.

18. Coles, D. E., Measurements in the Boundary Layer on a Smooth Flat Plate in Supersonic Flow", Jet Propulsion Lab Report No. 20-69, 1953.

19. Briley, W. R., "An Analysis of Laminar Separation - Bubble Flow using the Navier-Stokes Equations", Proceedings - Fluid Dynamics of Unsteady, Three-Dimensional and Separated Flows, Georgia Tech., June 1971.

20. Gaster, M., "The Structure and Behavior of Laminar Separation Bubbles", ARC 28-226, 1967.

21. Nash, J. F. and Patel, V. C., "A Generalized Method for the Calculation of Three-Dimensional Turbulent Boundary Layers", Proceedings - Workshop on Fluid Dynamics of Unsteady, Three-Dimensional and Separated Flows, Georgia Tech., Atlanta, June 1971.

22. Dvorak, F. A., "Calculation of Turbulent Boundary Layers and Wall Jets over Curved Surfaces", AIAA Journal, Vol. 11, No. 4, April 1973.

23. Crank, J. and Nicholson, P., "A Practical Method for Numerical Evaluation of Solutions of Partial Differential Equations of the Heat Conduction Type", Proc. Cambridge Phil. Soc., 43, 1947.

24. Dvorak, F. A., and Head, M. R., "Heat Transfer in the Constant Property Turbulent Boundary Layer", Int. J. Heat Mass Transfer, Vol. 10, 1967.

25. Squire, H. B. and Young, A. D., "The Calculation of the Profile Drag of Airfoils", Brit. Aero Res. Coun. R and M 1838, 1937.

26. McLellan, C. H., and Cangelosi, J. I., "Effects of Nacelle Position on Wing Nacelle Interference", NACA TN 1593, June 1948.

27. Hess, J. L., "Calculation of Potential Flow About Arbitrary Three-Dimensional Lifting Bodies", Report No. MDC J 5679-01, Douglas Aircraft Company, Oct. 1972.

28. Williams, B. L., "An Exact Test Case for the Plane Potential Flow About Two Adjacent Lifting Airfoils", RAE Tech. Report 71197, Sept. 1971.

29. Morgan, H., NASA Langley Research Center Private Communication.

30. Wenzinger, C. J. and Delano, J. B., "Pressure Distribution Over an NACA 23012 Airfoil with Slotted and Plain Flap, NACA TR 633.

31. Harris, T. A., and Lowry, J. G., "Pressure Distribution Over an NACA 23012 Airfoil with a Fixed Slot and a Slotted Flap", NACA TR 732, 1942.

32. Kelly, J. A. and Hayter, N. F., "Lift and Pitching Moment at Low Speeds of the NACA 64A010 Airfoil Section Equipped with Various Combinations of a Leading Edge Slot, Leading-Edge Flap, Split Flap and Double-Slotted Flap", NACA TN 3007, 1953.

33. Foster, D. N., Irwin, H. P., and Williams, B. R., "The Two Dimensional Flow Around a Slotted Flap", RAE Tech. Report 70164, Sept. 1970.

34. Cumpsty , N. A. and Head, M. R., "The Calculation of Three-Dimensional Turbulent Boundary Layers, Part IV: Comparison of Measurements with Calculations on the Rear of a Swept Wing", Brit. Aero Res. Coun. C. P. No. 1077, 1970.

35. Labrujere, Th. E., Loeve, W. and Sloof, J. W., "An Approximate Method for the Calculation of the Pressure Distribution on Wing-Body Combinations at Subcritical Speeds", AGARD C. P. No. 71, 1970.

36. Dvorak, F. A. and Woodward, F. A., "A Viscous/Potential Flow Interaction Analysis Method for Multi-Element Infinite Swept Wings", Volume II, NASA CR 137550, April 1974.

APPENDIX I

POTENTIAL FLOW THEORY

The potential flow theory is used to derive the influence of constant and linear distributions of sources and vorticity on planar two dimensional surfaces. Consider an elementary line source or line vortex located at a point ξ on the x axis and perpendicular to the x, z plane. In incompressible flow, the magnitude of the velocity induced by either singularity at an arbitrary point P(x,z) is given by:

$$V = \frac{1}{2\pi d} \tag{1}$$

where

$$d = [(x-\xi)^2 + z^2]^{1/2}$$

The geometry is illustrated by the following sketch:

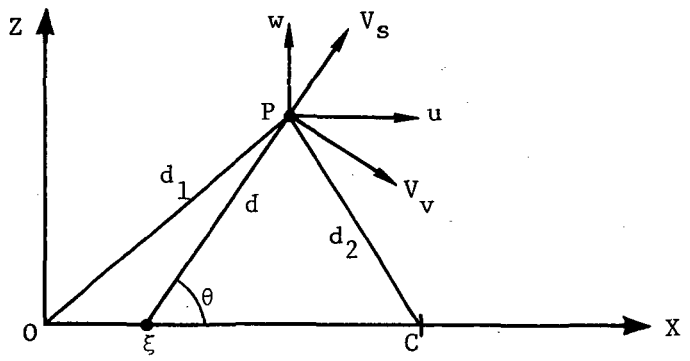

For an elementary source, the velocity V_s is in the direction of the line joining ξ and P, while for an elementary vortex, the velocity V_v is perpendicular to this line. The horizontal and vertical components of velocity corresponding to the line source or vortex are given by:

$$w_s = u_v = V\sin\theta = \frac{z}{2\pi d^2} \tag{2}$$

$$u_s = - w_v = V\cos\theta = \frac{x-\xi}{2\pi d^2} \qquad (3)$$

The contribution of a constant distribution of sources or vortices along the x axis is obtained by integrating equations (2) and (3) from 0 to c.

$$w_s = u_v = \frac{z}{2\pi} \int_0^c \frac{d\xi}{(x-\xi)^2 + z^2}$$

$$= \frac{1}{2\pi} \left[\tan^{-1} \frac{z}{x-c} - \tan^{-1} \frac{z}{x} \right] \qquad (4)$$

$$u_s = -w_v = \frac{1}{2\pi} \int_0^c \frac{(x-\xi)d\xi}{(x-\xi)^2 + z^2}$$

$$= - \frac{1}{2\pi} \log \sqrt{\frac{(x-c)^2+z^2}{x^2 + z^2}} \qquad (5)$$

The effects of compressibility may be obtained by applying Gothert's Rule, with $\beta = \sqrt{1-M^2}$

$$w_s = u_v = \frac{1}{2\pi} \left[\tan^{-1} \frac{\beta z}{x-c} - \tan^{-1} \frac{\beta z}{x} \right] \qquad (6)$$

$$u_s = - \frac{1}{2\pi\beta} \log \sqrt{\frac{(x-c)^2 + \beta^2 z^2}{x^2 + \beta^2 z^2}} \qquad (7)$$

and

$$w_v = - \beta^2 u_s = \frac{\beta}{2\pi} \log \sqrt{\frac{(x-c)^2 + \beta^2 z^2}{x^2 + \beta^2 z^2}} \qquad (8)$$

For a source or vortex distribution varying linearly with x, with zero strength at the origin and unit strength at x = c,

$$w_s = u_v = \frac{z}{2\pi c} \int_0^c \frac{\xi d\xi}{(x-\xi)^2 + z^2}$$

$$= \frac{1}{2\pi} \left\{ \frac{z}{c} \log \frac{\sqrt{(x-c)^2 + z^2}}{\sqrt{x^2 + z^2}} - \frac{x}{c} \left[\tan^{-1} \frac{z}{x} - \tan^{-1} \frac{z}{x-c} \right] \right\} \quad (9)$$

$$u_s = -w_v = \frac{1}{2\pi c} \int_0^c \frac{\xi(x-\xi)\, d\xi}{(x-\xi)^2 + z^2}$$

$$= \frac{-1}{2\pi} \left\{ 1 + \frac{z}{c} \left[\tan^{-1} \frac{z}{x} - \tan^{-1} \frac{z}{x-c} \right] + \frac{x}{c} \log \frac{\sqrt{(x-c)^2 + z^2}}{\sqrt{x^2 + z^2}} \right\} \quad (10)$$

Compressibility effects are obtained as before, i.e., by multiplying z and w_v by β, and dividing u_s by β.

A source or vortex distribution having unit strength at the origin, and zero strength at $x = c$, can be obtained by subtracting the previously derived linearly varying distributions from the constant distributions.

APPENDIX II

SOLUTION OF BOUNDARY CONDITION EQUATIONS

For single or multi-element airfoils, the boundary condition equations can be solved by direct inversion. For multi-element airfoils, use can also be made of a rapidly convergent iteration scheme reported in Reference (35). In this method the matrix is subdivided into smaller partitions, or blocks, with each block representing the influence of one element of the multi-element airfoil. The diagonal blocks represent the influence of the elements on themselves, the off-diagonal blocks represent the interference of one element on the others. The order of any block is restricted to 60, the maximum number of panels on the upper and lower surface of the element.

The initial iteration calculates the source and vortex strengths corresponding to each block in isolation. For this step, only the diagonal blocks are present in the aerodynamic matrix. Once the initial approximation to the source and vortex strengths is determined, the interference effect of each block on all the others is calculated by matrix multiplication. The incremental normal velocities obtained are subtracted from the normal velocities specified by the boundary conditions. This process is repeated 15 to 20 times, or until the residual interference velocities are small enough to ensure that convergence has occurred.

The procedure is illustrated below for an aerodynamic matrix consisting of nine blocks. The unknown singularity strengths are designated γ_j, the specified normal velocities C_i.

To solve

$$A_{ij} \quad \gamma_j \quad = \quad C_i$$

where

$$A_{ij} = \begin{bmatrix} A_{11} & A_{12} & A_{13} \\ A_{21} & A_{22} & A_{23} \\ A_{31} & A_{32} & A_{33} \end{bmatrix}$$

Put $A = D + E$

$$= \begin{bmatrix} A_{11} & 0 & 0 \\ 0 & A_{22} & 0 \\ 0 & 0 & A_{33} \end{bmatrix} + \begin{bmatrix} 0 & A_{12} & A_{13} \\ A_{21} & 0 & A_{23} \\ A_{31} & A_{32} & 0 \end{bmatrix}$$

Therefore $[D + E]\ \{\gamma\} = \{C\}$

or $$\{\gamma\} = D^{-1}\ [C - E\ \{\gamma\}]$$

First approximation:

$$\{\gamma\}^{-1} = D^{-1}\ \{C\}$$

Calculate $$\Delta C^{1} = E\ \{\gamma\}^{1}$$

Second approximation:

$$\{\gamma\}^{2} = D^{-1}\ \{C - \Delta C^{1}\}$$

Similarly, k^{th} approximation:

$$\{\gamma\}^{k} = D^{-1}\ \{C - \Delta C^{k-1}\}$$

Note that

$$D^{-1} = \begin{bmatrix} A_{11}^{-1} & 0 & 0 \\ 0 & A_{22}^{-1} & 0 \\ 0 & 0 & A_{33}^{-1} \end{bmatrix}$$

APPENDIX III

PROGRAM MACRO FLOW CHARTS

The general program overlay structure of each overlay is described briefly in the following paragraphs and flow charts. *

OVERLAY (0,0) Program VIP

Program VIP controls the entire computer program (Figure A1). All primary overlays are called from VIP. Overlay (0,0) also contains other subroutines which are commonly used in the other overlays.

OVERLAY (1,0) Program POTFLOW

Program POTFLOW controls the lofting of the configuration, the calculation of flap surface curvature, the calculation of the potential flow pressures, as well as the calculation of the lift and moment coefficients.

OVERLAY (2,0) Program IBL

Program IBL controls the integral boundary layer analysis from the calculation of initial conditions along a stagnation line to the turbulent boundary layer analysis. The program logic flow is shown in Figure A3.

OVERLAY (3,0) Program INSPAN

Program INSPAN controls the infinite swept wing finite difference boundary layer analysis. The overlay calls two secondary overlays, OVERLAY (3,1) Program BOUNDRY (Figure A4) and OVERLAY (3,2), Program DEVELOP (Figure A5). Program BOUNDRY initializes the grid network normal to the flap surface upon which the finite difference method is applied. Normal chord and spanwise velocity profiles are initialized in preparation for the analysis.

Program DEVELOP controls the actual calculation procedure used in determining the downstream development of the boundary layer.

OVERLAY (4,0) Program FELDPT

Program FELDPT calculates the off-body pressure distributions P(x,y) for input to INSPAN.

* Program input/output discription and a complete program listing is given in Reference 36.

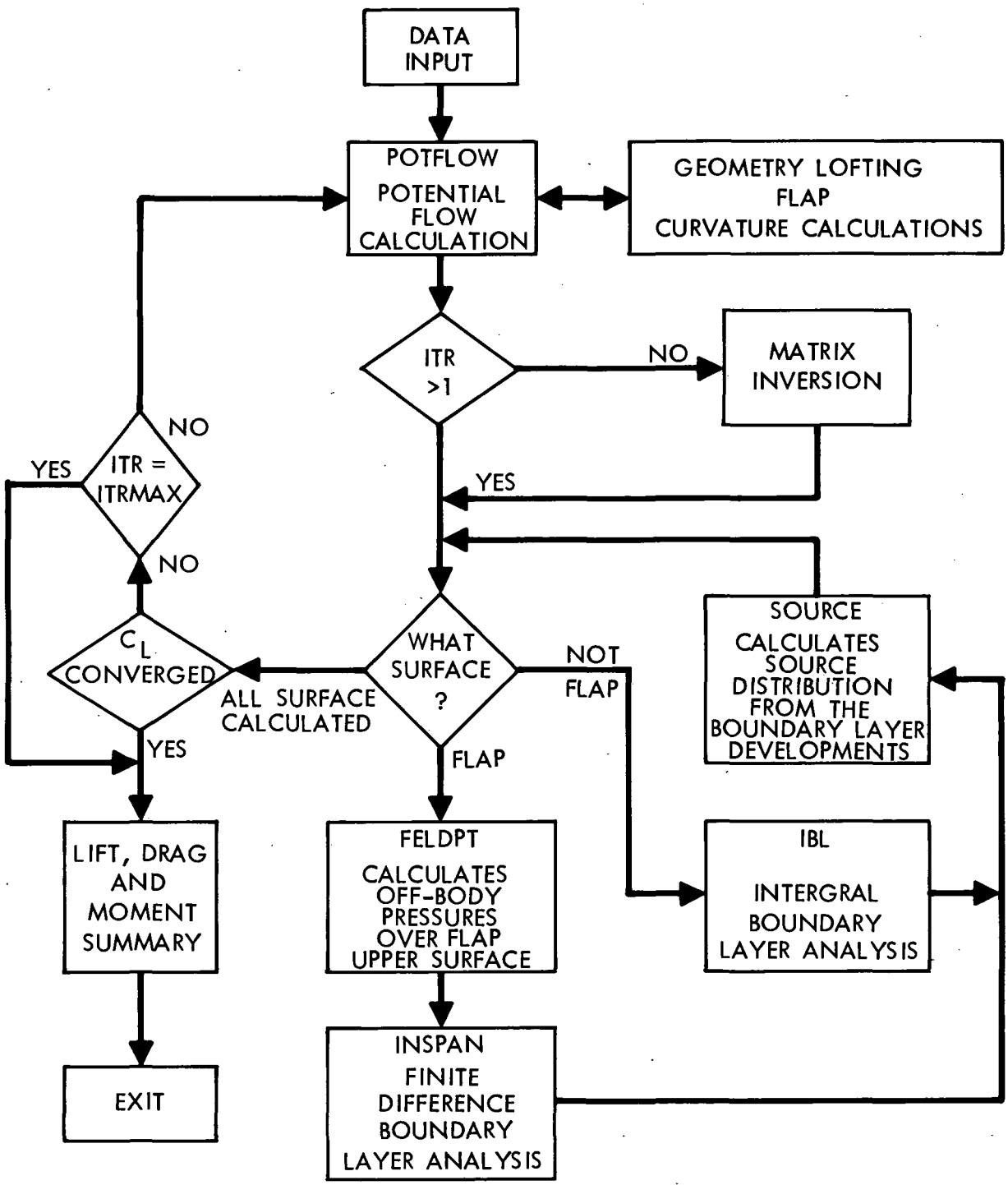

FIG. A1 OVERLAY (0,0) PROGRAM VIP

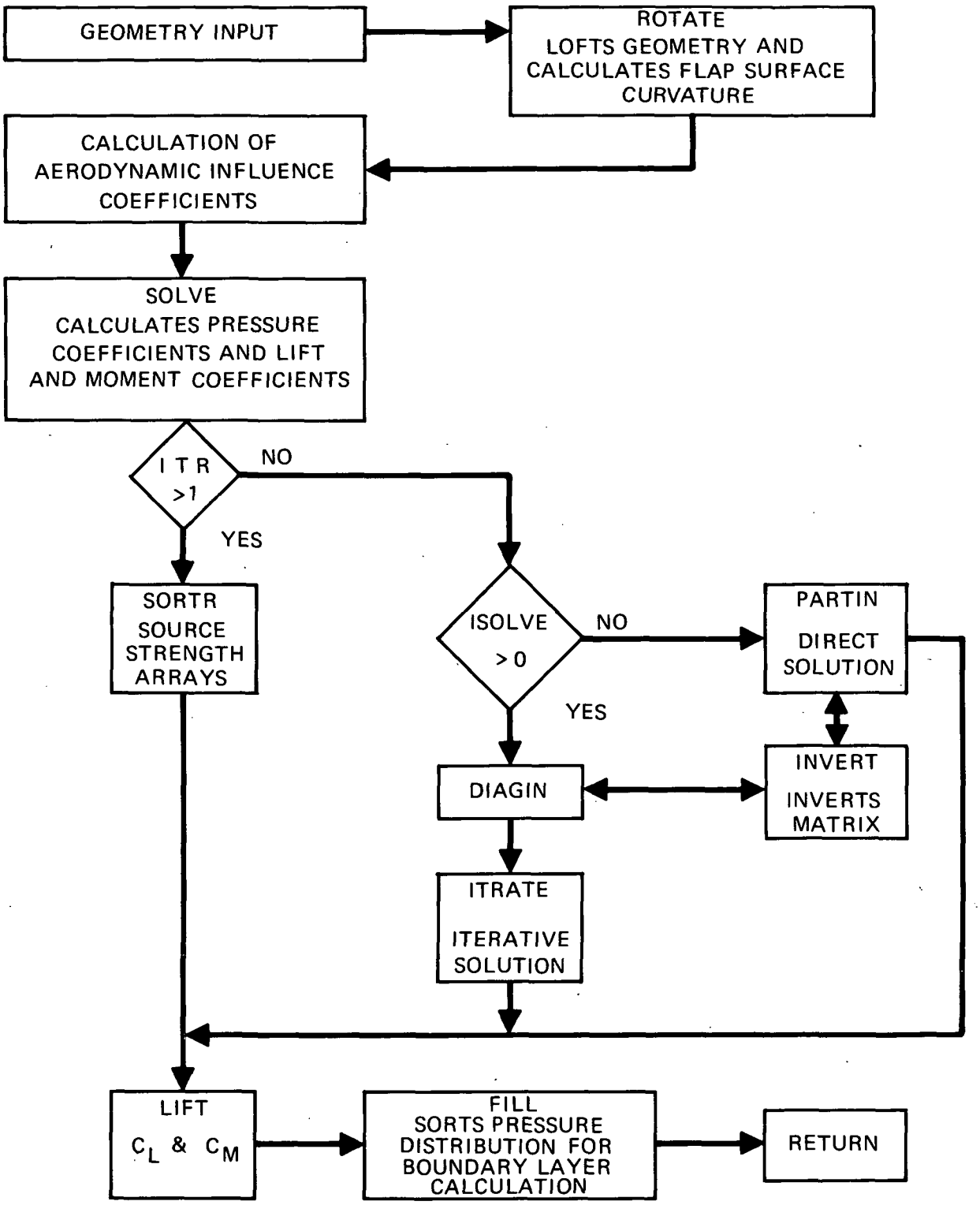

FIG. A - 2 OVERLAY (1, 0) PROGRAM POTFLOW

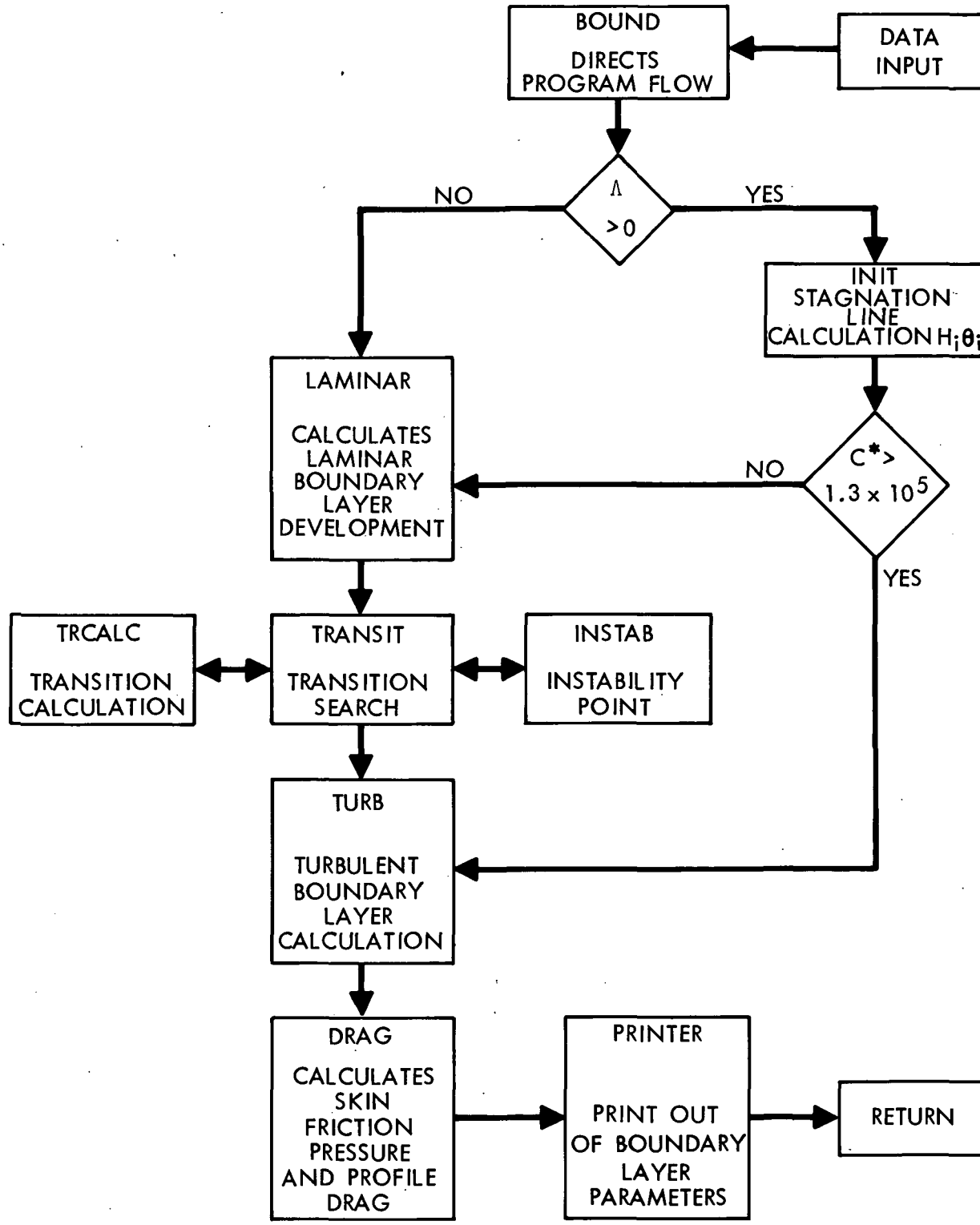

FIG. A3 OVERLAY (2,0) PROGRAM IBL

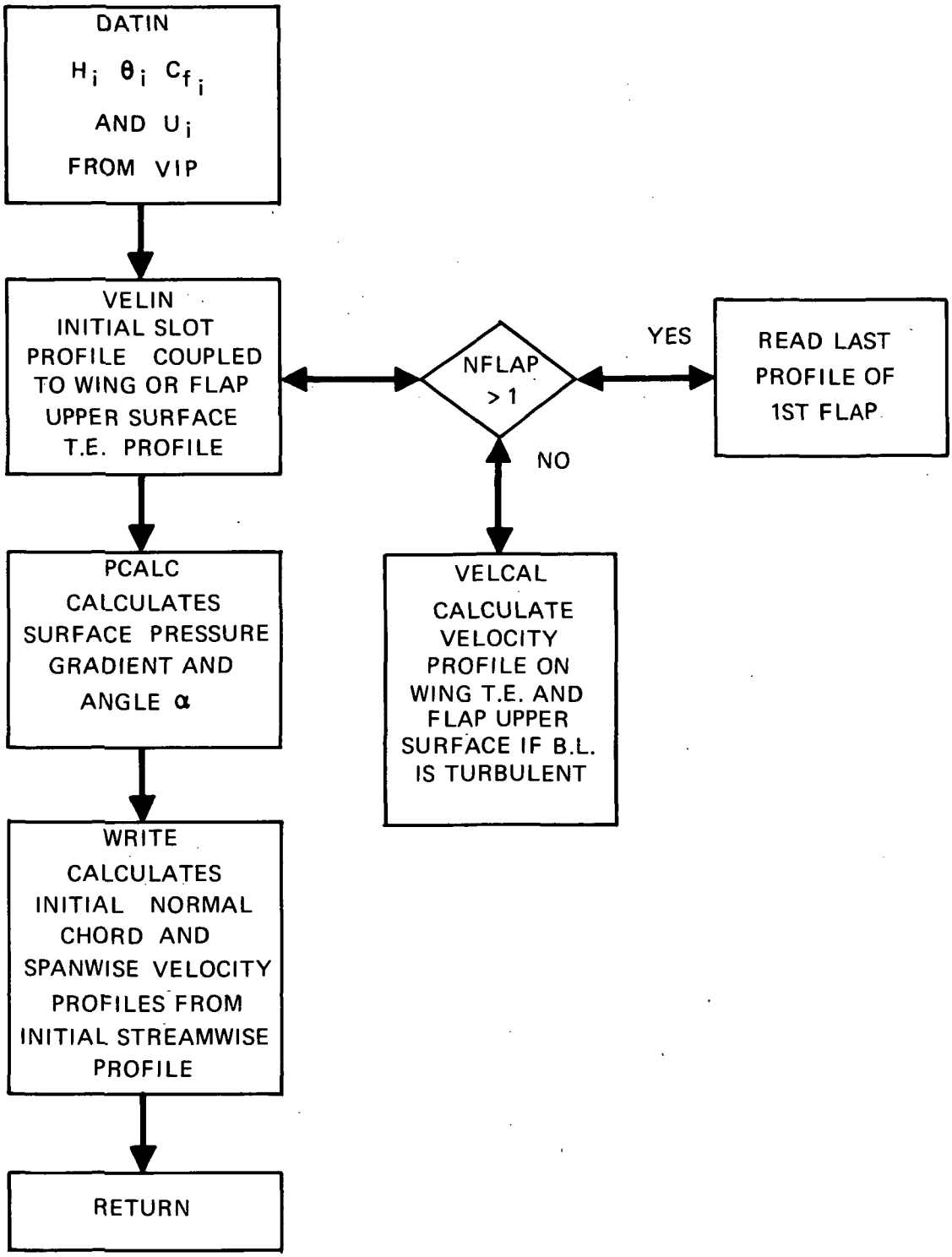

FIG. A - 4 OVERLAY (3, 1) PROGRAM BOUNDARY

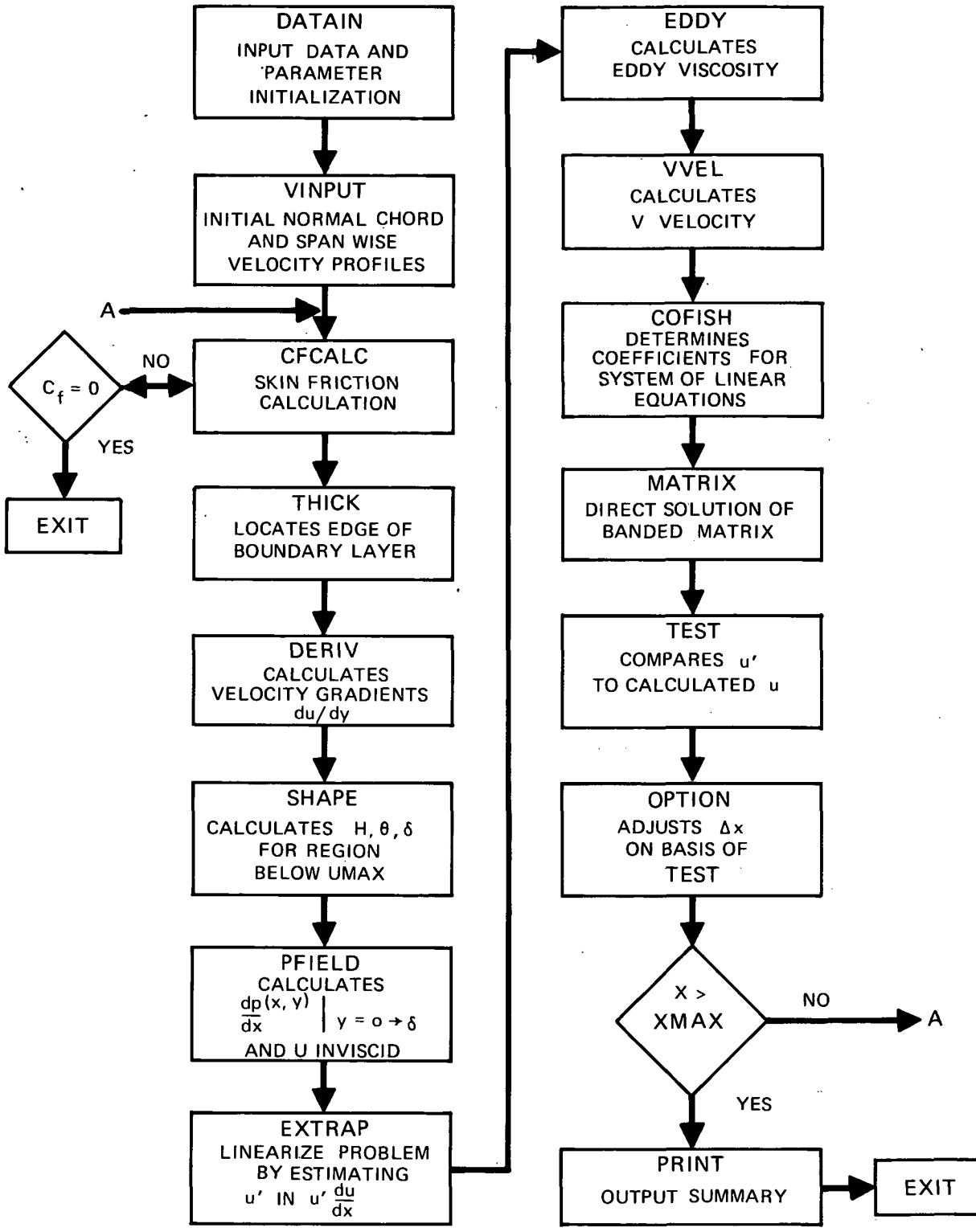

FIG. A - 5 OVERLAY (3, 2) PROGRAM DEVELOP